

1-1-2011

Surface-active solid lipid nanoparticles for emulsion stabilization

Renuka Tanmay Gupta
Ryerson University

Follow this and additional works at: <http://digitalcommons.ryerson.ca/dissertations>

 Part of the [Molecular Biology Commons](#)

Recommended Citation

Gupta, Renuka Tanmay, "Surface-active solid lipid nanoparticles for emulsion stabilization" (2011). *Theses and dissertations*. Paper 705.

This Thesis is brought to you for free and open access by Digital Commons @ Ryerson. It has been accepted for inclusion in Theses and dissertations by an authorized administrator of Digital Commons @ Ryerson. For more information, please contact bcameron@ryerson.ca.

SURFACE-ACTIVE SOLID LIPID NANOPARTICLES FOR EMULSION STABILIZATION

by

Renuka Tanmay Gupta

M. Pharm., SNDT Women's University, Mumbai, India, 2000

A thesis
presented to Ryerson University
in partial fulfilment of the
requirements for the degree of
Master of Science
in the Program of
Molecular Science

Toronto, Ontario, Canada, 2011

©Renuka Gupta 2011

I hereby declare that I am the sole author of this thesis. I authorize Ryerson University to lend this thesis to other institutions or individuals for the purpose of scholarly research.

* Signature

I further authorize Ryerson University to reproduce this thesis by photocopying or by other means, in total or in part, at the request of other institutions or individuals for the purpose of scholarly research.

*Signature

ABSTRACT

SURFACE-ACTIVE SOLID LIPID NANOPARTICLES FOR EMULSION STABILIZATION

©Renuka Gupta

Master of Science, Department of Chemistry and Biology

Ryerson University, Toronto, Canada, 2011

Solid lipid nanoparticles (SLNs) consisting of the food grade surfactant lipid glyceryl stearate citrate (GSC) were prepared using hot melt emulsification and high-pressure homogenization. Flash-cooling of the resultant oil-in-water nanoemulsions led to the formation of GSC SLNs. The effective mean particle size of the SLNs was ~ 180 nm by dynamic light scattering and the volume-weighted mean particle size was ~ 152 nm by laser diffraction, with a zeta (ζ) potential of ~ -49 mV. Effective mean particle size and ζ potential were stable for 24 wk. An equilibrium contact angle of $\sim 108.7^\circ$ measured through oil phase was obtained, suggesting a wettable lipid surface. The melting curve of the SLNs obtained by differential scanning calorimetry showed a significantly lower melting point and broader peak as compared to the bulk GSC, which was attributed to the nano-scale particle size. Unusually, the cooling curve showed an identical crystallization temperature as that for the bulk GSC, which suggested surface heterogeneous crystallization of the SLNs. Subsequent heating-cooling cycles confirmed the existence of nanosized particles in the sample during thermal analysis. Transmission electron (TEM) and atomic force microscopy (AFM) both revealed anisometric, flattened SLNs with circular or elliptical shapes.

SLNs were studied for their effectiveness as colloidal emulsifiers in oil-in-water (o/w) emulsions. The generated o/w emulsions had a volume-weighted mean droplet size of ~ 459 nm by laser diffraction and ζ potential of ~ -43 mV. The emulsions were stable for up to 12 wk as observed for macroscopic changes by inverted light microscopy. TEM images pointed to the presence of a Pickering-type network stabilizing the emulsions. With time, desorption of the SLNs from the oil droplet surface into the continuous aqueous environment, coupled with Ostwald ripening, resulted in destabilization of the emulsions. Overall, these results demonstrated that stabilization of o/w emulsions was achievable using SLNs as the sole emulsifiers.

ACKNOWLEDGEMENTS

I wish to express my gratitude to my supervisor, Dr. D errick Rousseau, for his insightful suggestions that have shaped the necessary progress of this thesis. Dr. Rousseau has been kind in providing a flexible work schedule due to my personal commitments. His boundless energy combined with his patience and support has enabled me to complete this work.

I extend my gratitude to my Committee members, Drs. Darrick Heyd & Christopher Evans, who have been equally enthusiastic and provided valuable insight to my work.

I thank Drs. Debora Foster and Daniel Foucher, Program Directors for their support during my enrolment as graduate student.

I wish to specially thank the Ministry of Training, Colleges and Universities for the Ontario Graduate Scholarship, the National Science and Engineering Research Council and Ryerson University for the Graduate scholarship that enabled these investigations.

For their kind support with characterization techniques, I would like to thank:

- Dr. Supratim Ghosh (DSC analysis, contact angle measurement, inverted microscopy)
- Mr. Shane Hodge (Introduction to AFM, Langmuir-Blodgett trough set up)
- Dr. Lanny Sapei and Mr. Muhammad Ali Naqvi (Particle size measurements)
- Mr. Steven Doyle, University of Toronto (TEM measurements)

I thank all my colleagues, especially Dr. Misael, Moumita, Tejas, Tu, Natasha, and Samira in the Rousseau Lab for the friendly and co-operative working atmosphere and wish them success in their research.

I extend my thanks to Toronto Public Library, Main Street & Ryerson University library.

I wish to thank my parents and my loving sisters Deepika, Leena, Neena, Seema and niece Tanishqa – you all make my life complete. Special thanks to my dear sister Seema for taking care of my son Nirmay. It would have been arduous to submit without her support.

Most of all, I deeply thank my husband Tanmay for his patience, love and positive support. Tanmay, I adore you for your continued encouragement and appreciation of what I do. My son Nirmay’s presence provides me immense bliss. To them, I dedicate this thesis.

Finally, I humbly acknowledge the glory of *The Supreme God*, the true essence and strength of life who provides perseverance during all tasks.

Renuka T. Gupta

TABLE OF CONTENTS

Abstract	iii
Acknowledgements.....	iv
Table of contents	v
List of tables.....	ix
List of figures.....	x
Acronyms & abbreviations.....	xii
List of symbols	xiv

CHAPTER 1 INTRODUCTION

1.0	Introduction.....	1
1.1	Colloids and interfaces	1
1.2	Fundamentals of colloidal systems	2
1.2.1	DLVO theory.....	2
1.3	Instability of colloidal systems	4
1.3.1	Lipid modification: Crystallinity and polymorphism	6
1.3.2	Flocculation	6
1.3.3	Creaming and sedimentation	6
1.3.4	Aggregation and coalescence	7
1.3.5	Ostwald ripening.....	7
1.3.6	Partial coalescence	8
1.3.7	Phase inversion	8
1.4	Improving stabilization in colloidal systems	9
1.4.1	SLN dispersion stabilization	9
1.4.2	Emulsion stabilization.....	10

1.5	Thesis objectives	12
1.6	Hypotheses.....	12
1.7	Methodology and approach.....	13
1.8	Thesis organization	13

CHAPTER 2 LITERATURE REVIEW

2.0	Introduction.....	15
2.1	Solid lipid nanoparticles	15
2.1.1	Production methods.....	16
2.1.2	Characterization of SLNs.....	16
2.1.2.1	<i>Particle size and size distribution</i>	16
2.1.2.2	<i>Surface charge</i>	17
2.1.2.3	<i>Particle morphology and ultra-structure</i>	17
2.1.2.4	<i>Polymorphism in SLNs</i>	19
2.2	Solid-stabilized emulsions.....	21
2.2.1	Contact angle and wettability.....	21
2.2.2	Particle size, shape and concentration.....	24

CHAPTER 3 EXPERIMENTAL TECHNIQUES

3.0	Introduction.....	27
3.1	SLN preparation.....	27
3.2	Emulsion preparation.....	28
3.3	Dynamic light scattering	29
3.4	Laser diffraction	30
3.5	Surface charge determination.....	31
3.6	Contact angle measurements.....	32
3.7	Thermal analysis.....	33

3.8	Inverted light microscopy	34
3.9	Transmission Electron Microscopy	34
3.10	Atomic Force Microscopy	35
3.11	Data analysis	36

**CHAPTER 4 SOLID LIPID NANOPARTICLES: PREPARATION,
CHARACTERIZATION AND APPLICATION AS NOVEL PARTICLE
STABILIZERS FOR OIL-IN-WATER EMULSIONS**

4.0	Summary.....	37
4.1	Introduction.....	38
4.2	Materials and methods	40
4.2.1	Materials	40
4.2.2	Methods.....	41
4.2.2.1	<i>Preparation of GSC SLNs.....</i>	<i>41</i>
4.2.2.2	<i>Preparation of SLN decorated oil-in-water (o/w) emulsions.....</i>	<i>42</i>
4.3	Characterization of developed systems.....	43
4.3.1	Characterization of GSC SLNs	43
4.3.1.1	<i>Particle size analysis.....</i>	<i>43</i>
4.3.1.2	<i>Surface charge measurement</i>	<i>44</i>
4.3.1.3	<i>Contact angle measurements.....</i>	<i>45</i>
4.3.1.4	<i>Differential Scanning Calorimetry (DSC).....</i>	<i>46</i>
4.3.1.5	<i>Transmission Electron Microscopy (TEM).....</i>	<i>47</i>
4.3.1.6	<i>Atomic Force Microscopy (AFM)</i>	<i>47</i>
4.3.2	Characterization of SLN decorated oil-in-water emulsions.....	48
4.3.2.1	<i>Particle size analysis.....</i>	<i>48</i>
4.3.2.2	<i>Surface charge measurement</i>	<i>48</i>
4.3.2.3	<i>Inverted light microscopy.....</i>	<i>48</i>
4.3.2.4	<i>Transmission Electron Microscopy (TEM).....</i>	<i>49</i>

4.4	Results.....	49
4.4.1	Characterization of GSC SLNs	49
4.4.1.1	<i>Particle size analysis</i>	49
4.4.1.2	<i>Surface charge measurement</i>	55
4.4.1.3	<i>Contact angle measurements</i>	56
4.4.1.4	<i>Differential Scanning Calorimetry (DSC)</i>	59
4.4.1.5	<i>Transmission Electron Microscopy (TEM)</i>	63
4.4.1.6	<i>Atomic Force Microscopy (AFM)</i>	64
4.4.2	Characterization of SLN decorated oil-in-water emulsions.....	65
4.4.2.1	<i>Particle size analysis</i>	65
4.4.2.2	<i>Surface charge measurement</i>	68
4.4.2.3	<i>Inverted light microscopy</i>	68
4.4.2.4	<i>Transmission Electron Microscopy (TEM)</i>	69
4.5	Conclusion	73
CHAPTER 5 OVERALL CONCLUSIONS		
5.0	Overall conclusions.....	74
CHAPTER 6 FUTURE STUDIES		
6.0	Future studies	75
CHAPTER 7 REFERENCES		
7.0	References	76

LIST OF TABLES

Table 4.1: DLS measurements showing unimodal and bimodal particle size distributions of 3 batches of GSC SLNs.	49
Table 4.2: LD measurements showing particle size distribution data of 3 batches of GSC SLNs.....	50
Table 4.3: DLS measurements showing unimodal and bimodal particle size distributions of refrigerated samples of GSC SLNs at various time points.	52
Table 4.4: LD measurements showing particle size distribution data of refrigerated samples of GSC SLNs at various time points.....	54
Table 4.5: Zeta potential of refrigerated samples of GSC SLNs at various time points.	55
Table 4.6: Melting and crystallization transitions for bulk GSC and GSC SLNs.....	60
Table 4.7: Melting and crystallization transitions for GSC SLNs for 5 heating-cooling cycles, along with the DLS particle size distribution data before and after the run.....	62
Table 4.8: SLN particle shape from AFM analysis initially and after 24 wk.	65
Table 4.9: LD measurements showing the particle size distribution data of 3 batches of SLN decorated o/w emulsions.	66
Table 4.10: LD measurements showing the particle size distribution data of refrigerated samples of SLN decorated o/w emulsions at various time points.	67
Table 4.11: Zeta potential measurements of refrigerated samples of SLN decorated o/w emulsions at various time points.....	68

LIST OF FIGURES

Figure 1.1: Schematic diagram of the DLVO theory showing overall potential energy of interaction as a plot of function of distance between two particles.	3
Figure 1.2: Mechanisms of instability in solid dispersions and emulsions.	5
Figure 1.3: Free energy and entropy changes in a system during emulsification.	10
Figure 2.1: Schematic view of contact angle of sessile drop.	22
Figure 2.2: Preferential position of small particles at (A) planar and (B) curved oil-water interface.	23
Figure 3.1: Schematic representation of the working principle of high-pressure homogenization technique used for producing SLNs.	27
Figure 3.2: Schematic representation of various potential gradients on the surface of a particle.	31
Figure 4.1: Chemical constituents of the lipid GSC.	40
Figure 4.2: Schematic representation of melt-emulsification homogenization for preparation of solid lipid nanoparticles.	41
Figure 4.3: Schematic representation of the preparation of SLN decorated oil-in-water (o/w) emulsions.	42
Figure 4.4: DLS particle size distributions (unimodal) of 3 batches of GSC SLNs.	50
Figure 4.5: LD particle size distributions of 3 batches of GSC SLNs.	51
Figure 4.6: DLS measurements showing particle size distributions (unimodal and bimodal) of refrigerated samples of GSC SLNs at various time points.	53
Figure 4.7: LD measurements showing particle size distribution of refrigerated samples of GSC SLNs at various time points.	54
Figure 4.8: Contact angle measurements of water droplet in canola oil spreading on a solid GSC surface at various time points.	56
Figure 4.9: Average contact angle (θ) of a water drop spreading over the GSC surface vs time (min).	57

Figure 4.10: Contact angle measurements of oil droplet in water on a solid GSC surface at various time points.....	58
Figure 4.11: Average contact angle (θ) of an oil drop spreading over the GSC surface vs time (min).....	58
Figure 4.12: DSC (A) melting and (B) crystallization thermograms of the bulk GSC (—) and GSC SLNs (-----).....	59
Figure 4.13: DSC (A) melting and (B) crystallization thermograms of GSC SLNs for 5 heating – cooling cycles.....	62
Figure 4.14: TEM micrographs of GSC SLNs at initial (A), 4 wk (B), 12 wk (C) and 24 wk (D) after preparation.....	63
Figure 4.15: AFM height images of GSC SLNs at initial (A) and 24 wk (B) after SLN preparation.....	64
Figure 4.16: LD-measured droplet size distributions showing the reproducibility of 3 batches of SLN decorated o/w emulsions.....	66
Figure 4.17: LD measurements showing the particle size distributions of refrigerated samples of SLN decorated o/w emulsions at various time points.....	67
Figure 4.18: Inverted light microscopy of SLN decorated o/w emulsions at initial (A) and 24 wk (B) after emulsion preparation.....	69
Figure 4.19: TEM micrographs of SLN decorated o/w emulsions at various time points.....	71
Figure 4.20: Probable positioning of GSC SLN at the oil-water interface in SLN decorated o/w emulsions.....	72

ACRONYMS & ABBREVIATIONS

(in alphabetical order)

2-D	:	2-dimensional
3-D	:	3-dimensional
AFM	:	Atomic force microscopy
ANOVA	:	Analysis of variance
ASTM	:	American Society for Testing and Materials
CCD camera	:	Charge-coupled device camera
CITREM	:	Citric acid esters of mono- and diglycerides of edible fatty acids
C_n	:	Carbon chain with n atoms
DLS	:	Dynamic light scattering
DLVO theory	:	Derjaguin, Landau, Verway and Overbeek theory
DSC	:	Differential scanning calorimetry
GRAS	:	Generally recognized as safe
GSC	:	Glyceryl stearyl citrate
HLB	:	Hydrophile-lipophile balance
LD	:	Laser diffraction
NLC	:	Nanostructured lipid carriers
o.d.	:	outer diameter
o/w	:	Oil-in-water
PCS	:	Photon correlation spectroscopy
PI	:	Polydispersity index
PIT	:	Phase inversion temperature
PTA	:	Phosphotungstic acid
PVDF	:	Polyvinylidene fluoride
Q10	:	Ubiquinone
QELS	:	Quasi-electric light scattering
rpm	:	revolutions per minute
SAXS/SAXD	:	Small-angle x-ray scattering/diffraction

SEM	:	Scanning electron microscopy
SLN	:	Solid lipid nanoparticles
TAG	:	Triacylglycerol
TEM	:	Transmission electron microscopy
w/o	:	Water-in-oil
WAXS/WAXD	:	Wide-angle x-ray scattering/diffraction
XRD	:	X-ray diffraction

LIST OF SYMBOLS

(in alphabetical order)

γ	:	Interfacial tension
θ	:	Contact angle
ΔA	:	Change in interfacial area
ΔG	:	Change in free energy
ΔP	:	Change in Laplace pressure
ΔS	:	Change in configurational entropy
a	:	Cross-sectional long semi-axis of non-spherical particle
A	:	Surface area of interface
b	:	Cross-sectional short semi-axis of non-spherical particle
D	:	Translational diffusion coefficient
$D(v, 0.1)$:	Diameter below which 10% of particles in a distribution lie
$D(v, 0.5)$:	Diameter below which 50% of particles in a distribution lie
$D(v, 0.9)$:	Diameter below which 90% of particles in a distribution lie
$d(H)$:	Hydrodynamic diameter
$D[3, 2]$:	Surface area-weighted mean diameter
$D[4, 3]$:	Volume-weighted mean diameter
$f(\chi a)$:	Henry's function
g	:	Acceleration due to gravity
k	:	Boltzmann's constant
p	:	The probability that a calculated test statistic has occurred by chance alone
r	:	Radius of a particle or droplet
T	:	Absolute temperature in Kelvin
U_e	:	Electrophoretic mobility
V	:	Sedimentation or creaming rate
V_a	:	Attractive van der Waals forces
V_r	:	Electrostatic repulsive forces
V_t	:	Total potential energy

w/v	:	weight by volume
w/w	:	weight by weight
wk	:	week(s)
$\bar{X} \pm s$:	mean \pm standard deviation
E	:	Dielectric constant of the dispersion medium
ζ	:	Zeta potential
η	:	Viscosity
ρ	:	Density

Chapter 1

INTRODUCTION

1.0 Introduction

The novelty of this thesis stems from the use of surface-active solid lipid nanoparticles as Pickering-type emulsion stabilizers. Many emulsions (*e.g.*, in foods, pharmaceuticals, cosmetics, and crude oil) are stabilized by crystals [paraffins, triacylglycerols (TAGs), polymers, *etc.*]. Though progress has been made in establishing the fundamentals of such crystal-stabilized emulsions, important questions regarding the stabilization capacity of so-called Pickering crystals in industrially-relevant multi-phasic systems remain¹⁻³.

1.1 Colloids and interfaces

Solid lipid nanoparticles (SLNs) are a type of colloidal carrier in which a physiological lipid is melted and dispersed in a continuous aqueous phase. Upon cooling, the melted lipid solidifies, giving rise to a solid lipid particle distributed in the aqueous system⁴. During SLN formation, the lipids used undergo physico-chemical modifications in particle size, surface charge, crystallization and polymorphism that will influence SLN stability⁵. Macro-scale changes such as creaming or sedimentation further promote instability.

Emulsions are a mixture of two immiscible liquids, with an internal liquid phase dispersed into another continuous or external liquid phase, and stabilized by the addition of a third component (surfactant) adsorbed at the liquid-liquid interface⁶. Depending on the nature of the dispersed and continuous phases, emulsions can be classified as oil-in-water emulsions (o/w) where oil is dispersed into the continuous water phase or water-in-oil emulsions (w/o) where water is dispersed into the continuous oil phase. Examples of food emulsions include butter, margarine, ice-cream, sauces, mayonnaise and spreads.

Emulsions are inherently unstable thermodynamically as an input of energy and an appropriate amount of surfactant(s) is required to achieve kinetic stability⁷. The input of energy causes breakdown of large drops into smaller droplets, thereby increasing their interfacial area. This increase, coupled with the presence of surfactant(s), lowers the interfacial tension at the liquid-liquid interface, which retards droplet-droplet flocculation

and coalescence and minimizes phase separation (*i.e.*, sedimentation or creaming) during the emulsion's shelf-life^{7,8}.

Although surfactants are largely used to reduce interfacial tension in emulsions, efficient emulsion stabilization can also be achieved with colloidal solid particles that adsorb at the oil/water interface, preventing droplet coalescence by steric hindrance⁸. Particle-stabilized emulsions have been reported to completely arrest Ostwald ripening in emulsions due to high desorption energy of the particles and resulting capillary effects⁹. Protein and nanoparticles^{10, 11}, hydrophobized fumed silica particles¹², silica and hydrophobized titania particles¹³ have been effectively used as solid stabilizers for o/w emulsions. Depending on whether the adsorbed particles are predominantly hydrophilic or hydrophobic, it is possible to generate o/w or w/o emulsions, respectively¹⁴.

Particle microstructure has been shown to influence droplet coverage, contact angles and aggregation behaviour in fat-stabilized emulsions, with smaller crystals providing better and full droplet coverage than larger crystals^{15, 16}. This can be seen in homogenized milk, where the damaged milk fat globule is replaced by casein micelles that stabilize the milk emulsion by adsorbing at the oil/water interface¹⁴. Recently, the presence of amphiphilic ions adsorbed at the droplet surface has been shown as one of the important requirements for the spontaneous formation of monodispersed solid particle-stabilized emulsions¹⁷.

Overall, this thesis aimed to show that SLNs generated from lipids possessing amphiphilic properties could be used as solid particle emulsifiers to stabilize o/w emulsions.

1.2 Fundamentals of colloidal systems

Since our systems were comprised of solid particles dispersed in an aqueous medium as well as o/w emulsions, interaction forces acting between colloidal particles in suspensions and emulsions are discussed as these forces greatly influence the stability of particulate systems.

1.2.1 DLVO theory

The forces involved during particle coagulation and flocculation can be described by the DLVO theory, named after Derjaguin, Landau, Verwey and Overbeek¹⁸. There exists an

attractive long range van der Waals force (V_a) arising from induced dipole-dipole interactions between particles. There also exist electrostatic repulsive forces (V_r) due to the interaction of identically-charged double layers surrounding particles.

The overall potential energy of interaction (V_t) is the sum of these attractive and repulsive potential forces¹⁹:

$$V_t = V_a + V_r \quad (\text{Eqn. 1.1})$$

Thus, if repulsive forces dominate, the total energy of the system increases and the system is stable. Correspondingly, if attractive forces dominate, the total energy decreases, destabilizing the system. Figure 1.1 shows the interplay of attractive and repulsive forces as a function of distance from the surface of a spherical particle.

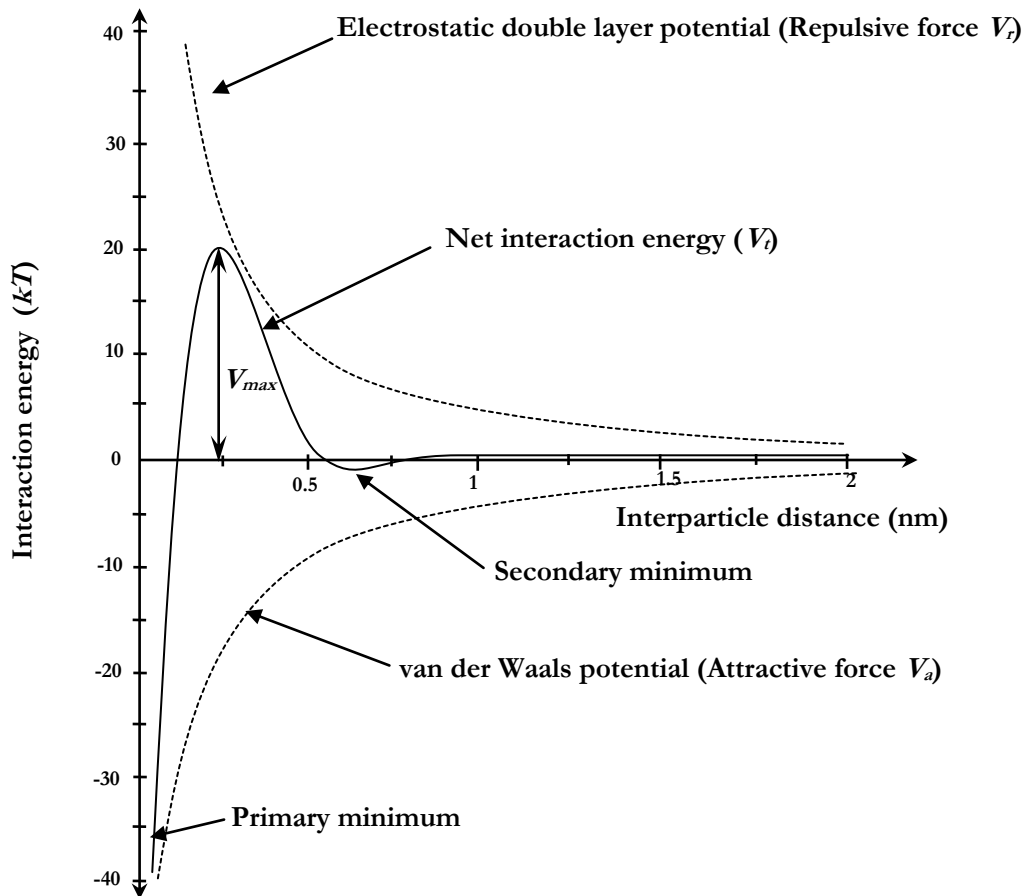


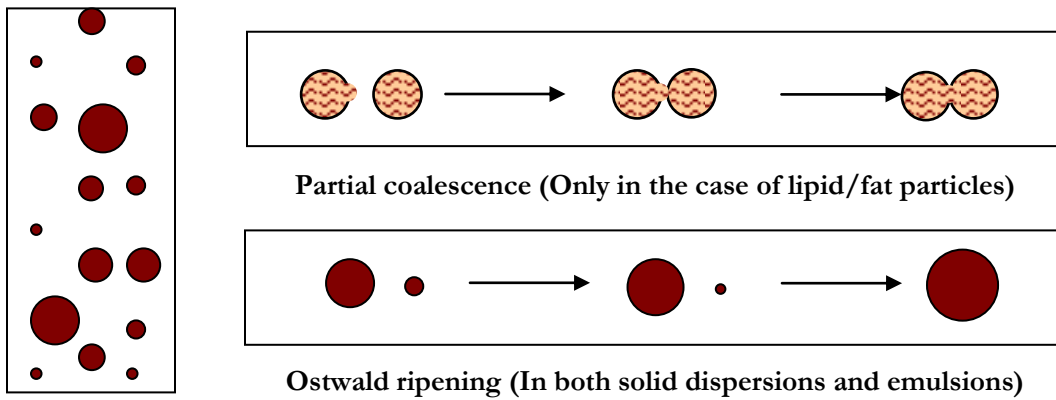
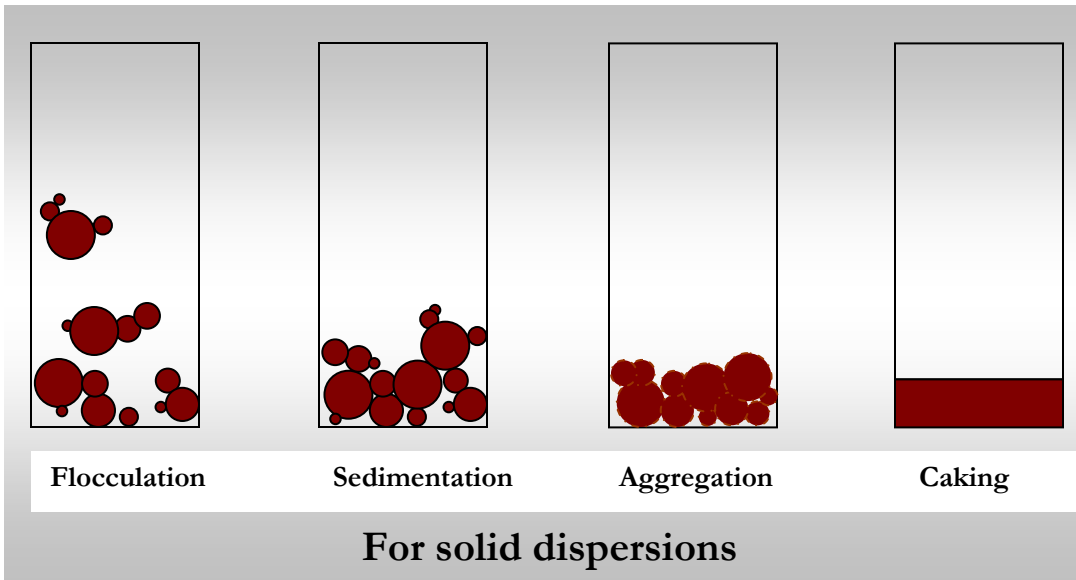
Figure 1.1: Schematic diagram of the DLVO theory showing overall potential energy of interaction as a plot of function of distance between two particles (Adapted from Refs # 19, 20).

When the interparticle distance between two particles is large, there is no interaction between them, and both potentials are near zero. As the particles approach each other, a repulsive force develops, which increases as the distance decreases due to the overlap of their electrostatic double layers. It reaches a maximum (V_{max}) when distance between the particle surfaces is equal to the distance between the repulsive barrier and surface. V_{max} when greater than $\sim 20 kT$ (thermal energy of the system), prevents agglomeration in the system and helps maintain stability over an extended period of time^{20, 21}. If the thermal energy of the system is higher than V_{max} , the particles are able to overcome the repulsive forces and cross the energy barrier to fall into the deep minimum that exists near the particle surface due to the van der Waals attractive potential. This is evidenced by a sharp fall in the net energy potential addressed as the primary minimum shown in the Figure. The secondary minimum exists only when the concentration of counter-ions in the system is high enough to develop weakly attractive forces²².

Although the DLVO theory successfully explains long-range interaction forces observed in colloidal systems, it cannot explain the interaction forces between particles a few nanometres from one another. Particle size, shape and chemistry will influence the interplay between these forces at small separation distances²³. Non-DLVO forces such as solvation or hydration forces, hydrophobic forces and steric interactions can be much stronger than either of the two DLVO forces, when two particles are very close to each other^{18, 23, 24}.

1.3 Instability of colloidal systems

Significant modifications in the composition and structure of the lipids used to generate nanoparticles occur gradually over time, altering their physico-chemical stability. Further instability arises due to processes such as sedimentation, aggregation, crystal networking and Ostwald ripening. In the case of emulsions, physical processes such as flocculation, creaming, coalescence, phase inversion and Ostwald ripening cause destabilization²⁵. In practice, initiation of one event is sufficient to trigger a cascade that ultimately causes instability in the colloidal system (Figure 1.2).



Kinetically stable dispersion or emulsion

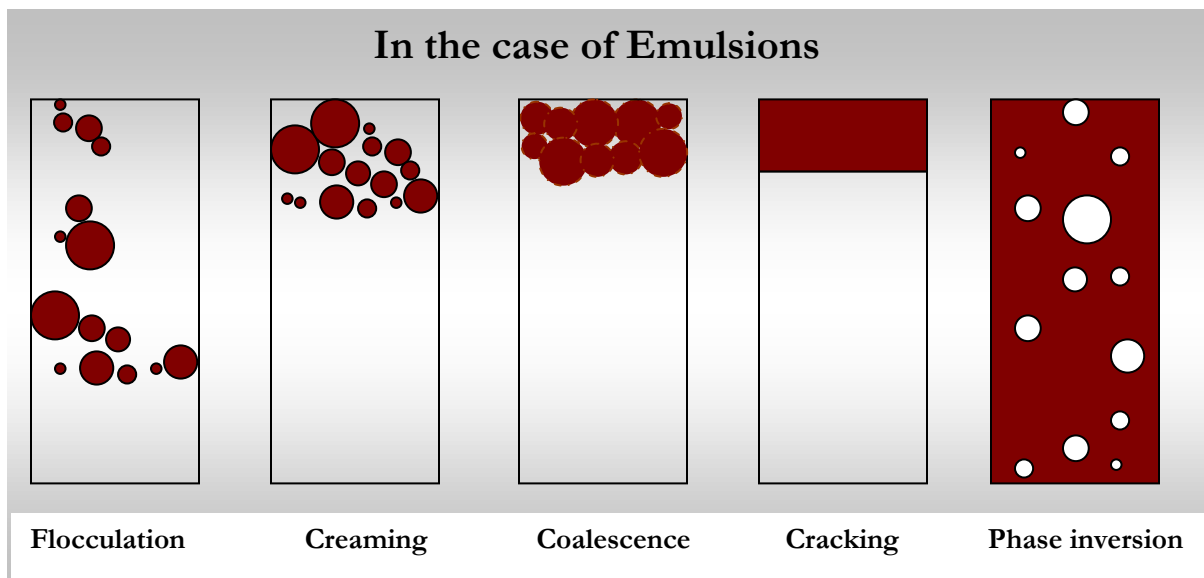


Figure 1.2: Mechanisms of instability in solid dispersions and emulsions (Adapted from Refs # 26, 27).

1.3.1 Lipid modification: Crystallinity and polymorphism

The ability of molecules to crystallize in more than one arrangement in the solid state is called polymorphism²⁸. Polymorphs possess unique melting points, X-ray diffraction patterns and solubilities and their identification in lipid dispersions is important²⁹. As a result of SLN processing conditions (shear, heat, cooling, *etc.*), the crystallization kinetics and polymorphism exhibited by dispersed lipid nanoparticles is often distinctly different from that observed in the bulk material³⁰.

In the case of triacylglycerols (TAGs), three main polymorphic forms, namely the α (alpha), β' (beta prime) and β (beta) forms, have been reported³¹. The α -form is the least stable, followed by β' which has an intermediate stability and the β -form which is the most stable polymorph. Because of their lower Gibb's free energy, unstable forms crystallize first³². The transition from α to β *via* β' tends to provide the optimum packing form of molecules.

1.3.2 Flocculation

Colloidal particles in Brownian motion will collide with neighbouring particles. Depending on the relative magnitudes of the attractive and repulsive forces, such particles may adhere or repel one another. At long separation distances, there is no effective interaction between the particles. However, as they move closer together, the van der Waals attraction dominates initially. These initial weak attractive forces give rise to the secondary minimum³³ (Figure 1.1) The depth of this minimum determines if the system will flocculate or remain non-aggregated. If the depth is larger compared to the thermal energy of the system, the particles will flocculate. If it is smaller, they remain in a non-aggregated state²¹. During flocculation, particles cluster together without merging^{18, 19, 34}. It is possible to re-disperse particles at this stage by gentle agitation. As flocculation increases, creaming and/or sedimentation ensues.

1.3.3 Creaming and sedimentation

Flocculates may either rise or sink depending on density differences between the dispersed and continuous phases. In the case of o/w emulsions, oil droplets typically have a lower density than the aqueous phase and will rise to the surface of the emulsion. In the case

of solid dispersions and w/o emulsions, due to higher density of the dispersed solid than water, the particles will sediment. The Stokes' equation provides an estimate of the rate of sedimentation or creaming^{34,35}:

$$V = \frac{2r^2(\rho_1 - \rho_2)g}{9\eta} \quad (\text{Eqn. 1.2})$$

where V is the sedimentation or creaming rate (m/s), r is the radius of the particle or droplet (m), ρ_1 and ρ_2 are the densities of the suspended particles (or dispersed phase) and the continuous phase medium (kg/m³), respectively, g is the acceleration due to gravity (m/s²), and η is the viscosity of the continuous phase (kg/m·s). From Equation 1.2, V increases with both an increase in particle size and density difference between the two phases and a decrease in the viscosity of the continuous phase. Creaming and sedimentation are reversible, only if the settled particles or globules have not formed a compact structure and progressed towards irreversible aggregation and/or coalescence.

1.3.4 Aggregation and coalescence

As more and more particles flocculate, they tend to overcome the repulsive energy barrier and attractive forces start to dominate. Rapid aggregation can occur in the absence of a primary maximum, leading to the formation of a strong, irreversible aggregated structure²⁰. A three-dimensional aggregated network with interconnections eventually fuses into a compact pack of particles, causing an irreversible “caking” of the dispersion³⁶.

Coalescence occurs when two or more droplets merge to form a single larger droplet. This process leads to an irreversible breakdown, referred to as “cracking” of an emulsion³⁴.

1.3.5 Ostwald ripening

Ostwald ripening, a phenomenon observed in both solid dispersions and emulsions³⁷, does not require physical contact of the colloidal particles. Rather, transport of dissolved matter through the continuous phase leads to emulsion destabilization. The mechanism responsible is due to existence of a pressure difference ΔP across curved interfaces (either liquid-liquid or solid-liquid), and is given by²⁷:

$$\Delta P = \frac{2\gamma}{r} \quad (\text{Eqn. 1.3})$$

where γ is the interfacial tension at the oil-water interface and r is the particle/droplet radius.

Thus, ΔP is inversely proportional to the particle/droplet radius. The difference in the Laplace pressure results in the molecular diffusion of dispersed phase material through the continuous phase³⁸, since the droplets try to maintain a state of low pressure and consequently larger radii. The net mass flux causes larger particles to grow at the expense of smaller particles, which eventually disappear^{7, 39}, thus causing an increase in average particle/droplet diameter with a corresponding reduction in their number³⁴. Ostwald ripening is primarily observed in systems when solubility differences between the continuous and dispersed phase is not very great.

1.3.6 Partial coalescence

Partial coalescence is a process when two or more partially crystalline droplets come into contact and fuse forming an irregularly-shaped aggregate²⁷. It occurs only if oil droplets contain solid particles such as fat crystals that form a solid network within the globules. Once they reach a certain size, they will protrude into the continuous aqueous phase. With either perikinetic and orthokinetic collisions, such protruding crystals will form an aggregate²⁶. This mechanism rarely occurs in w/o emulsions as the lipid phase is continuous.

1.3.7 Phase inversion

Emulsions can invert from an o/w to a w/o emulsion or *vice versa*, a process known as phase inversion. This instability can be induced by changes in composition, as a result of significant shear or at a set temperature called the phase inversion temperature (PIT). Binks and Lumsdon⁴⁰ reported the phase inversion of w/o emulsions stabilized solely by nanosized hydrophobic silica particles at a volume fraction of water close to 0.7, when water drops began to deform. A similar dispersed phase volume fraction was required for phase inversion of o/w emulsions stabilized with hydrophilic silica particles.

1.4 Improving stabilization in colloidal systems

The previous discussion highlighted factors that determine the stability of two types of colloidal systems - solid dispersions and emulsions. The following discussion describes various stabilization approaches.

1.4.1 SLN dispersion stabilization

Dispersions of SLNs can be stabilized *via* a number of composition and process-related approaches. SLN dispersions in water can be stabilized by eliminating the continuous aqueous phase *via* spray-drying or freeze drying. The spray- or freeze-dried powders can be reconstituted with water to obtain the original dispersion⁴¹⁻⁴⁴. The presence of surfactants such as polysorbate 80⁴⁵, phospholipid/bile salts⁴⁶ and poloxamers⁴⁷ provides steric stabilization, and help to ensure that the SLNs do not clump. For example, sodium taurocholate as a charged surfactant and ethanol as a co-surfactant were shown to impart a positive surface charge to SLN dispersions of stearic acid and glyceryl behenate⁴⁸. Along these lines, usage of surfactants in SLN formulations can provide considerable stability to metastable lipid polymorphs. For example, the metastable α -form in tristearin nanoparticles was maintained by the addition of saturated long-chain phospholipids and the bile salt sodium glycocholate⁴⁹. In another study, the α -form of tristearin SLNs was most stable in lipid dispersions stabilized with sodium glycocholate⁵⁰.

The type of lipid used for SLN production can have a significant effect on polymorphic stability. SLNs produced with TAGs will have a higher stability than those produced using mono- and diglycerides⁵¹. As well, the kinetics of polymorphic transitions are usually slower for longer-chained rather than shorter-chained TAGs⁵². In concert, by controlling processing conditions such as cooling rate, it is possible to obtain more stable polymorphs, which leads to dispersions with increased stability. Also, storage parameters can profoundly influence the stability of lipid dispersions. For example, an increase in production or storage temperature can promote the polymorphic transition of an SLN lipid towards a more stable polymorph³².

1.4.2 Emulsion stabilization

In the case of emulsions, apart from increasing viscosity or reducing particle size by efficient emulsification techniques, stability is achieved mainly by incorporation of surfactants. Thermodynamically, the initial and final states and associated energy changes of an emulsified system are shown in Figure 1.3.

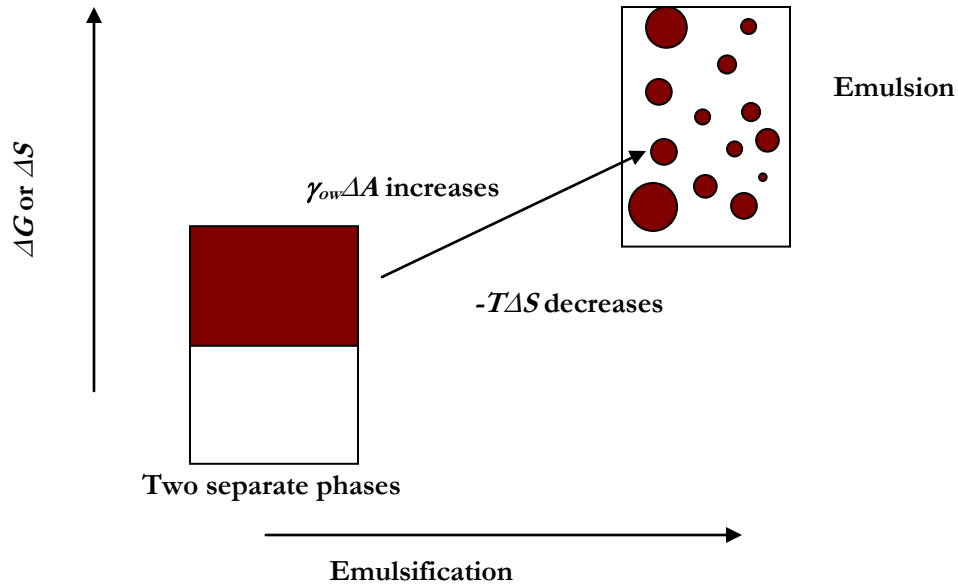


Figure 1.3: Free energy and entropy changes in a system during emulsification (Adapted from Ref # 53).

The free energy change in a system undergoing emulsification is given by⁵³:

$$\Delta G = \gamma_{ow}\Delta A - T\Delta S \quad (\text{Eqn. 1.4})$$

where ΔG is the free energy of emulsification, γ_{ow} is the interfacial tension at the oil-water interface, ΔA is the increase in interfacial area, T is the temperature and ΔS is the configurational entropy of the system (entropy change associated with a change in physical arrangement of the particles in a system).

A system is more stable when ΔG value is smaller or negative. When no surfactants are present in the system, $|\gamma_{ow}\Delta A| \gg |-T\Delta S| \therefore \Delta G = \gamma_{ow}\Delta A$. This indicates that the total change in free energy is positive and a thermodynamically unstable system exists. The presence of surfactant(s) lowers the interfacial tension, and consequently results in a smaller free energy of emulsification. If an emulsion with smaller droplets is desired, extra energy is

required to overcome the higher Laplace pressure that results from the smaller droplet radius.

When emulsions are stabilized solely by solid particles, the formation of emulsion droplets is initiated due to the preferential adsorption of particles at the liquid-liquid interface, which form a mechanical barrier preventing droplet-droplet coalescence⁵³.

Though it is well-known that complete droplet coverage best stabilizes Pickering-type emulsion droplets, complete stabilization has also been reported without full monolayer coverage of particles. Vignati *et al.* reported stabilization of o/w emulsion droplets by monodisperse, hydrophobic silica colloids with only 5 % droplet coverage. The authors proposed that stabilization was achieved by monolayer bridging between particles that helped to maintain a finite distance between droplets, preventing their coalescence⁸. This monolayer particle bridging sterically hindered coalescence, with stability governed by particle wettability. Horozov and Binks⁵⁴ studied octane-water interface stabilization with two types of particles: slightly hydrophobic silica particles with contact angle (θ) of 65° and very hydrophobic silica particles with θ of 152°, measured through the aqueous phase. Slightly hydrophobic particles yielded aggregated, disordered, planar monolayers due to lack of strong inter-particle repulsion resulting in the formation of a stabilizing bilayer arrangement between droplets that prevented coalescence by steric hindrance. In contrast, hydrophobic particles gave well-ordered, dilute planar monolayers that stabilized the emulsions by bridging the emulsion droplets.

Other means of stabilization occur *via* 2-D and 3-D particle networks^{14, 53}. In 2-D stabilization, adsorption of aggregated colloidal particles occurs when θ favours strong adsorption at the oil-water interface. In this case, the barrier consists of a rigid disordered layer or network of particles adsorbed to the oil-water interface, and the aggregated structure is held together by attractive inter-particle forces that dominate particle interactions at the droplet surface¹⁴.

By contrast, 3-D particle networks result when an abundance of particles is present in the continuous phase of an emulsion system. In addition to the presence of a tightly-packed particle layer at the droplet surface, a particle network through the continuous phase

is formed, resulting in improved emulsion stability^{15, 53}. With an increase in the concentration of solid particles, an envelope of solid particles forms around the droplets resulting in a 3-D network of particles connecting the droplets. This is called network stabilization and it heightens stability by decreasing droplet-droplet contact. Abend and Lagaly⁵⁵ combined bentonite with hydroxide particles at concentrations as low as 0.1% w/w solids to produce highly stable o/w emulsions. Addition of increasing amounts of bentonite further stabilized the system by providing a 3-D network consisting of both types of particles throughout the continuous phase.

1.5 Thesis objectives

Use of SLNs has been largely reported for drug delivery and cosmetic applications as against their use in functional foods and nutraceuticals where little has been reported. The overall objective of this thesis was to develop stable SLNs and explore their applicability as emulsion stabilizers for oil-in-water (o/w) emulsions for food applications. The specific objectives were as follows:

- i) To formulate SLNs using melt-emulsification homogenization and establish the stability of the resultant SLNs;
- ii) To study the effects of the local environment on SLN properties;
- iii) To explore the application of the developed stable SLNs as highly-effective food emulsion stabilizers in o/w emulsions, and;
- iv) To understand the mechanism of o/w emulsion stabilization by SLNs.

1.6 Hypotheses

The proposed hypotheses were:

- i) Stable SLNs based on food-grade lipids having emulsifying properties can be formulated solely without the aid of additional emulsifiers and;
- ii) The formulated SLNs can be used as emulsifiers to stabilize o/w emulsions *via* Pickering and/or solid particle network stabilization.

1.7 Methodology and approach

Stable SLNs were developed from food-grade lipids without the aid of emulsifiers as the lipid glyceryl stearyl citrate itself had emulsifying properties. The developed SLNs were characterized to determine their stability over a period of time. Well-characterized, stable SLNs were then used as the sole emulsion stabilizers for o/w emulsions. The emulsions were characterized and studied for stability, and the mechanisms responsible for imparting stability were established.

1.8 Thesis organization

The thesis is divided into seven chapters organized as follows:

Chapter 1: Introduction

The chapter briefly introduces the fundamentals of colloidal systems, interfaces and colloidal interactions. Instability encountered in both lipid dispersions and emulsions and methods to improve stability in these colloidal systems are discussed. Special mention is given to emulsions stabilized by solid particles and the mechanisms that govern the stability of such emulsions. The chapter also provides information on the thesis objectives, the hypotheses, methodology and approach adopted to achieve the aims of the research work and presents an overview of the thesis organization.

Chapter 2: Literature review

The chapter presents a review of recent work on SLNs related to their production and characterization techniques, with special emphasis on the challenges associated with elucidating the crystallinity and structure of lipid nanoparticles. Research work pertaining to the use of solid particles to stabilize emulsions, especially o/w emulsions is discussed.

Chapter 3: Experimental techniques

The chapter presents the experimental techniques used in this study. It describes the homogenization technique used for the production of SLNs and o/w emulsions. It provides a brief discussion of the concepts of the experimental techniques used for characterization of the SLNs and emulsions.

Chapter 4: Solid lipid nanoparticles: Preparation, characterization and application as novel particle stabilizers for oil-in-water emulsions

The chapter covers the formulation and characterization of the developed SLNs and o/w emulsions. It explains the detailed characterization of SLNs, including particle size and surface charge determination, contact angle measurements, thermal analysis and particle shape studies using TEM and AFM. It presents the formulation and characterization of o/w emulsions and discusses the results obtained, and attempts to elucidate the mechanisms responsible for emulsion stabilization using SLNs as emulsifiers.

Chapter 5: Overall conclusions

The chapter summarizes the results presented in the thesis and discusses their potential application in the context of proposed future studies in the area of SLN stabilized o/w emulsions.

Chapter 6: Future studies

The chapter highlights the potential areas for future research studies and feasible strategies to fine-tune this research.

Chapter 7: References

The chapter consists of the references used in this thesis.

Chapter 2

LITERATURE REVIEW

2.0 Introduction

SLNs were initially developed in the early 1980s and since then extensive research has been carried out to study their feasibility as carrier systems in pharmaceuticals, cosmetics and to a lesser extent, in foods. This chapter is divided into two parts. The first part is a review on SLNs regarding their preparation and characterization with special emphasis on understanding lipid crystallinity and polymorphic behaviour. The second part discusses concepts related to the stabilization of emulsions using solid particles.

2.1 Solid lipid nanoparticles

Solid lipid nanoparticles (SLNs) are submicron colloidal particles having particle size in the nanometre range (usually well below 1000 nm)⁵⁶. They are made from biocompatible lipids that melt when heated and solidify at room or body temperature^{57, 58}. The solid lipid protects incorporated biomolecules from degradation, a characteristic desirable for drug delivery. SLNs are easy to produce and can be well tolerated within the body⁵⁹.

In the past 20 years, SLNs have been investigated for their suitability as effective drug carrier systems by encapsulating both hydrophilic⁶⁰⁻⁶² and hydrophobic^{61, 63-65} molecules for oral⁶⁶⁻⁶⁸, parenteral^{58, 69} and topical drug delivery systems⁷⁰⁻⁷⁶.

As opposed to pharmaceutical applications, the study of SLNs to encapsulate food-related compounds has gained steam in the last five years⁷⁷⁻¹⁰⁰. Due to their solid nature, SLNs make an ideal carrier vehicle for lipophilic bioactive components such as omega-3 fatty acids, carotenoids or phytosterols^{79, 87}. However, saturated lipids generally used as the SLN building blocks are not always the preferred choices in terms of nutrition and health⁸⁴, as they are known to be an important risk factor in cardiovascular disease⁸⁰. As well, lipids exhibit polymorphic transformations during their preparation and shelf life, which further limits their use in food applications⁸⁴. Recently, structured systems such as nanoemulsions¹⁰¹, multilayered emulsions¹⁰², and SLNs⁸³ have been explored as carrier systems for functional food products. SLN production methods developed for pharmaceutical drug delivery

systems have been applied to food-grade (GRAS - generally recognized as safe) ingredients, which are substituted for polymers and surfactants used in pharmaceuticals⁷⁷.

2.1.1 Production methods

In early 1980s, Speiser and co-workers developed SLNs by spray-drying and lipid nanopellets using high speed mixing or ultrasound⁵⁷. However, particle size in the micron range excluded their use in parenteral administration. In the following years, Müller and co-workers demonstrated the application of high-pressure homogenization as an effective method for the production of colloidal dispersions of solid lipids with particle sizes below 500 nm⁵⁹, which attracted attention towards use of high-pressure homogenization to produce submicron-sized solid lipid dispersions.

Melt emulsification homogenization is the most widely reported technique for producing SLNs^{64, 103-113}, and has also been used to load hydrophobic bioactive compounds (*e.g.*, β -Carotene) into SLNs¹¹⁴ and nanostructured lipid carriers (NLCs)¹¹⁵. However, this approach cannot be used for shear and temperature-sensitive molecules such as heat-labile proteins, vitamins or aroma/flavour compounds. Cold homogenization is the alternative method for such compounds^{109, 116}. Another method is adsorptive SLN loading, where heat-sensitive biomolecules are adsorbed onto the SLN surface, after their preparation by high pressure homogenization¹¹⁷.

Other techniques reported for SLN production include melt emulsification homogenization with ultrasound¹¹⁸, microemulsions^{61, 119-122}, solvent-emulsification diffusion¹²³⁻¹²⁵, emulsion phase inversion¹²⁶, and *via* double emulsions^{60, 125, 127}.

2.1.2 Characterization of SLNs

The important characterization parameters to be investigated in SLNs are their particle size and size distribution, surface charge, determination of particle morphology and ultra-structure, as well as their polymorphic state (crystalline or amorphous)¹²⁸.

2.1.2.1 Particle size and size distribution

The determination of SLN particle size and size distribution is the foremost parameter to be evaluated. Particle size measurements are routinely performed on SLN

dispersions immediately after preparation as well as during their shelf life to ascertain changes in size. Most of the particle size determinations are performed using light scattering methods, primarily dynamic light scattering (DLS)^{104, 129}. For broader distributions, laser diffraction (LD) is frequently employed in conjunction with DLS^{117, 130}.

Jores *et al.*¹³¹ investigated the particle size and size distribution of SLNs using both DLS and LD and observed that particle sizes obtained by LD were consistently smaller than those *via* DLS. This was due to the fact that the latter determines the hydrodynamic radii which are usually larger than the solid radii determined by LD.

2.1.2.2 Surface charge

The surface charge of a dispersed system is best described by measuring the zeta (ζ) potential of the system. This parameter is a useful predictor of the storage stability of colloidal dispersions. A minimum ζ potential of ± 30 mV is considered the benchmark to obtain a physically stable system⁵¹. Surface charge measurements of SLN dispersions are routinely measured and reported along with particle size determinations.

2.1.2.3 Particle morphology and ultra-structure

Particle size results are often validated by TEM, which provides direct information on SLN morphology and ultra-structure. In a TEM, an electron beam is focused and directed through a sample by several magnetic lenses, with part of the beam adsorbed or scattered by the sample while the remaining is transmitted. The transmitted electron beam is magnified and then projected onto a screen to generate an image of the specimen. The fraction of electrons transmitted depends on sample density and thickness (typically < 100 nm)^{30, 128, 132}. Sample preparation techniques greatly influence the resolution of the observed images¹³³. Sample treatment by staining with contrast agents containing heavy metal compounds such as uranyl acetate, phosphotungstic acid (PTA) or osmium tetroxide helps to reveal the presence of smaller particles^{30, 128}.

Igartua *et al.*¹²² conducted TEM studies on magnetite-loaded SLNs by exposing them to a 4% aqueous osmium tetroxide solution for 3 hr. Osmium had an affinity for the double bonds in the lipid ethyl oleate as well as the unsaturated alkyl chains of the surfactant lecithin used in preparation of their SLNs. This allowed the visualization of both the lipid core as

well as the particle surface. Their SLNs consisted of fairly spherical particles with a mean diameter of 50 nm.

The high vacuum used in TEM¹³⁴ as well as sample preparation techniques^{128, 133} can lead to water loss and subsequent SLN structure alteration or collapse. In order to overcome these problems, alternative methods like freeze-fracture TEM and cryo-TEM have been employed. In both of these methods, the SLN dispersion is quench-frozen so that structures including the dispersion medium freeze instantly into an amorphous state^{30, 128, 134}. In freeze-fracture TEM, the frozen sample is subsequently fractured at a particular temperature and a replica of the fractured plane is created after shadowing with carbon/platinum whereas in cryo-TEM, the frozen hydrated samples are observed directly without any further preparation^{30, 128, 135}.

Bunjés *et al.* studied the ultra-structure of ubiquinone (Q10)-loaded SLN dispersions using cryo-TEM and freeze-fracture TEM and found a difference in the SLN structures with low and high drug loadings¹⁰⁴. A two-phase particle with a cap on one side of the particle was observed in dispersions loaded with higher amounts of Q10 while dispersions loaded with lower drug amounts did not exhibit such caps. The authors concluded that a fraction of the excess drug was expelled from the TAG matrix during crystallization forming a cap-like structure on one face of the crystalline platelets. In another study, cryo-TEM images showed that while monostearin, tristearin and tribehenin formed solid lipids, use of tricaprín, a liquid oil at room temperature, in combination with these solid lipids led to the formation of solid carriers with homogeneous liquid nano-compartments¹³⁶. Jores *et al.* observed a platelet structure for their SLNs characterized by cryo-TEM¹³¹.

TEM has also been used to discern the polymorphic form of SLNs. Bunjés *et al.* (2007) examined the α -form of solid tristearin SLNs using cryo-TEM and freeze fracture-TEM, and a spheroid shape with concentric rings was seen. In the β -form, plate-like, layered structures were observed¹³⁷. The structural investigation of SLNs containing high amounts of lecithin revealed the presence of ellipsoidal or disc-like platelets. No aggregates of lecithin and non-ionic emulsifier were observed, suggesting that the lipid nanoparticles consisted of two different layers: a crystalline TAG core covered either by monomolecular or multimolecular lecithin¹³⁰.

Scanning electron microscopy (SEM) has not been widely used for nanoparticle characterization, although it is routinely used for the characterization of microparticles¹³⁸⁻¹⁴⁰. SEM uses a focused electron beam to generate a variety of signals (*i.e.*, backscattered, or secondary electrons) at the surface of solid specimens. The signals derived from electron-sample interactions reveal information about the sample including morphology, chemical composition, and potentially crystalline structure. The yield of backscattered and/or secondary electrons emitted from the surface of the sample is plotted as a function of the position of the primary electron beam, yielding a 3-D image of the sample. Sample conductivity is increased by sputtering a thin film of gold on its surface after sample drying^{30, 132, 133}. SLNs observed *via* SEM have been shown to be smooth and spherical in shape¹⁴¹⁻¹⁴³.

Atomic force microscopy (AFM) is a newer technique to visualize SLN ultra-structure that avoids the high vacuum required in TEM, and the need for the sample to be conductive as required in SEM¹⁴⁴. A simple sample preparation procedure allows rapid visualization by providing a 3-D projection of the particles. Particle sizing by AFM has been shown to be in agreement with particle size measurements using DLS and LD¹⁴⁵⁻¹⁴⁷, although some reports point out that lower SLN heights observed with AFM could be due to the collapse of nanoparticles during sample preparation¹⁴⁸. SLNs loaded with prednisolone were characterized with AFM by zur Mühlen *et al.*¹⁴⁴ and the size observed was comparable to the results obtained from DLS. Dubes *et al.* characterized SLNs derived from amphiphilic cyclodextrins by SEM and AFM, with both techniques confirming the circular shape of the SLNs. Vacuum drying during sample preparation for SEM usage caused SLN shrinkage while the deposition method used for AFM led to the formation of small clusters of SLNs. The authors concluded that AFM allowed observation of SLNs in a hydrated state similar to that of SLN suspensions while SEM led to observation of SLNs in a less aggregated state¹⁴⁹.

2.1.2.4 Polymorphism in SLNs

Differential scanning calorimetry (DSC), X-ray diffraction (XRD), small-angle x-ray scattering/diffraction (SAXS/SAXD), and wide-angle x-ray scattering/diffraction (WAXS/WAXD) have been used in concert with particle size and electron microscopy techniques to confirm the polymorphic state and properties of SLNs in lipid dispersions.

DSC is the preferred technique for monitoring phase transitions in colloidal systems, as different lipid forms possess unique melting points and enthalpies⁴³. Bunjes *et al.* have extensively studied the crystallization behaviour and polymorphic transitions in lipids. The influence of emulsifiers on the crystallization of tripalmitin SLNs was investigated by DSC and synchrotron WAXS⁵⁰. No major differences were observed on the crystallization temperature, but remarkable differences were noticed after crystallization of the particles. Fast cooling of glycocholate-stabilized dispersions led to the formation of an uncommon type of α -crystals that displayed very weak reflections in the WAXS diffractogram, indicating poor order between TAG layers.

In another study, C₁₂-C₁₈ TAGs were investigated by DSC and XRD for their ability to form SLNs after melt homogenization. It was found that although longer-chained lipids could form SLNs, the lipids with C₁₂ chain did not form solid particles. C₁₄ nanoparticles were obtained in both solid and liquid forms, but showed a higher drug loading capacity in the liquid state. The polymorphic transitions were slowest for longer-chained TAGs. Combining C₁₈ with C₁₄/C₁₆ raised the crystallization temperature of the shorter-chain TAGs facilitating solidification and leading to a more complex structure and melting behaviour as observed in DSC and XRD scans⁵². In an extension to this study, saturated long-chain phospholipids and soybean phospholipids were studied for their effects on the crystallization of SLNs made from TAG lipids containing C₁₂-C₁₈ chains. Saturated phospholipids increased the crystallization temperature of the TAG sharply compared to soybean phospholipids and crystallization of phospholipid chains was induced prior to TAG crystallization, observed in DSC runs⁴⁹.

Schubert *et al.* conducted similar investigations on SLNs containing high amounts of lecithin as emulsifiers using isothermal heat-conduction microcalorimetry and WAXD. There was an accelerated polymorphic transition to the stable β -modification with increasing lecithin content and a corresponding decrease in the rate of the polymorphic transition. Lecithin concentration did not influence the melting and crystallization points, but a 10% decrease was observed in the crystallization index, indicating incomplete crystallization¹⁵⁰. Furthermore, a decrease in particle size resulted when the lecithin concentration was increased up to a critical concentration of 30 %, above which there was no further change in particle size. Nuclear magnetic resonance measurements were corroborated by SAXS data,

which suggested strong attachment of lecithin and emulsifiers to SLN surfaces, and no emulsifier aggregation in the aqueous phase¹³⁰.

Awad *et al.* investigated temperature-scanning ultrasonic velocity as an alternative technique to study complex thermal transformations in SLNs and compared the results with those obtained by DSC. Both techniques were sensitive to the complex melting behaviour of solidified tripalmitin SLNs, and excellent correspondence between thermal transitions was obtained, indicating that this technique could be a useful alternative to conventional DSC methods in studying lipid transitions¹⁵¹.

2.2 Solid-stabilized emulsions

As early as 1903, Professor W. Ramsden described the stabilization of emulsion drops and bubbles in foams using solid particles. Professor S. U. Pickering carried on these investigations and in 1907, reported the first recorded scientific study of particle-stabilized emulsions of water and paraffin with basic copper and iron sulfate particles precipitated *in situ*¹⁵². Since then, solid-stabilized emulsions have been referred to as ‘Pickering emulsions’, although Pickering credited their initial development to Ramsden¹⁵². Examples of so-called Pickering emulsions in foods include the stabilization of whipped cream by fat particles and of ice cream by ice crystals¹⁵³. In the case of whipped cream, solid fat globules cover the surface of hydrophobic bubbles and stabilize foam formation, while in the case of ice cream, conversion of a portion of the water to ice crystals upon freezing forms a solid phase together with fat globules. In this and other examples, effective stabilization with solid particles at fluid interfaces strongly depends on contact angle and wettability, as well as particle size, shape and concentration.

2.2.1 Contact angle and wettability

The contact angle θ provides an indication of how well a liquid will spread on a surface. The mechanical equilibrium of a sessile water drop resting atop a plane solid substrate immersed in oil depends on three surface tensions - γ_{ow} at the oil-water interface, γ_{sw} at the solid-water interface and γ_{so} at the solid-oil interface (Figure 2.1) and is described by Young’s equation^{154, 155}:

$$\gamma_{so} - \gamma_{sw} = \gamma_{ow} \cos \theta \quad (\text{Eqn. 2.1})$$

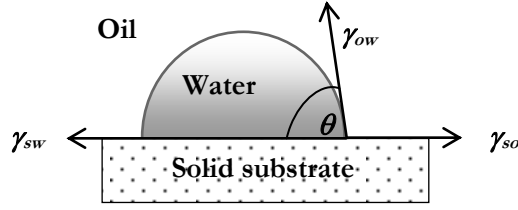


Figure 2.1: Schematic view of contact angle of sessile drop (Adapted from Ref # 154).

At $\theta = 0^\circ$, the liquid wets the solid completely and spreads freely over the surface at a rate depending on liquid viscosity and surface roughness¹⁵⁴. The tendency of a liquid to spread increases as θ decreases, thus contact angle serves as an important criterion for establishing wettability or spreadability of solid by a liquid^{53, 152, 154}.

The Gibbs free energy (kJ) of interactions between two liquids and a solid per unit area is given by¹⁵⁵:

$$\begin{aligned} \Delta G_{so} &= \gamma_{s,vac} - \gamma_{so} \\ \Delta G_{sw} &= \gamma_{s,vac} - \gamma_{sw} \end{aligned} \quad (\text{Eqn. 2.2})$$

where $\gamma_{s,vac}$ is the excess free energy of the solid substrate in a vacuum.

Substituting Eqn. 2.2 into Eqn. 2.1 yields the Gibbs-Young equation¹⁵⁵:

$$\cos \theta = \frac{\Delta G_{sw} - \Delta G_{so}}{\gamma_{ow}} \quad (\text{Eqn. 2.3})$$

Thus, the solid substrate interacts with the liquids to either enhance or oppose the spreading of a drop of liquid onto the surface. Extending the above concept to the situation of solid-stabilized emulsions, the three phase contact angle θ is the key parameter that dictates the attachment or detachment of particles from the oil-water interface. Particles with θ less than and greater than 90° (measured through the aqueous phase) are referred to as hydrophilic and hydrophobic particles, respectively⁵³. Figures 2.2 (A) and (B) depict the generally-accepted configuration showing the positioning of particles at planar and curved

oil-water interfaces, respectively. For hydrophilic particles, a larger fraction of the particle surface is in water than in oil, and accordingly particles will stabilize o/w emulsions. In the case of hydrophobic particles, particles reside more in oil than in water, and now will stabilize w/o emulsions. In the case where the particles are either too hydrophilic ($\theta \ll 90^\circ$) or too hydrophobic ($\theta \gg 90^\circ$), they preferentially remain dispersed in either the aqueous or oil phase, respectively, giving rise to very unstable emulsions¹.

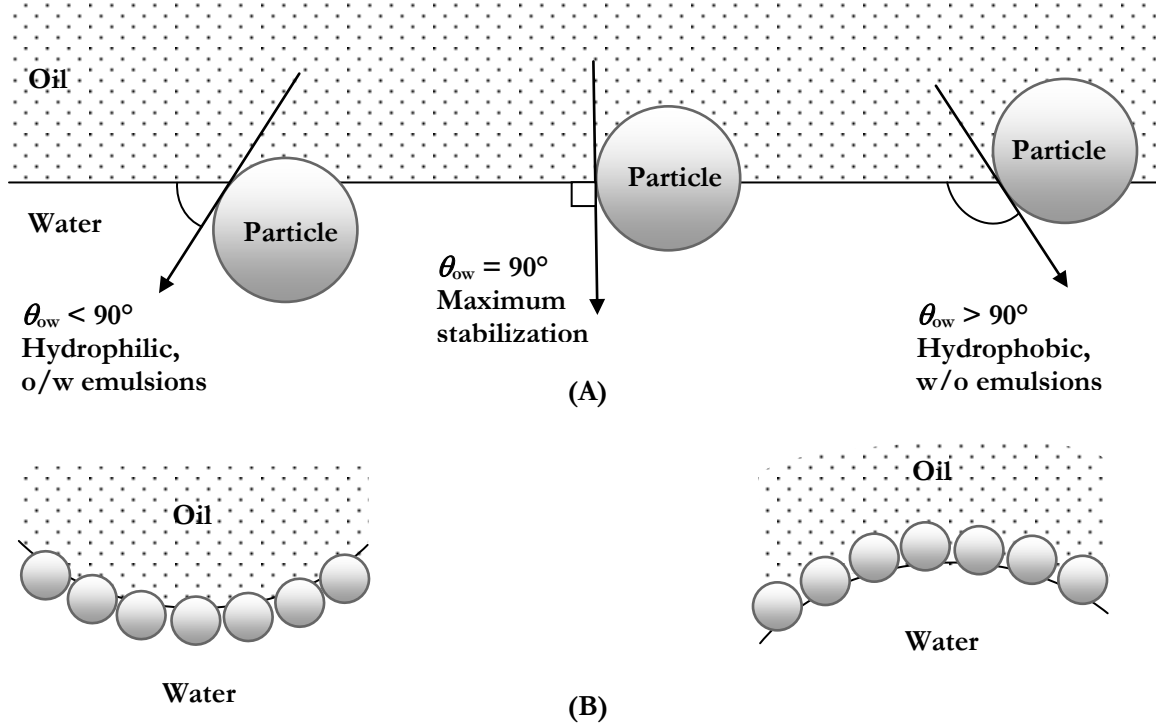


Figure 2.2: Preferential position of small particles at (A) planar and (B) curved oil-water interface (Adapted from Ref # 1).

The Gibbs free energy of particle detachment into oil phase ΔG_{do} is given by the equation¹⁵²:

$$\Delta G_{do} = \gamma_{ow} (A_c + A_{pw} \cos \theta) \quad (\text{Eqn. 2.4})$$

where γ_{ow} is the interfacial tension at the oil-water interface, A_c is the surface area of the oil-water interface occupied by the particle when it is attached at the fluid particle, and is described as $A_c = A_{ow(2)} - A_{ow(1)}$, where $A_{ow(2)}$ and $A_{ow(1)}$ are the surface areas of the oil-water interface before and after particle attachment, respectively, and A_{pw} is the surface area of the particle-water interface.

Similarly, the free energy of particle detachment into water ΔG_{dw} is given by the expression¹⁵²:

$$\Delta G_{dw} = \gamma_{ow} (A_c - A_{po} \cos \theta) \quad (\text{Eqn. 2.5})$$

where A_{po} is the surface area of the particle-oil interface.

The total surface area of the particle A_p is given by the equation¹⁵²:

$$A_p = A_{pw} + A_{po} \quad (\text{Eqn. 2.6})$$

Subtracting Eqn. 2.5 from Eqn. 2.4 and combining with Eqn. 2.6 and rearranging, a relationship between the two free energies of particle detachment is obtained as follows:

$$\Delta G_{do} = \Delta G_{dw} + \gamma_{ow} A_p \cos \theta \quad (\text{Eqn. 2.7})$$

As can be seen from the equation, the detachment of a hydrophilic particle ($\cos \theta > 0$) into the oil phase needs more energy than into water ($\Delta G_{do} > \Delta G_{dw}$), while for the detachment of a hydrophobic particle ($\cos \theta < 0$), the opposite is true ($\Delta G_{do} < \Delta G_{dw}$). At $\theta = 0$, both energies are equal to each other. The minimum free energy of particle detachment ΔG_d is written as¹⁵²:

$$\Delta G_d = \begin{cases} \Delta G_{dw} & \text{for } 0 \leq \theta \leq 90^\circ \\ \Delta G_{do} & \text{for } 90^\circ \leq \theta \leq 180^\circ \end{cases} \quad (\text{Eqn. 2.8})$$

The respective free energies of particle attachment ΔG_a to the fluid interface are given by the same equation as above, with the opposite sign ($\Delta G_a = -\Delta G_d$), hence particle attachment is a thermodynamically-favourable and spontaneous process¹⁵². Both the attachment and detachment free energies depend on particle shape, as explained below.

2.2.2 Particle size, shape and concentration

In the case of a spherical particle, the minimum free energy of particle detachment ΔG_d from the interface is given by the equation derived by Koretsky and Kruglyakov¹⁵²:

$$\Delta G_d = \pi r^2 \gamma_{ow} (1 - |\cos \theta|)^2 \quad (\text{Eqn. 2.9})$$

The resistance energy would be highest with a contact angle of 90°. Also, the minimum energy needed to detach a spherical particle from the oil-water interface rapidly decreases with particle size (r^2) and very small particles (<10 nm radius) are easily detachable and may not be effective stabilizers¹.

Particle shape is another critical factor that controls the adsorption-desorption of particles at the oil-water interface. In the case of non-spherical rod-shaped particles with a and b as cross-sectional long and short semi-axes, and keeping particle volume constant, ΔG_d is given by the following equations¹⁵²:

$$\Delta G_{dw,rod} = \gamma_{ow} \pi b^2 (1 - \cos \theta)^2 \left[1 + \frac{4(a/b - 1)(\sin \theta - \theta \cos \theta)}{\pi (1 - \cos \theta)^2} \right] \quad (\text{Eqn. 2.10})$$

$$\Delta G_{do,rod} = \Delta G_{dw,rod} + 4\pi\gamma_{ow} b^2 \cos \theta (a/b) \quad (\text{Eqn. 2.11})$$

$$\Delta G_{d,rod} = \begin{cases} \Delta G_{dw,rod} & \text{for } 0 \leq \theta \leq 90^\circ \\ \Delta G_{do,rod} & \text{for } 90^\circ \leq \theta \leq 180^\circ \end{cases} \quad (\text{Eqn. 2.12})$$

Thus, at a fixed particle volume, the free energy of detachment of a rod-shaped particle is dependent on the particle aspect ratio and θ , and is higher compared to that of a spherical particle of the same volume. Hence, rod-like particles with rounded ends oriented parallel to the fluid surface are held more strongly at an oil-water interface than spherical particles with same volume. In the case of a rounded disk-like particle with a and b as cross-sectional long and short semi-axes respectively, the free energy of detachment is given by¹⁵²:

$$\Delta G_{dw,disk} = \gamma_{ow} \pi b^2 (1 - \cos \theta)^2 \left[1 + \frac{(a/b - 1)^2}{1 - \cos \theta} + \frac{2(a/b - 1)(\sin \theta - \theta \cos \theta)}{(1 - \cos \theta)^2} \right] \quad (\text{Eqn. 2.13})$$

$$\Delta G_{do,disk} = \Delta G_{dw,disk} + 2\pi\gamma_{ow} b^2 \cos \theta [(a/b - 1)^2 + \pi(a/b - 1) + 2] \quad (\text{Eqn. 2.14})$$

$$\Delta G_{d,disk} = \begin{cases} \Delta G_{dw,disk} & \text{for } 0 \leq \theta \leq 90^\circ \\ \Delta G_{do,disk} & \text{for } 90^\circ \leq \theta \leq 180^\circ \end{cases} \quad (\text{Eqn. 2.15})$$

The free energy of detachment in disk-shaped particles is even higher than that for a rod shaped particle, thus $\Delta G_{d, disk} > \Delta G_{d, rod} > \Delta G_{d, sphere}$. Accordingly, the driving force of attachment of the particles decreases in the order disk > rod > sphere. Thus, disk- and rod-shaped particles with the same volume as spherical particles can have better attachment and lower detachment at fluid interfaces, suggesting formation of more stable emulsion systems with an appropriate change in particle shape.

Particle concentration at the oil-water interface influences droplet coverage which in turn depends on particle microstructure. Full droplet coverage is best with small particles, with better stabilization observed if particle size is substantially smaller than the droplet size, *i.e.*, submicron-sized particles have the ability to stabilize micron-sized emulsion droplets^{15,16}.

To conclude, it is expected that SLNs can function as solid particles that adsorb effectively to oil-water interfaces, thus stabilizing o/w or w/o emulsion systems. Their size, shape, structure and contact angle at the oil-water interface will determine effective droplet coverage and consequently adsorption-desorption kinetics from oil-water interfaces, thus dictating stability.

Chapter 3

EXPERIMENTAL TECHNIQUES

3.0 Introduction

The following chapter introduces the experimental methods used to formulate and characterize the SLNs and o/w emulsions herein studied. Specific measurements related to each experiment are addressed within the experimental sections of the subsequent chapters. Unless otherwise indicated, all experiments were performed in triplicate, as were their respective measurements.

3.1 SLN preparation

SLNs were generated by the melt-emulsification homogenization method. In this technique, the lipid is heated above its melting point and added to the aqueous phase maintained at the same temperature, under high-speed stirring. This pre-emulsion is passed through a valve homogenizer under high pressure. Figure 3.1 is the schematic representation of the working principle of high-pressure homogenization.

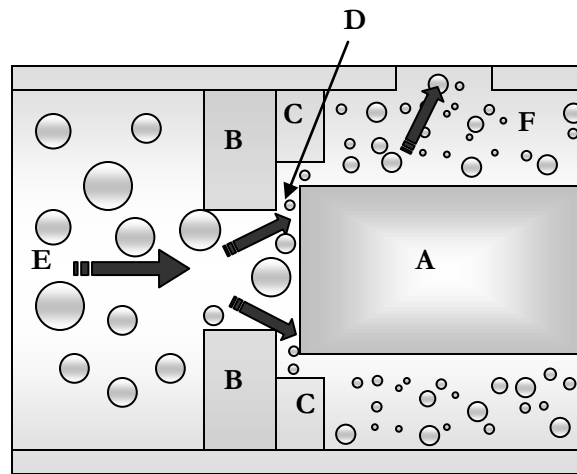


Figure 3.1: Schematic representation of the working principle of high-pressure homogenization technique used for producing SLNs (Adapted from Ref # 156).

The pre-emulsion E enters the adjustable clearance area between the valve A and valve seat B of the homogenizer under high pressure and low velocity. The volume of the clearance area is inversely proportional to the applied pressure. During homogenization, an

intense energy transition occurs within microseconds producing a turbulent 3-D mixing layer that disrupts the particles during discharge from gap D. The homogenized product F exits the impact ring C at low pressure and high velocity¹⁵⁶. The hot nanoemulsion is flash-cooled to solidify the dispersed lipid in the aqueous system and obtain SLNs.

Multiple passes through the homogenizer cause a further reduction in particle size and a corresponding increase in the interfacial area. Thus, after homogenization, the same amount of surfactant gets distributed over a larger interfacial area³⁸.

Glyceryl stearyl citrate (GSC) was selected as the lipid for preparation of SLNs. The GSC used in all experiments was Imwitor 372P (>98 % w/w purity, Sasol Chemicals, Mississauga, ON, Canada). Reverse osmosis water was used for all experiments. GSC was melted and added to hot water (85 °C) under high-speed stirring to form a pre-emulsion. The hot pre-emulsion was passed through a valve homogenizer (APV 1000, Albertslund, Denmark). The homogenization pressure was maintained at 14,500 psi for 5 cycles. The nanoemulsion was flash-cooled to obtain the GSC SLNs. All samples were transferred to Falcon tubes with screw caps and stored under refrigeration at ~4 °C.

3.2 Emulsion preparation

The GSC SLN dispersions maintained at ~4 °C were used as the aqueous phase for the preparation and stabilization of o/w emulsions. Canola oil purchased from a local grocery store was used as the oil phase (acid value < 0.2) and cooled to ~4 °C. Where needed, a drop of 0.1% (w/v) Nile Red in mineral oil solution was added to the oil phase to characterize instability such as creaming or coalescence with light microscopy. Based on preliminary studies of different ratios of oil: SLN, a ratio of 1:4 of canola oil: GSC SLNs was selected as the composition for o/w emulsion characterization.

Emulsions using GSC SLNs as the continuous phase were prepared using valve homogenization (APV 1000, Albertslund, Denmark) at ~4 °C. The homogenization pressure was maintained at 7000 psi for 5 cycles. The prepared o/w emulsions were transferred to Falcon tubes with screw caps and stored at ~4 °C.

3.3 Dynamic light scattering

Particle size determination is one of the prime characterization parameters for SLN dispersions. Measuring particle size confirms the existence of a desired colloidal size range after processing and during storage and helps establish dispersion stability^{30, 42, 43, 57, 134, 157-159}.

Dynamic light scattering (DLS) also referred as Photon Correlation Spectroscopy (PCS) or Quasi-Electric Light Scattering (QELS) is the standard method for rapid determination of nano-sized particle diameter and size distribution. Dynamic processes such as random Brownian motion of the particles in the dispersion medium result from collisions with each other and solvent molecules. Upon irradiation with a laser beam, these motions cause time-dependent variations in the intensity of scattered coherent light³⁰. Intensity fluctuations of the scattered beam are inversely proportional to the particle size. The velocity of the Brownian motion is measured as the translational diffusion coefficient and particle size is calculated from this coefficient by using the Stokes-Einstein equation¹⁵⁹:

$$d(H) = \frac{kT}{3\pi\eta D} \quad (\text{Eqn. 3.1})$$

where $d(H)$ is the effective or hydrodynamic diameter or ζ -average diameter (nm), k is Boltzmann's constant (1.38054×10^{-23} J/K), T is absolute temperature (K), η is viscosity (cP) and D (cm^2/sec) is the translational diffusion coefficient.

The light scattering effect due to the Brownian motion exhibited by particles over time is used to calculate particle size. Multimodal particle size distributions are calculated by applying complex advanced algorithms and the use of a numerical approach called the non-negatively constrained least squares algorithm integrated within the software¹⁶⁰. The main assumptions of this approach are that only positive intensity-weighted distributions are considered, and the ratio between any two successive diameters is kept constant and the method of least squares is followed at each interval. The corresponding conversion of the intensity-weighted distribution to a volume-weighted or number-weighted distribution was performed by calculating the scattering Mie factors using the integrated software.

The instrument used was the Brookhaven 90Plus/BI-MAS DLS Particle Size Analyzer (Brookhaven Instruments Corporation, Holtsville, NY, USA). The DLS

measurements provided the effective hydrodynamic diameter or \bar{z} -average diameter, as well as the polydispersity index (PI), an indicator of the width of the particle size distributions for the GSC SLNs.

3.4 Laser diffraction

DLS gives reliable results for narrow, unimodal distributions of particles in the nanometre range, and is also capable of sensing the presence of very small amounts of aggregation^{30, 43, 57}. Laser light diffraction (LD) or scattering is a better method to investigate larger particle sizes in polydispersed samples. This technique is based on the determination of the angular diffraction of light scattered from the dispersion when irradiated with a laser beam. The intensity of scattered light is inversely proportional to the particle radius, *i.e.*, smaller particles show more intense scattering at higher angles compared to larger ones. Particle size distributions are calculated based on comparisons of the angular information with a scattering model (the Mie theory), that applies to absorbing or non-absorbing spherical particles, essentially without any size restriction. Calculations using the Mie theory require an input of the illumination wavelength and polarization state, the refractive index (both real and imaginary) of both the particles and the medium, the diameter of the particles and the angle of observation relative to the incident illumination (also called the scattering angle)^{134, 161}.

The instrument used was the Malvern Mastersizer 2000S (Malvern Instruments, Worcestershire, UK). The instrument calculates a distribution based around volume terms independent of the number of particles in the sample¹⁶². It measures the volume or mass moment mean diameter $D [4,3]$ also called the De Brouckere mean diameter, and assuming that particle density is constant, generates a volume distribution data equal to the weight distribution directly from the initial measurements. The $D [3,2]$ is based on the surface area moment mean and is also called the Sauter mean diameter. The diameters calculated by LD indicate the percentage of particle volume below a certain size. For instance, $D (v, 0.5)$ means that 50% of the particle diameters lie below this value. The parameters generated by the instrument include the $D (v, 0.1)$, $D (v, 0.5)$ and $D (v, 0.9)$ *i.e.*, particle size values below which 10%, 50% and 90% of the sample distributions lie, respectively. The software also

calculated the span or width of the distribution, analogous to the polydispersity index in PCS measurements, defined as¹⁶³:

$$Span = \frac{D(0.9) - D(0.1)}{D(0.5)} \quad (\text{Eqn. 3.2})$$

LD was used to characterize SLN particle and emulsion droplet sizes.

3.5 Surface charge determination

Each particle suspended in a liquid medium is surrounded by an electrical double layer consisting of an inner region (or Stern layer) where counter-ions are strongly bound to the particle and an outer region (or diffuse layer) where they are associated less firmly (Figure 3.2).

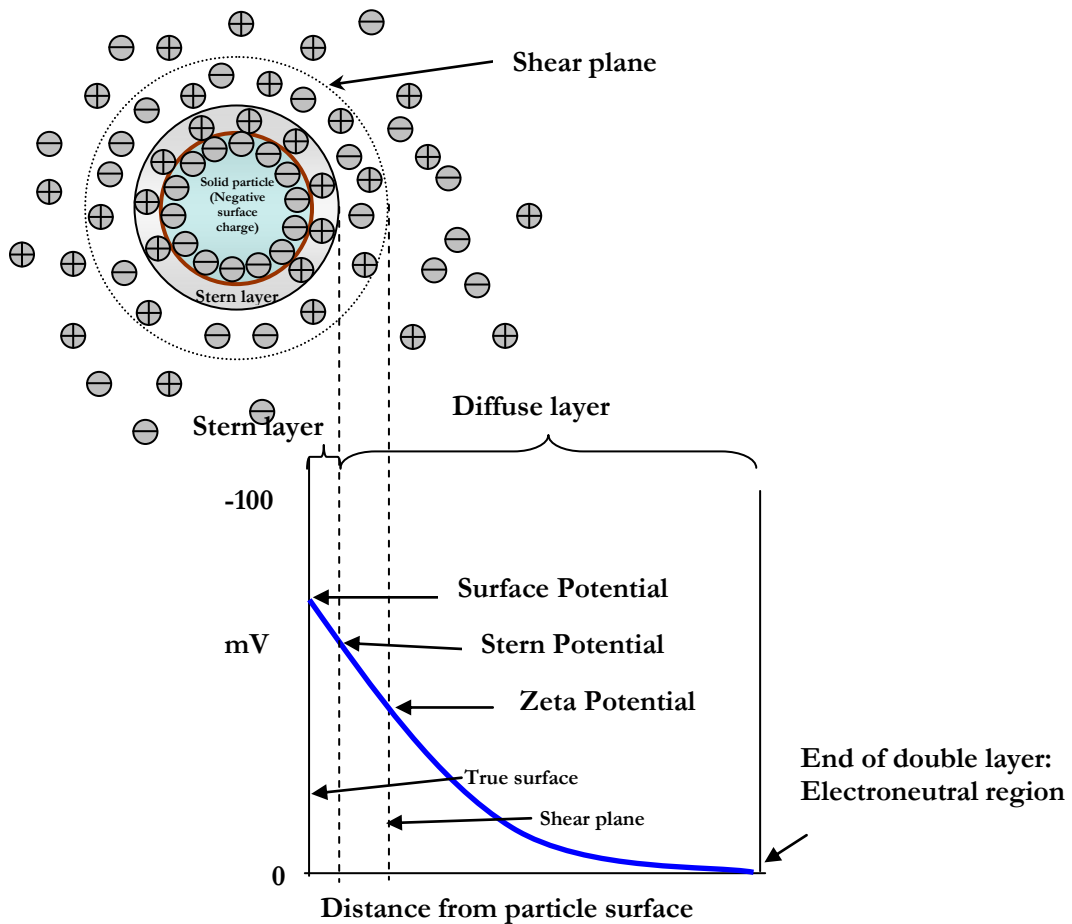


Figure 3.2: Schematic representation of various potential gradients on the surface of a particle (Adapted from Refs # 159, 164, 165).

The surface potential of particles in the Stern layer cannot be measured directly¹⁶⁴. Within the diffuse layer, an imaginary boundary exists where charges are assumed to be stable. The electric potential at the surface of this boundary (or surface of hydrodynamic shear) is called the zeta (ζ) or electrokinetic potential^{159, 165} and can be measured by laser Doppler electrophoresis. The instrument measures the electrophoretic mobility U_e of the sample and converts it into the ζ potential by Henry's equation¹⁵⁹:

$$U_e = \frac{2E\zeta f(\kappa a)}{3\eta} \quad (\text{Eqn. 3.3})$$

where U_e is the electrophoretic mobility, E is the dielectric constant of the dispersion medium, ζ is the zeta potential (mV), $f(\kappa a)$ is Henry's function (most often the Hückel and Smoluchowski approximations of 1 and 1.5, respectively, are used)¹⁶⁴ and η is the viscosity of the solvent medium.

The ζ potential is an important parameter to determine electrostatic colloidal dispersion stability. The instrument used to measure the ζ potential of the GSC SLNs and o/w emulsions was the Brookhaven 90Plus PALS Zeta Potential Analyzer (Brookhaven Instruments Corporation, Holtsville, NY, USA).

3.6 Contact angle measurements

The contact angle is a critical parameter in the design of an emulsion stabilized by solid particles and provides information on particle orientation at the oil-water interface. In order to measure contact angles, GSC was melted at ~ 75 °C with stirring and poured into aluminium weigh boats at room temperature. It was allowed to crystallize for ~ 24 hr. The crystallized lipid was used to determine the contact angle of water or oil droplets on the lipid surface.

For determination of contact angle of water droplet on the lipid surface, the solidified disks were cut into ~ 1 cm³ cubes and placed in transparent spectrophotometer cuvettes, with the smooth side facing upwards. Cuvettes were filled with canola oil and a small droplet (~ 1 mm o.d.) of water was injected from a needle onto the surface of the solid lipid. Images of the water droplet as it spread over the lipid surface were captured with a Teli

CCD camera with macro lens assembly and IDS Falcon/Eagle Framegrabber (DataPhysics Instrument GmbH, Filderstadt, Germany) at regular intervals up to 10 hr and a final reading at 24 hr. Image analysis was performed to determine the contact angle of the water droplet against the lipid surface using SCA 20 software Version 2.1.5 build 16 (DataPhysics Instrument GmbH, Filderstadt, Germany).

The contact angle of an oil droplet on the lipid surface was determined by modifying the method of Campbell¹⁶⁶. The solidified lipid was cut into 1 cm diameter circular disk and placed into a 2 ml capacity Eppendorf tube with the smooth surface of the lipid exposed. A tiny aperture was made into the centre of the solid lipid disk with a hypodermic needle. This assembly was placed upturned into a transparent spectrophotometer cuvette which was filled with water. A small droplet (~ 1 mm o.d.) of canola oil was injected from a microsyringe needle onto the surface of the solid lipid through the aperture. Images of the oil droplet were captured at regular intervals up to 12 hr as described before for water droplet contact angle measurements.

Additionally, interfacial tension measurements at the canola oil-water interface were performed using ASTM method D971¹⁶⁷, with the Du Nouy ring method (Fisher surface tensiometer Model 21, Fisher Scientific, Nepean, ON, Canada).

3.7 Thermal analysis

Thermal analysis broadly covers various techniques that measure chemical or physical changes that occur when a known quantity of a material is subjected to a controlled temperature program over time. Differential Scanning Calorimetry (DSC) is one such technique designed to measure the heat exchange (*e.g.* heat uptake during melting or heat release during crystallization) accompanying structural alterations of a material subjected to a controlled temperature program¹⁶⁸. An alteration in the enthalpy (ΔH) or entropy (ΔS) of a system causes phase transitions, accompanied by free energy changes. Enthalpy changes associated with endothermic (or consumption of energy as during melting of lipid, a solid-liquid transition) or exothermic (or release of energy as upon recrystallization, a liquid-solid transition) events are quantified¹³⁴.

In power-compensation DSC (used in our DSC system), the sample and empty reference pans are supplied with individual heaters, and any temperature difference between the two is detected and adjusted immediately to maintain almost identical temperatures in both¹⁶⁸. The increase (or decrease) in heating power is directly correlated with the heat flow into or out of the sample. The DSC curve is displayed as a function of time or temperature on the abscissa and the rate of energy absorption (heat flow) on the ordinate axis. Transitions accompanying changes in specific heat are demonstrated as peaks with areas proportional to the total enthalpy changes.

DSC measurements of the bulk GSC and GSC SLNs were performed using a Pyris-Diamond DSC (Perkin-Elmer, Markham, ON, Canada). Samples were weighed into DSC aluminum pans using a Mettler M3 microbalance (Mettler Toledo Canada, Mississauga, ON, Canada) and then sealed with a universal press B013-9005 (Perkin Elmer, Markham, ON, Canada). An empty sealed pan was used as reference. From the DSC curves obtained for the bulk lipid and GSC SLNs, onset temperature, peak temperature and enthalpy during both melting and crystallization transitions were determined by extrapolation.

3.8 Inverted light microscopy

In an inverted light microscope, the light source and condenser are located above the stage and point down while the objectives and turret are located below, pointing up towards the stage¹⁶⁹. Emulsion droplets were observed for particle size and shape using inverted light microscope. Images of emulsion samples were observed at a magnification of 1008X using a Zeiss Axiovert 200M inverted light microscope (Zeiss Canada, Toronto, ON, Canada). Images captured on CCD camera were analysed with Northern Eclipse software, Version 7.0. (Empix Imaging, Inc., Mississauga, ON, Canada).

3.9 Transmission Electron Microscopy

Transmission Electron Microscopy (TEM) is a powerful tool that provides direct visualization of the particle morphology and ultra-structure of colloidal system in terms of particle size, shape, and ultra-structure^{30, 134}. Contrast images of fairly good resolution can be obtained by staining with contrast agents such as uranyl acetate and PTA^{30, 128}. Although

TEM is expensive and requires expertise to distinguish between true images and artefacts, it is the most widely-used technique for the structural elucidation of SLN dispersions.

SLN samples were studied by TEM using the direct application method^{30, 128}. Diluted SLN samples were applied to a copper grid (400 mesh) and negatively-stained with 2 % (w/v) aqueous PTA. Excess fluid was drawn off the grid with a filter paper and the sample film was dried on the grid. Samples were examined and photographed on Hitachi H-7000 TEM (Hitachi, Tokyo, Japan) operating at an acceleration voltage of 75-80 kV. Digital images were captured using an AMT XR60 CCD camera.

3.10 Atomic Force Microscopy

The atomic force microscope, invented in 1986, is part of the family of scanning probe microscopes directed towards elucidating the nano-scale surface properties of materials²⁴. Currently, Atomic Force Microscopy (AFM) is the only available surface imaging technique that directly offers three-dimensional structural, mechanical, functional and topographical information of surfaces with dimensions in the nanometre to Angstrom range¹⁵⁷.

AFM produces images by sensing sample surface imperfections using an oscillating thin metallic cantilever, with a sharp tip on the end²⁴. The tip, usually fabricated from silicon or silicon nitride, has an extremely sharp pointed spike with dimensions as small as 1 nm at the apex. Its sharpness strongly influences the resolution of an AFM image. The tip is mounted on a cantilever that allows free up or down movement of the tip as it scans the surface of the sample. The cantilever position is controlled in three dimensions (x, y and z axes) by a set of oriented piezo-electric transducer crystals. The cantilever deflection is detected by means of an optical lever consisting of a laser in conjunction with a photodiode assembly in a closed loop feedback system. Based on the amount of cantilever deflection, the deflection angle of the laser beam and subsequently the laser intensity changes, which is captured by the position-sensitive photodiode detector. The signal thus obtained is processed into an image that is seen on a computer monitor and can be captured and digitally analyzed using appropriate software. The most common scanning mechanisms are the contact mode, where the tip directly touches the sample to be scanned, and tapping

mode where the cantilever vibrates near the surface of a sample at its resonant frequency (typically from 100 to 400 kHz)^{170, 171}.

SLN samples mounted on mica slides and placed to air dry in a fume hood were examined under ambient conditions using a Bioscope atomic force microscope with Nanoscope IIIa controller (Digital Instruments, Santa Barbara, CA, USA), operated in tapping mode. The AFM tips had a cantilever spring constant of 40 mNm⁻¹ and were oscillated at ~350 kHz with an end-point radius of 10 nm and a body angle of 30°.

3.11 Data analysis

Results are reported in all experiments as arithmetic mean \pm standard deviation. Statistical analysis was performed using either a two-tailed student's *t*-test (for single pair comparisons) or one-way ANOVA with single-step Tukey's multiple comparison *post-hoc* test. For data with control groups, one-way ANOVA with Dunnett's multiple comparison *post-hoc* test was applied. Differences were considered statistically significant at $p \leq 0.05$.

Chapter 4

SOLID LIPID NANOPARTICLES: PREPARATION, CHARACTERIZATION AND APPLICATION AS NOVEL PARTICLE STABILIZERS FOR OIL-IN-WATER EMULSIONS

4.0 Summary

Oil-in-water (o/w) emulsions solely stabilized by surface-active solid lipid nanoparticles (SLNs) were developed. The SLNs were generated in hot o/w nanoemulsions consisting of glyceryl stearyl citrate (GSC) in water quench-cooled from 80 °C to 4 °C to promote the liquid-solid phase transition of the dispersed GSC. The effective mean particle size of the resulting oblate spheroidal SLNs was ~180 nm by dynamic light scattering and the volume-weighted mean particle size was ~152 nm by laser diffraction, with a ζ potential of ~-49 mV. Effective mean particle size and ζ potential were stable for 24 wk. Oil-in-water emulsions (oily phase volume fraction: 0.2) containing 7.5% (w/w) GSC SLNs in the aqueous phase were kinetically stable for 12 wk, though they did not visually phase-separate over 24 wk. The generated o/w emulsions were found to have a volume-weighted mean droplet size of ~459 nm by laser diffraction and ζ potential of ~-43 mV. The emulsions were stable for up to 12 wk as observed for microscopic changes by inverted light microscopy. Emulsion microstructure evaluated with TEM revealed Pickering-type SLNs adsorbed as mono- and multilayers to the dispersed oil droplets. Overall, surface-active SLNs developed within nanoemulsions effectively kinetically stabilized oil-in-water emulsions.

Key words: Solid lipid nanoparticles, emulsifier, oil-in-water emulsions, Pickering-type stabilization

4.1 Introduction

Solid lipid nanoparticles (or SLNs) are colloidal particulate systems with a mean particle size below 500 nm and a narrow particle size distribution^{115, 129}. They typically consist of physiological lipids that are biodegradable, non-toxic, cost effective, possess high dispersibility in an aqueous medium and offer ease of preparation and scale-up possibilities¹⁷². The exclusion of organic solvents and the ability to encapsulate both lipophilic and hydrophilic compounds within the lipid makes them an ideal carrier system for functional foods⁸⁷.

It is well-known that the increase in specific surface area of a material is inversely proportional to its particle size. Thus, when a cubic solid particle of 1 cm is micronized to 1 μm and 10 nm, there is an increase in its specific surface area from 6 cm^2/g to 6 x 10⁴ cm^2/g and 6 x 10⁸ cm^2/g , respectively. This increase alters the particle's surface properties and directly influences its physicochemical, structural, thermal, electromagnetic, optical and mechanical properties compared to the bulk material. This effect also greatly influences the interactions of nanoparticles with their local environment¹⁷³.

An emulsifier is a component that aids in mixing two immiscible phases such as water and oil. Due to the presence of both hydrophilic and hydrophobic moieties, an emulsifier adsorbs at the oil-water interface and lowers the interfacial tension between them, thereby enhancing emulsification and increasing emulsion stability¹⁷⁴. If the continuous phase is oil with water as dispersed phase, the system is water-in-oil (w/o) emulsion and if *vice versa*, the system is an oil-in-water (o/w) emulsion. Food products such as butter, margarine and chocolate are w/o emulsions while mayonnaise, salad dressings and hollandaise sauce are o/w emulsions, all stabilized by the addition of emulsifiers.

Emulsifiers may be of natural origin (*e.g.*, lecithin) or may be chemical in nature such as polysorbates and sorbitan esters. Emulsifier concentration is one of the key factors that influence size of the emulsion droplets which in turn governs emulsion stability¹⁷⁵. At optimum emulsifier concentration, there is sufficient coverage of the dispersed droplets and coalescence is retarded. Inadequate emulsifier concentrations result in coalescence and an increased droplet size whereas an excess emulsifier concentration does not aid in further decreasing particle size or providing additional stability. Emulsifiers are added typically alone

or in combination in concentrations ranging from 0.5% w/w (in ice creams) to 10% w/w (in whipped creams) for stabilization¹⁷⁶.

Mono- and diglycerides are amongst the most widely used synthetic emulsifiers in the food industry and possess a significant lipophilic functionality¹⁷⁷. In order to impart hydrophilicity, their headgroup size and charge can be varied *via* reaction with polar functional groups such as acids^{177, 178}. If the hydroxyl group is esterified with citric acid, the hydrophilic, anionic emulsifier CITREM, or citric acid esters of mono- and diglycerides of edible fatty acids, is formed¹⁷⁴. Glyceryl stearyl citrate (GSC) is a plant-derived CITREM emulsifier with carboxylic head groups of citric acid¹⁷⁸ that has a melting range of 59-63 °C and an HLB value of 10-12¹⁷⁹⁻¹⁸¹. It is an approved food-grade lipid and used mainly as an anti-spattering agent in margarine and as emulsifier in meat sausages or beverage emulsions in concentrations in the range 0.3 % - 5 % (w/w)^{174, 182}.

The use of solid particles as stabilizers of o/w emulsions, also known as Pickering stabilization, is well-documented^{1, 14, 152}. Depending on the nature of particles and the emulsion system, there are at least two mechanisms by which colloidal particles can stabilize emulsions. Pickering stabilization results by adsorption of particles to the oil-water interface and their ability to form rigid structures that prevent droplet coalescence by steric hindrance¹⁸³. Smaller particles are likely to provide better coverage than larger particles^{15, 16}, although very small particles (<10 nm radius) would have a very low energy of interfacial attachment, rendering them ineffective as stabilizers^{1, 184}. By contrast, network stabilization arises when particle-particle interactions lead to the formation of a 3-D particle network in the continuous phase surrounding the droplets¹. A modification of the Bancroft rule which states that the phase in which the surfactant is dissolved usually becomes the continuous phase applies to these systems. Particles that are preferentially wetted by water mostly form o/w emulsion while particles that are preferentially wetted by oil form w/o emulsion^{8, 163}. The effectiveness of particles in stabilizing emulsions depends therefore, on their particle size, wettability, initial location and the level of interparticle interactions¹⁸³.

The objective of this research was to fabricate SLNs using melt-emulsification homogenization. As the functionality of solid particles is magnified several fold at the

nanoscale, it is postulated that SLNs of GSC in their sub-colloidal dimensions should effectively stabilize o/w emulsions *via* Pickering and perhaps crystal networking.

4.2 Materials and methods

4.2.1 Materials

Glyceryl stearyl citrate (GSC) (Imwitor 372P) was a gift from Sasol Germany GmbH and was procured through Multichem Inc. (Mississauga, ON, Canada). GSC is a partially neutralized ester of monoglycerides and diglycerides of plant-derived, saturated fatty acids obtained by esterification of citric acid and edible fatty acids with glycerol¹⁷⁸ (Figure 4.1).

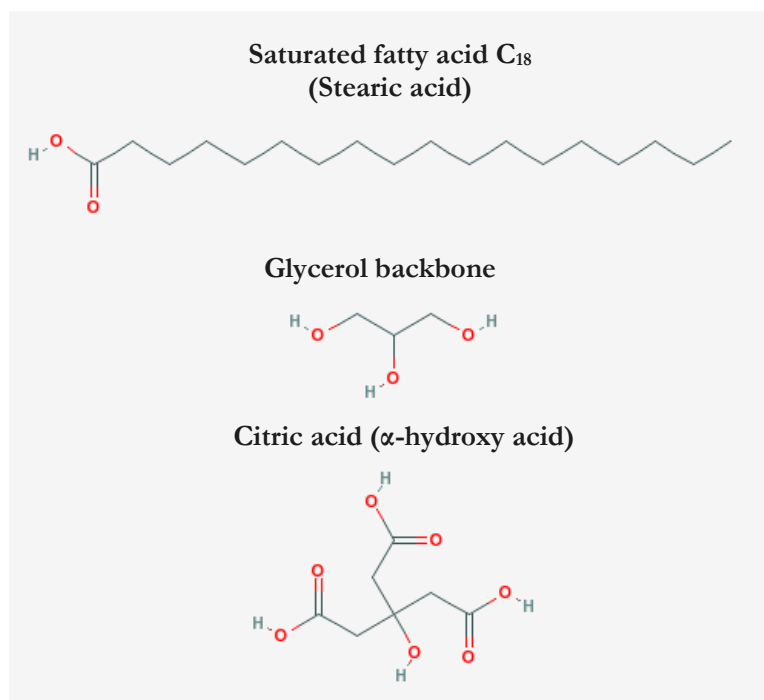


Figure 4.1: Chemical constituents of the lipid GSC (Adapted from Ref # 185).

GSC contains a saturated fatty acid chain (hydrophobic tail) with even carbon atoms (stearic acid, C₁₈). The 1-monoglyceride content in Imwitor 372P is 10-30 % (w/w)¹⁷⁹. The distribution of the principal components depends on the proportion of citric acid (typically 12-20 % by weight of the finished product), fatty acids, glycerol and the reaction conditions being used^{174, 178} for its preparation.

Canola oil was purchased at a local grocery store and used without further purification (acid value < 0.2). Nile Red was purchased from Sigma-Aldrich (Mississauga, ON, Canada). Deionized particulate-free water was used throughout the work.

4.2.2 Methods

4.2.2.1 Preparation of GSC SLNs

SLNs were prepared by the melt-emulsification homogenization technique (Figure 4.2).

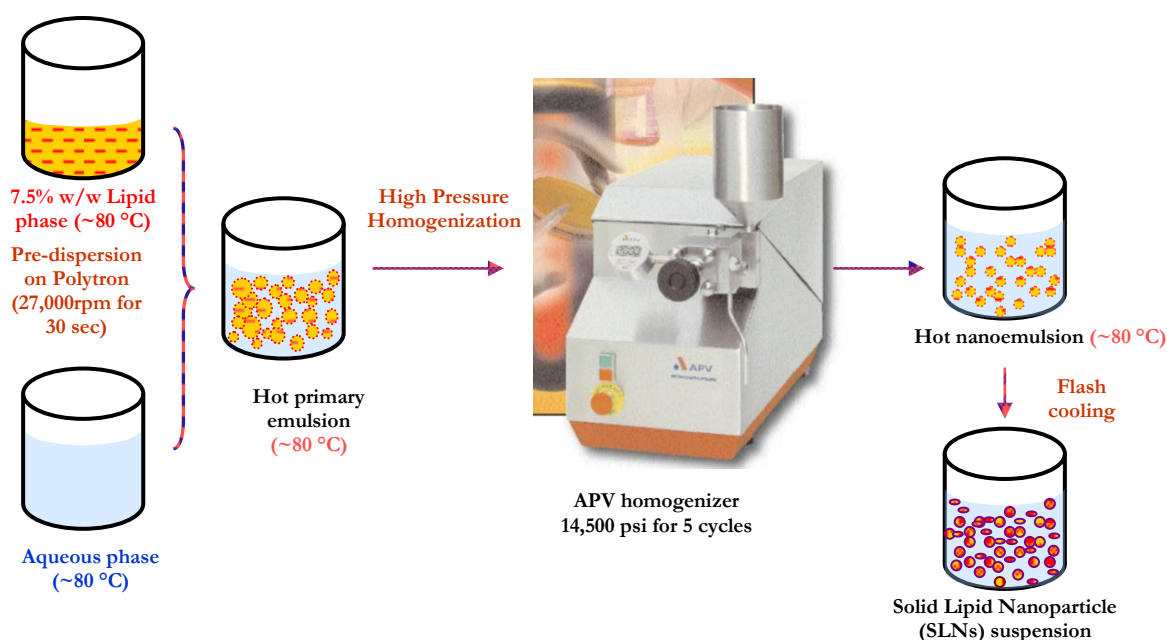


Figure 4.2: Schematic representation of melt-emulsification homogenization for preparation of solid lipid nanoparticles.

GSC (7.5% w/w) was heated to 70-80 °C. The aqueous phase was maintained at the same temperature and added to the molten lipid phase by vigorous dispersion with a Polytron PT-10/35 high speed homogenizer with PCU-2 control (Kinematica GmbH, Switzerland) at ~27,000 rpm for ~30 sec to produce the hot primary emulsion. The primary emulsion at ~75-80 °C was immediately passed through a heated high pressure homogenizer (APV 1000, Albertslund, Denmark) at a pressure of 14,500 psi for 5 cycles to obtain a lipid nanoemulsion. To prevent lipid solidification in the homogenizer, both the homogenizer and emulsion were heated at 85 °C by means of a copper coil connected to a circulating water

bath with thermostatic control (Lauda GmbH Eco100, Lauda-Konigshofen, Germany). During homogenization, the emulsion was stirred in the homogenizer hopper at 500 rpm with an IKA RW 14 Basic S1 overhead stirrer (IKA Works, Inc., Wilmington, DE, USA). The nanoemulsion was collected in a hot container and thereafter flash-cooled in a pre-conditioned ice bath to obtain the GSC SLNs. The samples were stored at refrigerator temperature (4 - 8 °C). SLNs were prepared in triplicate and analyzed immediately after their manufacturing.

4.2.2.2 Preparation of SLN decorated oil-in-water (o/w) emulsions

The o/w emulsions were made with an 80% (w/w) aqueous phase containing the SLNs and 20% (w/w) canola oil (containing 0.1 ml of 0.1% w/v Nile Red in mineral oil) as the oil phase (Figure 4.3).

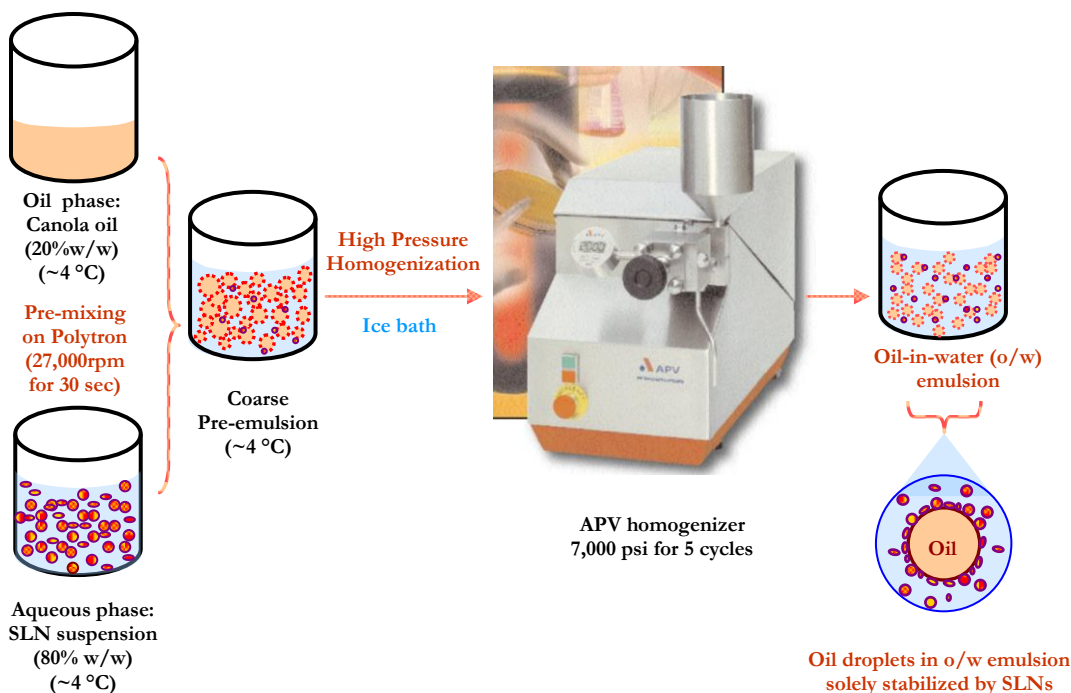


Figure 4.3: Schematic representation of the preparation of SLN decorated oil-in-water (o/w) emulsions.

Emulsions were processed at ~4 °C to avoid melting the SLNs. Canola oil cooled to ~4 °C was dispersed into the cold SLN suspension with a Polytron PT-10/35 high speed homogenizer with PCU-2 control (Kinematica GmbH, Switzerland) at ~27,000 rpm for ~

30 sec to produce the pre-emulsion, with the temperature maintained at ~ 4 °C by means of an ice bath. The pre-emulsion was immediately passed through a high pressure homogenizer (APV 1000, Albertslund, Denmark) at a pressure of 7,000 psi for 5 cycles to obtain o/w emulsion. During homogenization, the emulsion was stirred at 500 rpm with IKA RW 14 Basic S1 overhead stirrer (IKA Works, Inc., Wilmington, DE, USA). The o/w emulsion was collected in a cold container for re-circulation to avoid melting of SLNs. The resultant o/w emulsions were stored at refrigerated temperature (4 - 8 °C). The emulsions were prepared in triplicate and analyzed immediately after production.

4.3 Characterization of developed systems

4.3.1 Characterization of GSC SLNs

4.3.1.1 Particle size analysis

Particle size was determined by DLS at 25 °C using a Multi Angle Brookhaven 90 Plus Particle Size Analyzer (Brookhaven Instruments Corporation, Holtsville, NY, USA). The detection was performed at a scattering angle of 90° at a wavelength of 659.0 nm in a transparent 5 ml capacity 1 cm² polystyrene cell with lid, equilibrated at 25 °C. The viscosity of the dispersant water was 0.890 cP with a refractive index of 1.330. For multimodal analysis, the particle optical properties were defined as refractive index of 1.450 (real) and 0.000 (imaginary) and the refractive index of dispersant water was kept at 1.330. Prior to measurement, samples were diluted in filtered dust-free deionized water (0.22 µm PVDF Millex[®] GV Filter, Millipore Corporation, Bedford, MA, USA) to an appropriate scattering intensity. Measurements were carried out with a sample processing time of 120 sec for 10 min. The particle size (effective mean diameter or \bar{x} -average diameter) and particle size distribution (polydispersity index or PI) were calculated by the Brookhaven software by processing the time-dependent fluctuating scattered light intensity signal with a digital autocorrelator yielding the particle diffusion coefficient, from which the equivalent spherical particle size was calculated using the Stokes-Einstein equation (Eqn. 3.1). Values reported are the average of three successive 10 min runs with independent samples.

To determine the presence of particles with diameters larger than 1000 nm, if any, particle size distributions were also measured using LD. The measurements were performed with a Malvern Mastersizer 2000S with the Hydrosizer 2000S module (Malvern Instruments,

Worcestershire, UK). The sample was rapidly dispersed in deionized water at 1200 rpm until an obscuration rate of 5 - 10 % was obtained. The background and sample integration times were 12 sec and 10 sec, respectively. Optical properties were defined as refractive index 1.450 (particles), 1.330 (dispersant water) and absorption index 0.01, with the normal instrument calculation sensitivity and general purpose irregular particle shape selected. Each sample was measured in triplicate. Results were calculated with Malvern Version 5.54 software integrating the Mie theory of diffraction¹⁸⁶.

Particle size distribution and characteristic particle size values such as D [4, 3], D [3, 2], D (v, 0.1), D (v, 0.5) and D (v, 0.9) as well as span of the distribution were obtained (Eqn. 3.2). Values reported are the averages of three consecutive runs using different samples. Both techniques were used to measure particle size distribution immediately, and at 4, 12, 24 and 28 wk after SLN preparation.

4.3.1.2 Surface charge measurement

The zeta (ζ) potential of a colloidal sample can be used to establish its stability against inter-particle flocculation or collisions. It may be defined as the potential within the hydrodynamic shear or slipping plane of the electric double layer of a charged particle¹⁸⁷ (Fig. 3.2). The ζ potential of the SLNs was measured using a Brookhaven Zeta PALS Zeta Potential Analyzer (Brookhaven Instruments Corporation, Holtsville, NY, USA). The Zeta PALS determines zeta potential using the Phase Analysis Light Scattering technique, which is up to 1000 times more sensitive than traditional light scattering methods and avoids the application of large electrical fields that cause thermal problems seen in laser Doppler electrophoresis. Measurements were performed using an electrophoresis chamber with Kevlar-supported Pd electrodes in a transparent 1 cm polystyrene cell. SLN samples were diluted in filtered dust-free deionized water (0.22 μm PVDF Millex[®] GV Filter, Millipore Corporation, Bedford, MA, USA) and the ζ potential was determined at 25 °C. The instrument specified values for the dispersant (pure water) were a viscosity 0.890 cP, refractive index 1.330, dielectric constant 78.54 and sample pH of 4.5. The obtained electrophoretic mobility (U) values were used to estimate ζ potential by applying the Henry equation¹⁵⁹ (Eqn. 3.3) explained in section 3.5.

All measurements were performed in triplicate on three different samples and the average ζ potential calculated immediately, and at 4, 12, 24 and 28 wk after SLN preparation.

4.3.1.3 Contact angle measurements

In order to measure contact angle, molten GSC (~ 75 °C) was poured into 2-inch diameter aluminium weigh boats at room temperature and allowed to crystallize undisturbed for ~ 24 hr. The crystallized lipid was used to determine the contact angle of water or oil droplets on the lipid surface.

For determination of contact angle of water droplet on the lipid surface, solidified cubic disks of ~ 1 cm³ were cut from the crystallized lipid and placed in transparent square polystyrene cuvettes (1 cm² dimension), with the smooth side facing upwards. Cuvettes were then filled with canola oil. A small droplet (~ 1 mm o. d.) of water was injected from a needle onto the surface of the solid lipid using a 10 ml syringe and a programmable syringe pump (KD Scientific, Markham, Canada) operated at 0.1 ml/min. Images of the water droplet were captured with a Teli CCD camera with macro lens assembly and IDS Falcon/Eagle Framegrabber (DataPhysics Instrument GmbH, Filderstadt, Germany). The spreading of the water droplet over the lipid surface was monitored for 24 hr. Image analysis to determine the contact angle of the droplet against the solid surface at every time point was performed using SCA 20 version 2.1.5 build 16 (DataPhysics Instrument GmbH, Filderstadt, Germany).

The contact angle of an oil droplet on lipid surface was determined by modifying the method described by Campbell¹⁶⁶. The solidified lipid was cut into 1 cm diameter circular disk of ~ 5 mm thickness and placed into a 2 ml capacity Eppendorf tube with the smooth surface of the lipid exposed. A tiny aperture was made into the centre of the solid lipid disk with a 23 G1 hypodermic needle. This assembly was placed upturned into a transparent spectrophotometer cuvette filled with water. A small droplet (~ 1 mm o.d.) of canola oil was injected using a 100 μ l syringe needle onto the surface of the solid lipid through the aperture. Images of the oil droplet were captured at regular intervals up to 12 hr as described before for water droplet contact angle measurements.

The right and left contact angles of the water/oil droplet were determined and average of the two values taken as the contact angle for that time point. All readings were repeated in triplicate and average values were calculated. The spreading rates of water droplet over the lipid surface were calculated from the plot of contact angle (θ) *vs.* time (min), by linear regression analysis and r^2 values obtained for the various spreading rates. The equilibrium contact angle of oil droplets on the lipid surface was determined.

The water-canola oil interfacial tension was determined using ASTM method D971¹⁶⁷, with the DuNouy ring method (Fisher surface tensiometer Model 21, Fisher Scientific, Nepean, ON, Canada).

From the equilibrium contact angle θ and water-canola oil interfacial tension γ_{ow} values, water-solid lipid and oil-solid lipid interfacial tensions, γ_{sw} and γ_{so} , were calculated by using the formulae¹⁶:

$$\cos \theta = \frac{(0.015 \gamma_{sw} - 2.00)(\gamma_{ow} \gamma_{sw})^{1/2} + \gamma_{ow}}{\gamma_{ow} [0.015 (\gamma_{ow} \gamma_{sw})^{1/2} - 1]} \quad (\text{Eqn. 4.1})$$

$$\gamma_{ow} \cos \theta = \gamma_{sw} - \gamma_{so}, \text{ through oil phase} \quad (\text{Eqn. 4.2})$$

4.3.1.4 Differential Scanning Calorimetry (DSC)

The degree of crystallinity of the SLNs was determined on Pyris Diamond DSC (Perkin-Elmer, Markham, Canada). Thermal analysis was performed on both pure GSC and GSC SLNs. Approximately 3-6 mg samples were weighed into DSC aluminum pans using a Mettler M3 microbalance (Mettler Toledo Canada, Mississauga, ON, Canada) and then sealed with a universal press B013-9005 (Perkin Elmer, Markham, ON, Canada). The thermal behaviour was determined against an empty pan in the range of 1 °C to 85 °C at a heating rate of 5 °C/min. The cooling rate during flash cooling to obtain our SLNs was monitored and was ~150 - 200 °C/min. Due to instrumental limitations, a cooling rate of 50 °C/min was selected to observe the crystallization behaviour of the bulk and GSC SLNs. Freshly-prepared hot nanoemulsion samples were cooled against an empty reference pan from 85 °C to 1 °C at a cooling rate of 50 °C/min to simulate the flash cooling procedure

during SLN preparation. Additionally, GSC SLNs were subjected to 5 heating-cooling cycles to establish their stability during thermal analysis.

All measurements were performed in triplicate for bulk GSC as well as GSC SLN samples immediately after preparation.

4.3.1.5 Transmission Electron Microscopy (TEM)

Copper grids (400 mesh) (Gilder, Canemco & Marivac Inc., Québec, Canada) coated with Formvar/carbon were glow-discharged for 15 sec to impart hydrophilicity to the surface and facilitate spreading of the SLNs samples onto the grid. Diluted SLN samples (10 μ l of a 1 % w/w dispersion) were placed on the grid. After 2 min, excess sample was blotted off with filter paper and 6 μ l of aqueous 2 % (w/w) PTA were added. After 30 sec, excess solution was removed and the grid was dried at room temperature. Samples were viewed in a Hitachi H-7000 TEM (Hitachi, Tokyo, Japan) operating at an acceleration voltage of 75 - 80 kV. Digital images were captured using an AMT XR-60 CCD camera system and analyzed with AMT 5.34.2 Imaging Studio (Advanced Microscopy Techniques Corporation, Danvers, MA, USA). Samples were observed initially and at 4, 12 and 24 wk after SLN preparation.

4.3.1.6 Atomic Force Microscopy (AFM)

A Bioscope Atomic Force Microscope with Nanoscope IIIa controller (Digital Instruments, Santa Barbara, CA, USA) was used under ambient conditions. Tapping mode AFM was performed with silicon nitride tips attached to cantilevers with a spring constant of 40 mNm^{-1} ; the tip had an end-point radius of 10 nm and body angle of 30°. For sample preparation, the SLN dispersion was diluted (1 μ l ml^{-1}) in filtered dust-free deionized water (0.22 μm PVDF Millex[®] GV Filter, Millipore Corporation, Bedford, MA, USA). Pelco[®] Mica discs of 0.21 mm thickness and 9.9 mm diameter (Ted Pella, Inc., Redding, CA, USA) were used as substrates for SLN mounting. The discs were mounted onto glass slides with double-sided tape and the glass slide was immersed into the diluted SLN solution for 30 sec, after which the slides were removed and air dried. This gentle treatment was assumed to cause no or little alteration in the specimens resulting in a much easier interpretation of images. Samples were analyzed initially and at 24 wk after SLN preparation.

4.3.2 Characterization of SLN decorated oil-in-water emulsions

4.3.2.1 Particle size analysis

The droplet size distributions of o/w emulsions were analyzed by laser diffraction technique using a Malvern Mastersizer 2000S (Malvern Instruments, Worcestershire, UK) equipped with a Hydro S dispersion cell. A small sample of each emulsion was dispersed into a bath of deionized water within the dispersion cell. The diluted emulsion was circulated through the measuring cell at a speed of 1200 rpm until obscuration in the range of 5 - 10 % was obtained. The scattering recorded was deconvoluted to produce a particle size distribution using a conversion algorithm based on the Mie theory. Samples were analyzed immediately and at 4, 12 and 24 wk following emulsion preparation. Volume-weighted particle sizes and distributions were obtained from the analysis.

4.3.2.2 Surface charge measurement

As per the SLN analyses, the emulsion droplets' ζ potential was also measured using a Brookhaven ZetaPALS unit (Brookhaven Instruments Corporation, Holtsville, NY, USA). Emulsion samples were diluted in filtered dust-free deionized water (0.22 μm PVDF Millex[®] GV Filter, Millipore Corporation, Bedford, MA, USA) and the ζ potential determined at 25 °C. The instrument specified values for the dispersant (pure water) were a viscosity 0.890 cP, refractive index 1.330, dielectric constant 78.54 and sample pH of 4.6 with the Smoluchowski approximation applied. All measurements were done in triplicate on three different samples and the average ζ potential measured immediately and after 4, 12 and 24 wk following emulsion preparation.

4.3.2.3 Inverted light microscopy

The o/w emulsion droplets were examined using inverted light microscope. Images were observed with a 63X objective and a 10X lens using a 1.6 magnifier (giving a total magnification of 1008X) using a Zeiss Axiovert 200M inverted light microscope (Zeiss Canada, Toronto, ON, Canada). Images were captured with a CCD camera and analysed with Northern Eclipse software, Version 7.0 (Empix Imaging, Inc., Mississauga, ON, Canada). Microscopy was performed initially and at 24 wk after emulsion preparation.

4.3.2.4 Transmission Electron Microscopy (TEM)

As per the SLN characterization, the ultra-structure of smaller-sized SLN-stabilized emulsion droplets were also investigated by TEM using negative staining. Copper grids (400 mesh) (Gilder, Canemco & Marivac Inc., Québec, Canada) coated with Formvar/carbon were glow-discharged for 15 sec as per the SLN samples. A 10 μ l of the diluted sample of the emulsion (1 in 25) was placed on the grid. The procedure outlined earlier for GSC SLNs was followed for the o/w emulsions. Samples were characterized initially and at 4, 12, 15 and 24 wk after emulsion preparation.

4.4 Results

4.4.1 Characterization of GSC SLNs

4.4.1.1 Particle size analysis

Particle sizing is an indicator of SLN (in)stability as in most cases, an increase in particle size takes place before macroscopic (visual) changes occur⁵. A well-formulated submicron colloidal system will typically display a narrow particle size distribution. Tables 4.1 and 4.2 show the mean diameter values and reproducibility of the SLN production process by DLS and LD, respectively. Figures 4.4 and 4.5 show the particle size distributions via DLS and LD measurements, respectively. As seen from the results, excellent reproducibility is demonstrated.

Table 4.1: DLS measurements showing unimodal and bimodal particle size distributions of 3 batches of GSC SLNs. All data are means \pm standard deviations ($\bar{X} \pm s$) for $n = 3$ replicates per batch. No significant differences were observed between batches ($p > 0.05$).

Parameters	Batch 1	Batch 2	Batch 3
Unimodal distribution			
Effective diameter(nm)	175.5 \pm 4.1	171.7 \pm 8.1	179.6 \pm 5.7
Polydispersity index	0.19 \pm 0.02	0.20 \pm 0.01	0.14 \pm 0.00
Bimodal distribution			
Mean diameter (nm)	201.2 \pm 7.0	193.6 \pm 6.8	205.3 \pm 1.7

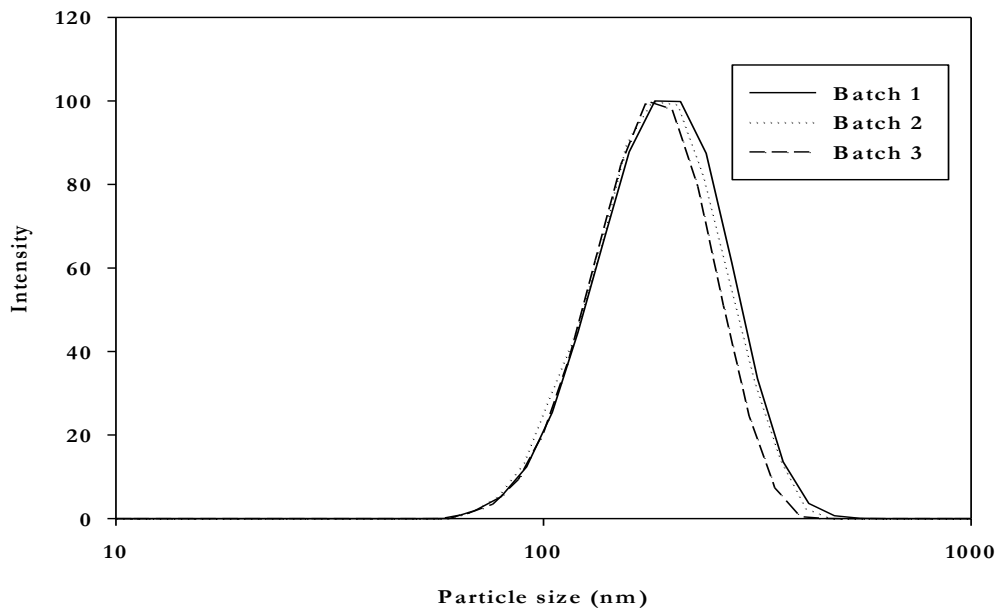


Figure 4.4: DLS particle size distributions (unimodal) of 3 batches of GSC SLNs.

Table 4.2: LD measurements showing particle size distribution data of 3 batches of GSC SLNs. All data are means \pm standard deviations ($\bar{X} \pm s$) for $n = 3$ replicates per batch. No significant differences were observed between batches ($p > 0.05$).

Parameters	Batch 1	Batch 2	Batch 3
$D [4, 3]$ (nm)	157.7 ± 0.6	160.3 ± 0.6	157.2 ± 1.5
$D [3, 2]$ (nm)	143.0 ± 1.0	143.3 ± 0.6	145.0 ± 2.5
$D (v, 0.1)$ (nm)	100.0 ± 1.7	97.7 ± 0.6	95.4 ± 3.2
$D (v, 0.5)$ (nm)	152.0 ± 0.0	153.7 ± 1.2	151.3 ± 1.7
$D (v, 0.9)$ (nm)	221.7 ± 3.2	227.7 ± 2.3	226.3 ± 2.1
Span	798.0 ± 32.9	868.0 ± 13.0	849.0 ± 45.5

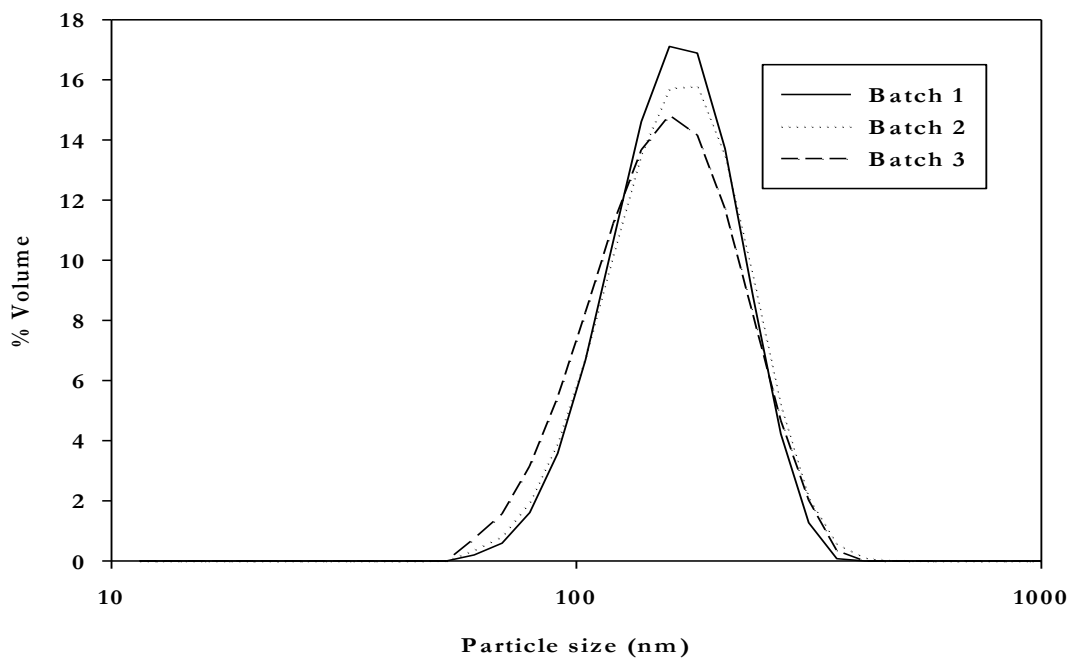


Figure 4.5: LD particle size distributions of 3 batches of GSC SLNs.

There were no within-replicate differences in average particle size observed ($p > 0.05$). The LD mass median diameter $D(v, 0.5)$ was always smaller than with DLS, as the latter determines hydrodynamic radii, which are usually larger than the solid sphere radii determined *via* LD^{131, 188, 189}. The intensity-based polydispersity occurred as a result of a small population of larger-sized SLNs that skewed the distribution towards higher values. LD measurements indicated that $> 90\%$ of particles were < 230 nm in all batches.

Investigations were made as to whether the process of flash cooling was required to generate the SLNs. A trial batch was cooled to room temperature without flash cooling and particle size analysis by DLS and LD performed. DLS measurements revealed an effective diameter of 173.6 ± 0.5 nm, with a polydispersity index of 0.30 ± 0.1 and bimodal mean particle size of 250.4 ± 7.7 nm. Thus, although no significant difference ($p > 0.05$) was observed in effective diameter, a significantly higher ($p < 0.05$) polydispersity index and bimodal mean particle size values than those for flash-cooled SLNs were observed for room temperature-cooled SLNs. Micron-sized particles were detected with LD measurements. The $D[3, 2]$, $D(v, 0.1)$, and $D(v, 0.5)$ values were 149.6 ± 4.4 nm, 81.7 ± 0.6 nm and 156.3 ± 3.2 nm, respectively. These values were not significantly different ($p > 0.05$) from the values

for flash-cooled SLNs. However, $D [4, 3]$ and $D (v, 0.9)$ values were $14.7 \pm 6.9 \mu\text{m}$ and $54.0 \pm 48.6 \mu\text{m}$, respectively, ($p < 0.05$), suggesting that flash cooling was an important step in the generation of the SLNs.

The SLN colloidal suspensions appeared milky white and homogeneous with no sedimentation over 28 wk. While the DLS unimodal results (Table 4.3 and Figure 4.6) suggested no significant changes in effective diameter up to 28 wk, multimodal analysis revealed a truer picture of the particle size distribution.

Table 4.3: DLS measurements showing unimodal and bimodal particle size distributions of refrigerated samples of GSC SLNs at various time points. All data are means \pm standard deviations ($\bar{X} \pm s$) for $n = 3$ replicates per time point.

Parameters	Initial	4 wk	12 wk	24 wk	28 wk
Unimodal distribution					
Effective diameter(nm)	175.5 ± 4.1	182.5 ± 0.9	180.1 ± 7.1	173.8 ± 2.2	178.3 ± 2.7
Polydispersity index	0.19 ± 0.02	0.14 ± 0.01	0.18 ± 0.04	$0.22 \pm 0.01^*$	$0.22 \pm 0.01^*$
Bimodal distribution					
Mean diameter (nm)	201.2 ± 7.0	200.7 ± 3.5	207.2 ± 0.9	208.4 ± 2.6	$213.8 \pm 3.7^*$

* Statistically significant at $p < 0.05$

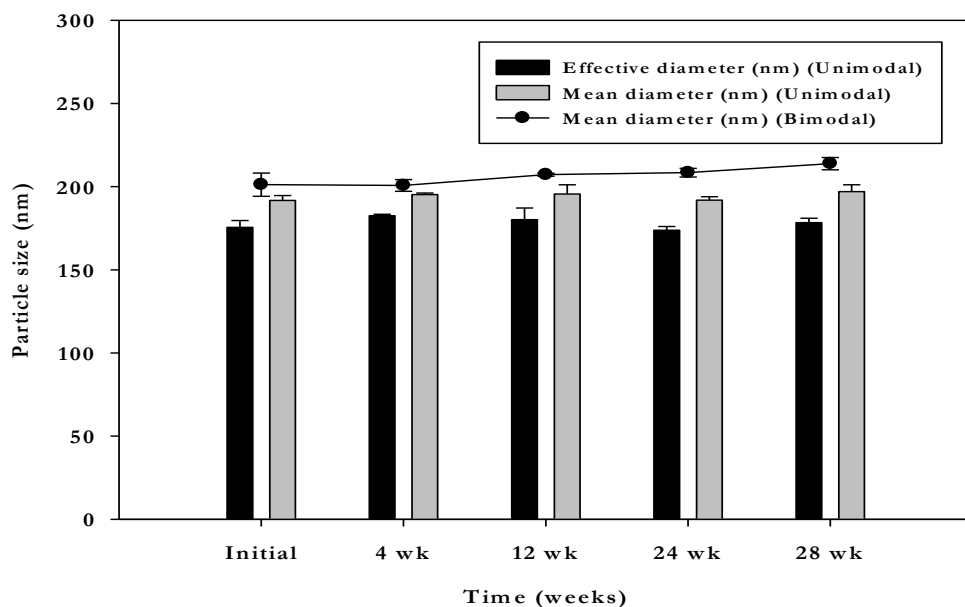


Figure 4.6: DLS measurements showing particle size distributions (unimodal and bimodal) of refrigerated samples of GSC SLNs at various time points.

Significant differences were observed in both the lower and upper ranges (data not shown) of the bimodal distribution curves from 12 wk onwards ($p < 0.05$). Two factors likely explained these results. In a polydisperse sample, Ostwald ripening dictates that smaller particles will have a higher solubility than larger particles and will tend to dissolve whereas larger droplets will tend to grow³⁵. It was observed that smaller particles disappeared with time, resulting in an increase in the lower and upper particle range values in the multimodal data. The end result was the formation of larger particles, based on a significant increase in the polydispersity index of the distribution, observed at 24 wk. Secondly, there may have been SLN-SLN accretion, resulting in larger particles. The bimodal distribution pointed towards changes in mean diameter only at 28 wk. Thus, a critical evaluation of both unimodal and multimodal data, including lower and upper particle range limits, obtained by DLS measurement was necessary to correctly assess the stability of the SLNs.

By contrast, the LD results (Table 4.4 and Figure 4.7) showed a statistically significant increase ($p < 0.05$) in the span of the distribution from 12 wk onwards, suggesting SLN aggregation and/or particle growth.

Table 4.4: LD measurements showing particle size distribution data of refrigerated samples of GSC SLNs at various time points. All data are means \pm standard deviations ($\bar{X} \pm s$) for $n = 3$ replicates per time point.

Parameters	Initial	4 wk	12 wk	24 wk	28 wk
$D [4, 3]$ (nm)	157.7 \pm 0.6	163.7 \pm 1.2	158.7 \pm 2.5	164.3 \pm 1.5	3958.0 \pm 178.9
$D [3, 2]$ (nm)	143.0 \pm 1.0	145.7 \pm 2.1	137.3 \pm 4.5	140.7 \pm 3.1	149.0 \pm 1.0
$D (v, 0.1)$ (nm)	100.0 \pm 1.7	98.7 \pm 3.1	88.3 \pm 5.5	90.3 \pm 3.5	97.0 \pm 1.1
$D (v, 0.5)$ (nm)	152.0 \pm 0.9	157.3 \pm 1.5	150.7 \pm 3.5	155.0 \pm 2.0	151.0 \pm 0.9
$D (v, 0.9)$ (nm)	221.7 \pm 3.2	228.3 \pm 2.0	241.7 \pm 3.2*	251.7 \pm 1.5*	254.0 \pm 1.7*
Span	798.0 \pm 32.9	884.3 \pm 36.7	1019.0 \pm 82.7*	1043.0 \pm 46.1*	1039.0 \pm 12.3

* Statistically significant at $p < 0.05$

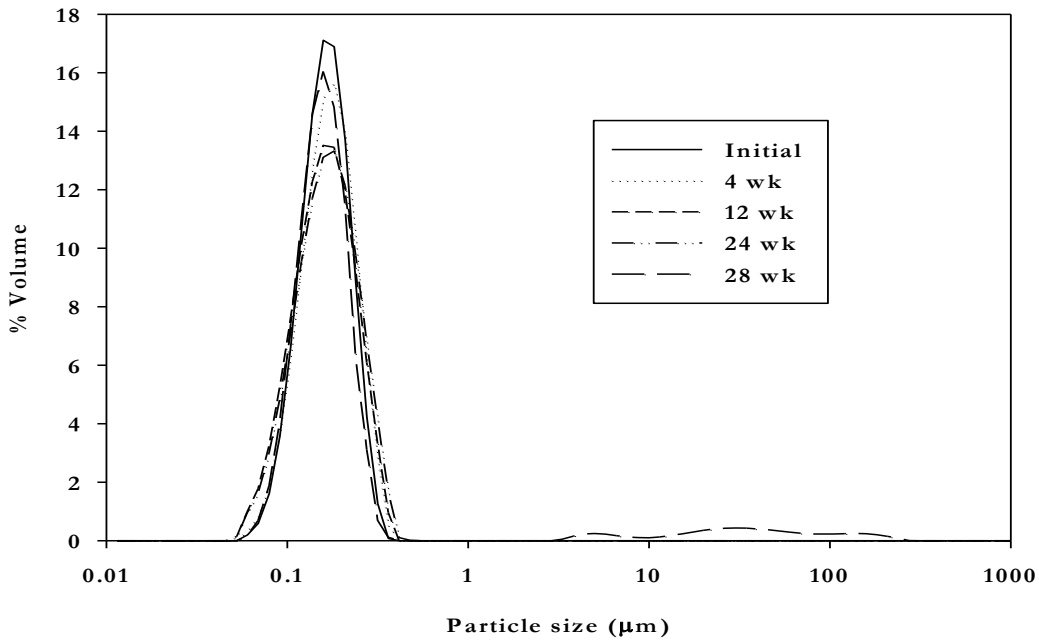


Figure 4.7: LD measurements showing particle size distribution of refrigerated samples of GSC SLNs at various time points

The $D [4, 3]$ and $D [3, 2]$ values were significantly higher ($p < 0.05$) at 28 wk than at 0, 4, 12 and 24 wk, which was due to the presence of particles in the 2-200 μm range that appeared with time. The $D (v, 0.9)$ diameter is sensitive to the presence of even a few large particles, with higher values indicating the presence of micron-sized particles¹⁹⁰. The $D (v,$

0.9) of the SLN suspensions up to 4 wk was below 230 nm, indicating the absence of micrometre-sized particles. However, $D(v, 0.9)$ values significantly increased ($p < 0.05$) from 12 wk onwards, suggesting an increase in particle size. LD does not differentiate between agglomerated and larger individual particles¹⁷³. Unimodal data, obtained by DLS measurements, though useful, does not accurately reflect the true particle size distribution. Rather, multimodal data provides a truer idea of the distribution, leading to a more conclusive view of the stability of SLN dispersions.

4.4.1.2 Surface charge measurement

The ζ potential is a measure of the global surface charge on a colloid. As a result, it can help predict the physical stability of colloidal dispersions. Large negative or positive values indicate a higher stability as the particles are more highly-charged, and repel one another more intensely preventing aggregation¹⁸⁷. ζ potential values of ± 30 mV are generally considered the dividing line between stable and unstable emulsions^{14, 51, 187}, with optimal electrostatic repulsion at $> \pm 60$ mV. Values between 5-15 mV suggest systems that are undergoing limited flocculation whereas values of 3-5 mV indicate unstable systems that rapidly flocculate⁵. For systems that contain a steric stabilizer, the cumulative electrostatic and steric stabilization effects provide accrued stability at lower values⁵¹.

An initial net negative ζ potential value of ca. -49 mV was observed at pH 4.5 at 25 °C, and stayed constant for 28 wk ($p > 0.05$) (Table 4.5). As GSC is esterified with citric acid¹⁷⁹, GSC-based SLNs have surface -OH and -COOH groups that dissociate in an aqueous environment¹⁹¹, leading to a net negative charge.

Table 4.5: Zeta potential of refrigerated samples of GSC SLNs at various time points. All data are means \pm standard deviations ($\bar{X} \pm s$) for $n = 3$ replicates per time point. No significant differences were observed between batches ($p > 0.05$).

Parameter	Initial	4 wk	12 wk	24 wk	28 wk
ζ (mV)	-48.8 ± 1.9	-47.7 ± 2.0	-46.3 ± 4.1	-49.0 ± 1.3	-46.7 ± 3.7

Although the particle size data indicated the presence of aggregates and an increase in particle size suggesting particle growth, ζ potential values did not reflect this change. Fine

particles repeatedly collide with each other due to their thermal motion and van der Waals interactions. As per the DLVO theory, highly-charged or polar surfaces will in theory demonstrate strong long-range repulsion, as the energy barrier is too high for the particles to overcome¹⁹². Nevertheless, perikinetic collisions between SLNs and/or Ostwald ripening led to an increase in particle size. As noted, the ζ potential for the SLN dispersions was smaller than the -60 mV threshold required for full electrostatic stabilization^{5, 193}

4.4.1.3 Contact angle measurements

In order to understand how the water, GSC and oil interacted, the θ evolution of a water droplet in canola oil on solid GSC was monitored for 24 hr (Figure 4.8). Following deposition, there was a significant change in θ .

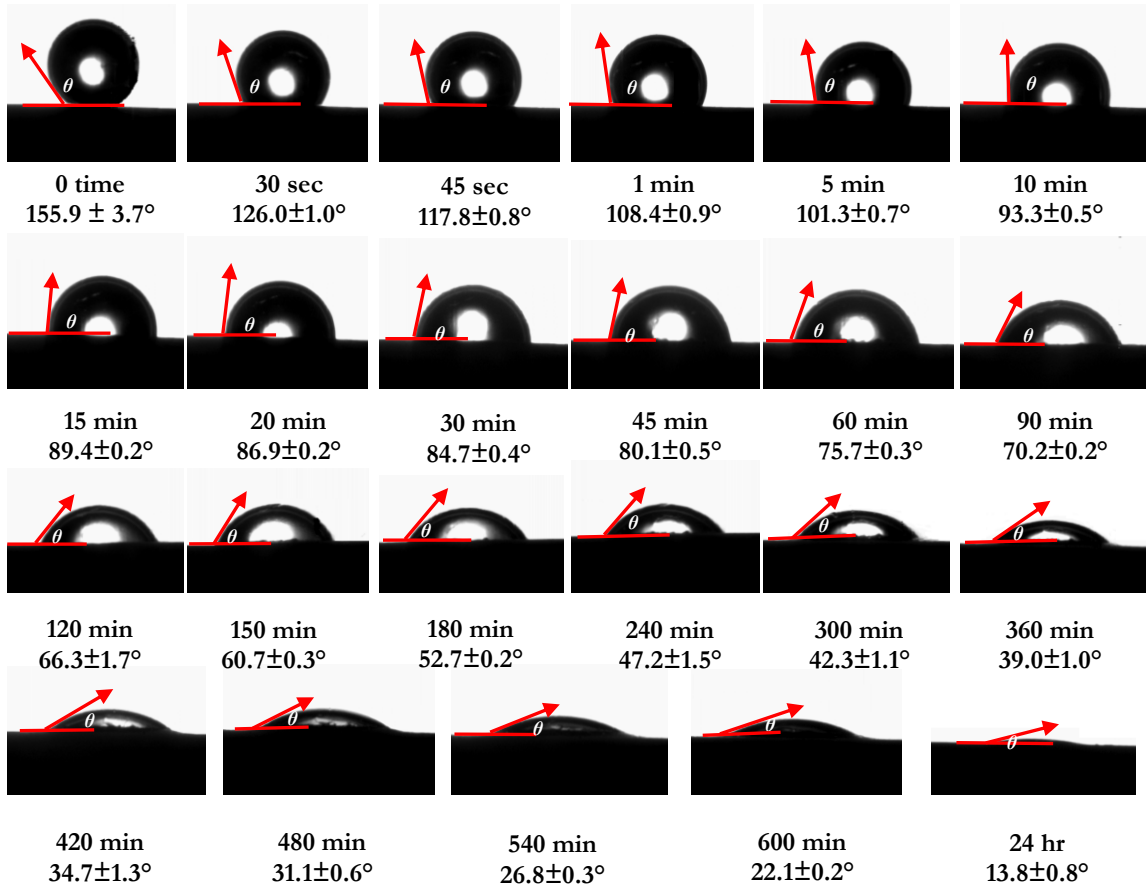


Figure 4.8: Contact angle measurements of water droplet in canola oil spreading on a solid GSC surface at various time points. All data are means ± standard deviations ($\bar{X} \pm s$) for $n = 3$ replicates per time point.

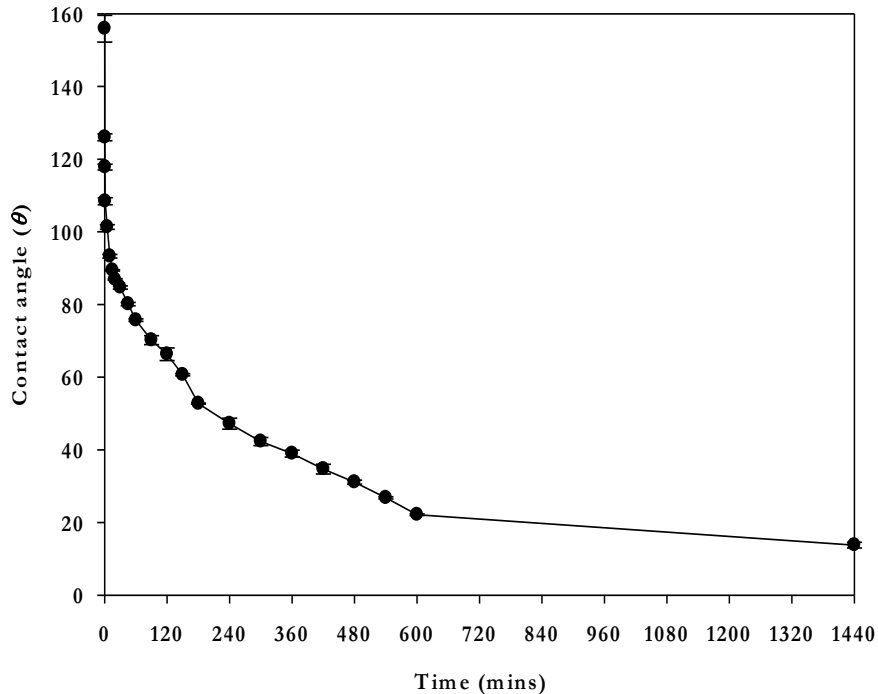


Figure 4.9: Average contact angle (θ) of a water drop spreading over the GSC surface vs time (min).

Initially, θ decreased rapidly, only to slow with time. The spreading rate was calculated from the curve (Figure 4.9) and distinct regions were identified:

- An initial region of instantaneous spreading: Within 1 min of placing the drop on the lipid surface, the spreading rate was $47.6^\circ/\text{min}$ ($r^2 = 0.99$).
- An intermediate region of gradual spreading stratified into: A rapid spreading phase within the first 15 min - the spreading rate was $1.37^\circ/\text{min}$ ($r^2 = 0.99$), followed by a gradual spreading phase up to 3 hr - the spreading rate was $0.21^\circ/\text{min}$ ($r^2 = 0.99$).
- A final region of slow spreading (up to 10 hr), with a spreading rate of $0.07^\circ/\text{min}$ ($r^2 = 1$). After 10 hr, the spreading rate further decreased to $0.01^\circ/\text{min}$ ($r^2 = 1$) up to 24 hr.

Thus, an equilibrium θ could not be obtained from the water droplet θ measurements. In order to understand how the oil drop would spread on the surface of GSC, the θ evolution of an oil droplet in water on solid GSC was monitored for 12 hr (Figure 4.10).

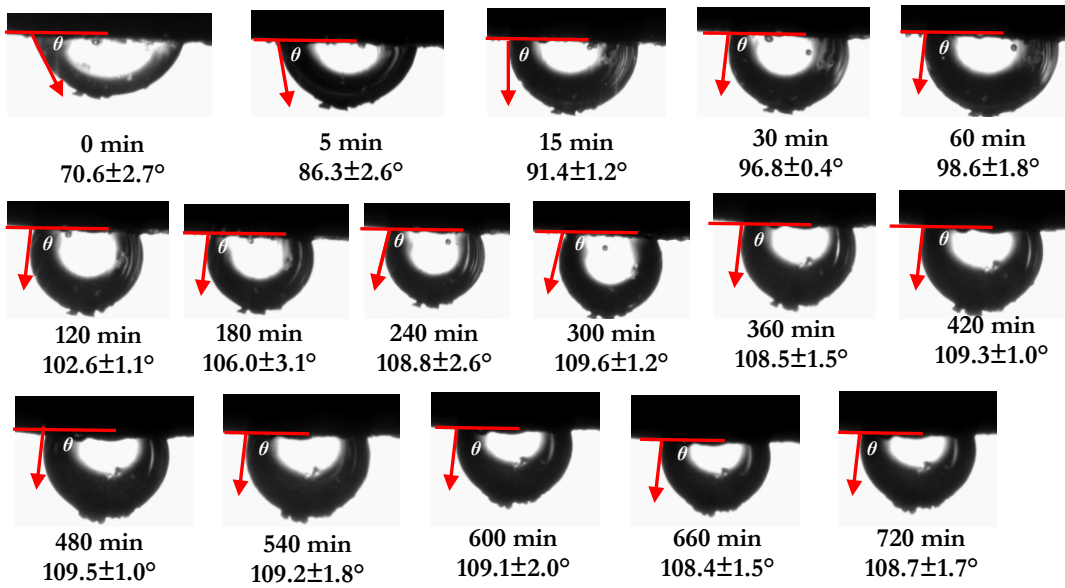


Figure 4.10: Contact angle measurements of oil droplet in water on a solid GSC surface at various time points. All data are means \pm standard deviations ($\bar{X} \pm s$) for $n = 3$ replicates per time point.

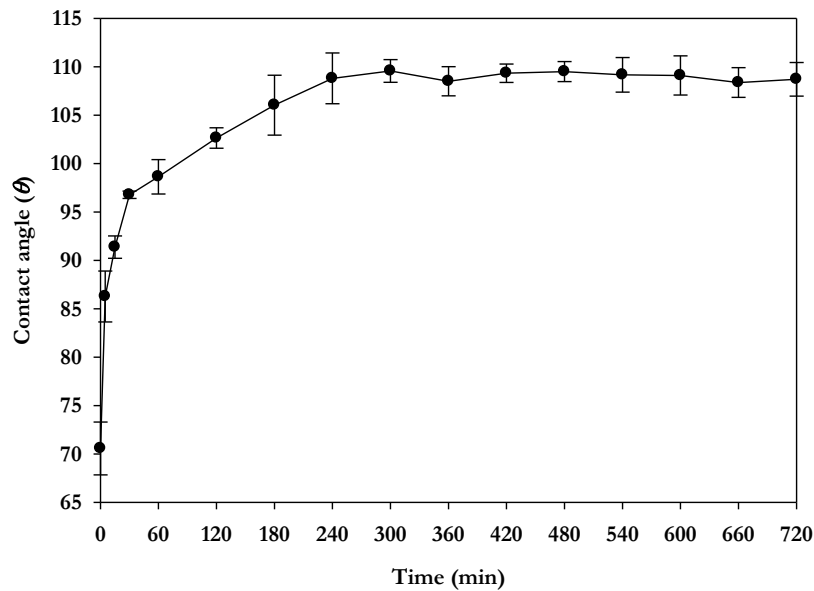


Figure 4.11: Average contact angle (θ) of an oil drop spreading over the GSC surface vs time (min).

Following deposition, the initial spreading rate (Figure 4.11) was $3.14^\circ/\text{min}$ within 5 min of placing the drop on the solid lipid ($r^2=1$). The spreading rate dropped to $0.42^\circ/\text{min}$ at

30 min ($r^2=0.99$), and further to $0.06^\circ/\text{min}$ at 240 min ($r^2=0.99$), after which equilibrium was observed up to 720 min. The equilibrium θ was $108.7 \pm 1.7^\circ$ measured through oil phase. During the equilibrium phase, the spreading rate fluctuated between $0.02\text{-}0.01^\circ/\text{min}$ ($r^2=1$). With $\gamma_{ow} = 28.8 \text{ mN}\cdot\text{m}^{-1}$, from Equations 4.1 and 4.2, γ_{sw} and γ_{so} were 99.8 and $109.0 \text{ mN}\cdot\text{m}^{-1}$, respectively. It is known that if $\gamma_{ow} > \gamma_{sw} + \gamma_{so}$, the particles will be wetted by both phases and position themselves at the interface¹⁶. From Equations 4.1 and 4.2 and our calculated interfacial tension values, $28.8 > 109.0 - 99.8 (= 9.2)$, thus suggesting that the GSC SLNs would effectively position themselves at the oil-water interface.

4.4.1.4 Differential Scanning Calorimetry (DSC)

DSC was used to investigate the melting and crystallization behaviour of the SLNs. Thermograms presented in Figures 4.12A and B show the melting and crystallization curves of the GSC in the bulk and as SLNs, respectively. Table 4.6 presents the values of the onset and peak temperatures and enthalpy for the bulk GSC and GSC SLNs during their melting and crystallization transitions.

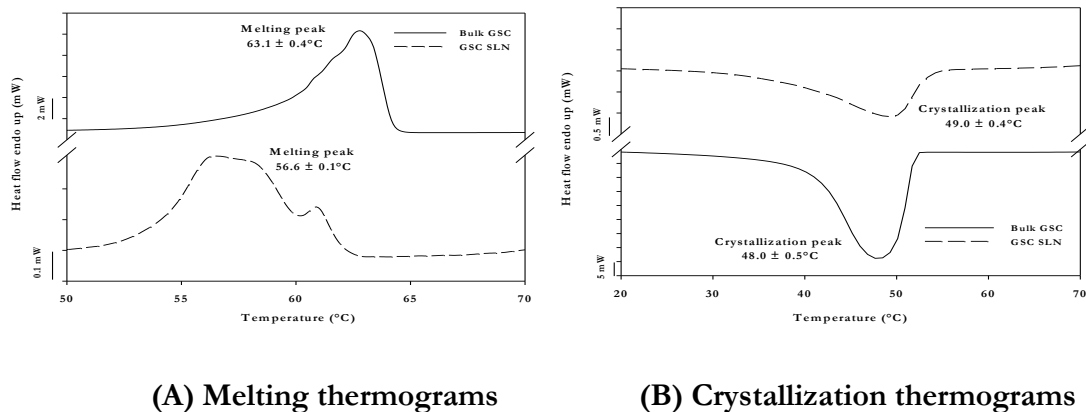


Figure 4.12: DSC (A) melting and (B) crystallization thermograms of the bulk GSC (—) and GSC SLNs (-----). Samples were heated from 1°C to 85°C at a rate of $5^\circ\text{C}/\text{min}$ for the melting curves and cooled from 85°C to 1°C at a rate of $50^\circ\text{C}/\text{min}$ for the crystallization curves. Note differences in the y-axis scales.

Table 4.6: Melting and crystallization transitions for bulk GSC and GSC SLNs. All data are means \pm standard deviations ($\bar{X} \pm s$) for $n = 3$ replicates per run.

Parameters	Bulk GSC		GSC SLNs	
	Melting	Crystallization	Melting	Crystallization
Onset temperature (°C)	59.8 \pm 0.4	52.1 \pm 0.1	53.7 \pm 0.1*	53.1 \pm 0.4*
Peak temperature (°C)	63.1 \pm 0.4	48.0 \pm 0.5	56.6 \pm 0.1*	49.0 \pm 0.4
Enthalpy ΔH (J/g)	91.2 \pm 0.4	-77.8 \pm 1.6	87.9 \pm 2.4	-135.3 \pm 10.2*

* Statistically significant at $p < 0.05$

For the melting curves, bulk GSC showed a single broad endothermic peak with an onset temperature of ~ 60 °C and an enthalpy of ~ 91 J/g. By comparison, the SLNs melted at significantly lower temperatures (~ 54 °C) ($p < 0.05$) with an enthalpy similar to the bulk GSC. Dispersions usually exhibit broader transitions and lower melting points than an equivalent material in the bulk, which is strongly dependent on particle size¹⁹⁵. The broad peak of GSC SLNs is thought to result from multiple melting events that take place due to different-sized particles present^{196, 197}. For the crystallization curves, bulk GSC showed a single broad exothermic peak with an onset temperature of ~ 52 °C and an enthalpy of ~ 78 J/g. The SLNs crystallized at essentially the same temperature as the bulk GSC, with a significantly higher enthalpy of ~ -135 J/g. The similar crystallization temperatures were unexpected, and contrary to widely-reported results that commonly indicate a delay of ~ 20 °C in lipid dispersions compared to bulk lipids^{52, 151, 196}.

The crystallization curves thus provided useful information on the nucleation mechanism in SLNs, *i.e.*, whether homogeneous, surface-heterogeneous or volume-heterogeneous nucleation was dominant¹¹⁴. During lipid crystallization, heterogeneous nucleation normally occurs much more readily than homogeneous nucleation since it is kinetically more favourable¹⁹⁸. The presence of catalytic impurities such as phase boundaries, dust or foreign particles reduces free energy and promotes heterogeneous nucleation.

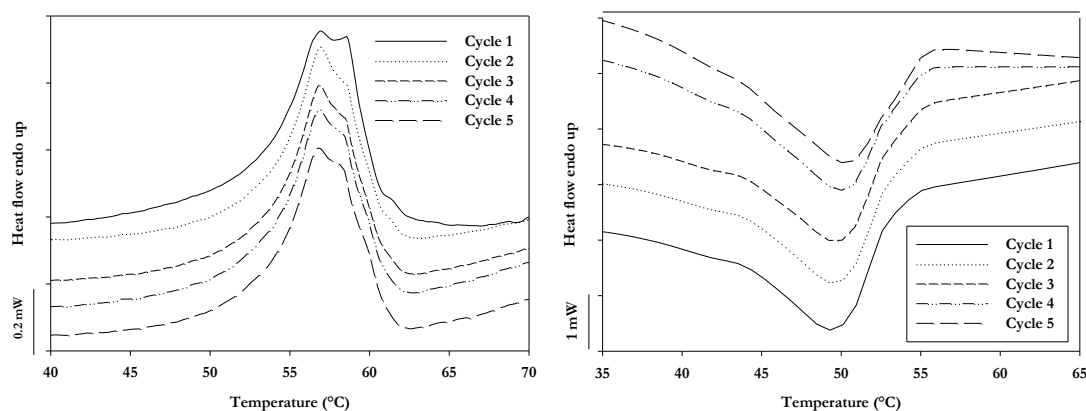
At the nano-scale, the small size of nanodroplets results in a low probability of finding now-compartmentalized catalytic impurities within individual droplets, thereby suppressing heterogeneous nucleation^{32, 199}. Homogeneous nucleation thus predominates,

resulting in decreased crystallization temperatures , as has been reported in many SLN studies, *e.g.*, with palm stearin²⁰⁰ and trilaurin¹⁹⁷.

Unexpectedly, this was not the case in the present work, suggesting that heterogeneous nucleation was the dominant process. In seminal work by Krog and Larsson, they hypothesized that monoglycerides (as per the present research) accumulate at the interface in such a way that their orientation resembles that in the crystalline state²⁰¹. In the crystalline form, the hydrocarbon chains are arranged in monolayers and polar head groups of adjacent layers interact *via* hydrogen bonding, reflecting their amphiphilic characteristics²⁸. Upon emulsification and cooling, the emulsifier crystals expose their methyl end group towards oil and polar heads towards water, thus behaving as surface-active crystals and initiating monoglyceride crystallization at the oil-water interface²⁰¹. Thus, interaction at the interface between the solidifying particle and supersaturated fluid acts as a template for heterogeneous nucleation²⁰².

In our SLN systems, such interfacial heterogeneous nucleation likely occurred, as has been reported by Bunjes *et al.* in phospholipid-stabilized dispersions⁴⁹, Helgason *et al.* for high-melting surfactants¹¹⁴, Ueno *et al.* in *n*-alkane crystal-stabilized emulsion droplets²⁰³ and Arima *et al.* in o/w emulsions stabilized by hydrophobic sucrose palmitic acid oligoesters²⁰⁴.

To further evaluate the influence of thermal treatment on crystallization behaviour and assess the crystallization stability of the nano-dispersions, GSC SLNs were melted and crystallized repeatedly for 5 cycles *via* DSC. Figure 4.13 (A) and (B) represent the melting and crystallization transitions of the 5 cycles, respectively, and Table 4.7 displays the melting and crystallization peaks obtained along with the particle size distributions before and after the completion of the cycle.



(A) Melting thermograms

(B) Crystallization thermograms

Figure 4.13: DSC (A) melting and (B) crystallization thermograms of GSC SLNs for 5 heating – cooling cycles. Samples were heated from 1 °C to 85 °C at a rate of 5 °C/min and cooled from 85 °C to 1 °C at a rate of 50 °C/min for 5 consecutive cycles.

Table 4.7: Melting and crystallization transitions for GSC SLNs for 5 heating-cooling cycles, along with the DLS particle size distribution data before and after the run. All data are means \pm standard deviations ($\bar{X} \pm s$) for $n = 3$ replicates per run.

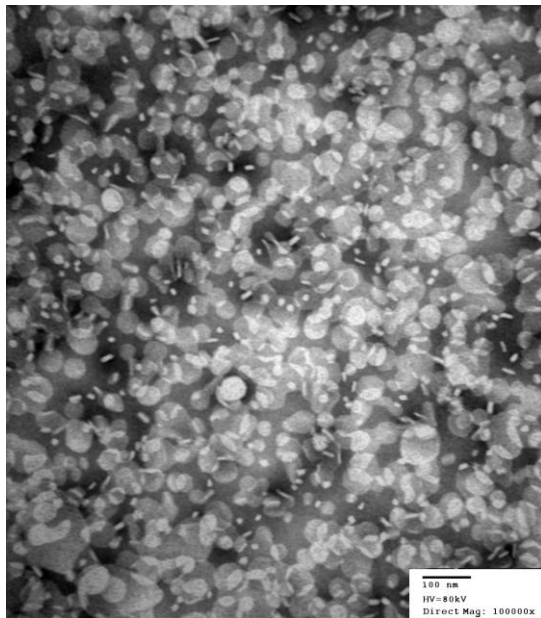
Peak temperature (°C)	GSC SLNs				
	Cycle 1	Cycle 2	Cycle 3	Cycle 4	Cycle 5
Melting	57.9 \pm 0.1	56.6 \pm 0.1*	57.7 \pm 0.1	57.8 \pm 0.0	57.8 \pm 0.1
Crystallization	49.2 \pm 0.8	49.5 \pm 0.5	49.7 \pm 0.5	49.7 \pm 0.5	49.7 \pm 0.5
Effective diameter (nm)	191.9 \pm 4.2	-	-	-	193.2 \pm 1.2
Polydispersity index	0.20 \pm 0.02	-	-	-	0.23 \pm 0.01

* Statistically significant at $p < 0.05$

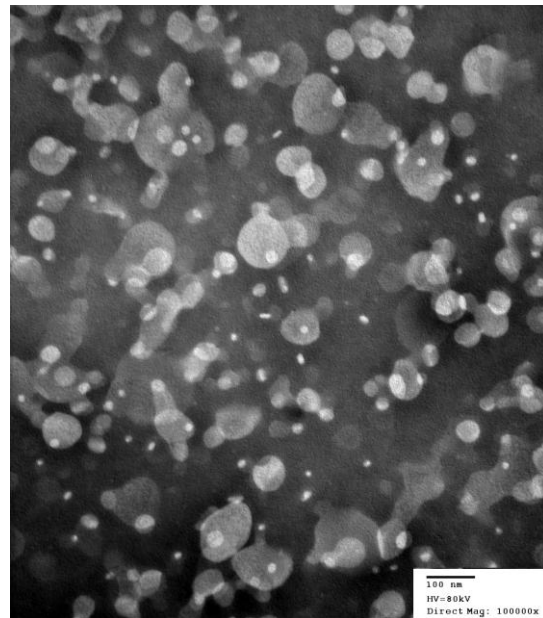
The thermal treatment of the dispersions did not cause a significant increase ($p > 0.05$) in the effective mean particle diameter at the end of 5 cycles, thus indicating and confirming the stability of the sample. The crystallization temperatures showed excellent overlap strongly supporting the hypothesis of interfacial heterogeneous nucleation occurring during crystallization of the surface-active GSC SLNs.

4.4.1.5 Transmission Electron Microscopy (TEM)

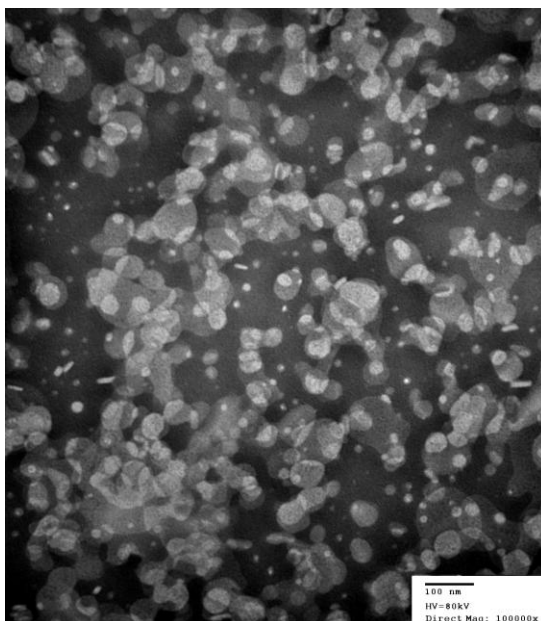
Figures 4.14A, B, C and D shows TEM micrographs recorded initially, and at 4 wk, 12 wk and 24 wk after SLN preparation.



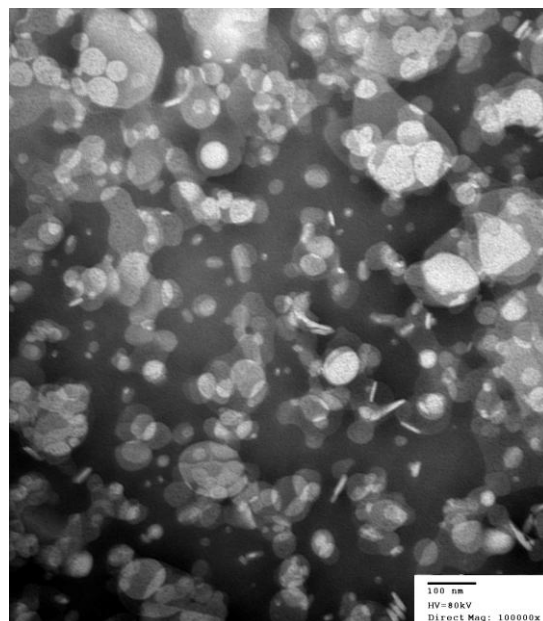
(A) Initial



(B) At 4 wk



(C) At 12 wk



(D) At 24 wk

Figure 4.14: TEM micrographs of GSC SLNs at initial (A), 4 wk (B), 12 wk (C) and 24 wk (D) after preparation.

TEM examination of freshly-prepared SLNs revealed well-defined anisometric, ellipsoidal particles. Edge-on, the particles appeared as rods or needles with a thickness of ~10-20 nm. The mean particle size obtained was in the range of 20-140 nm, which was closer to the lower range of mean particle size distributions observed in DLS and much closer to the $D [4, 3]$ data obtained by LD measurements. Little change was observed after 4 and 12 wk. After 24 wk, the particle size and shape remained essentially unaltered. However, some aggregates were observed.

4.4.1.6 Atomic Force Microscopy (AFM)

AFM imaging of SLNs were conducted to further obtain information on SLN morphology and size. Figures 4.15A and B show the 2-D AFM height scans of the SLNs dispersions initially and at 24 wk.

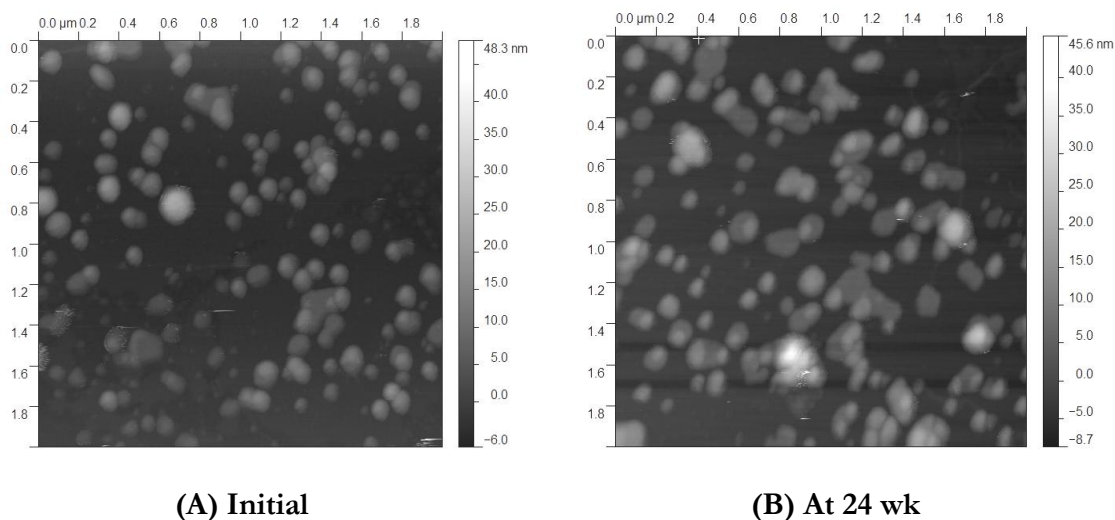


Figure 4.15: AFM height images of GSC SLNs at initial (A) and 24 wk (B) after SLN preparation.

As observed with TEM, AFM confirmed that the SLNs were circular to ellipsoidal in shape with a smooth surface. The SLNs tended to cluster, which may have been due to the sample preparation method where the colloidal suspension was dried onto the mica surface, causing some aggregation.

Two indices that provide information on the overall shape of a particle are the degree of elongation and the degree of flatness. The degree of elongation or aspect ratio is

an index that provides information on whether the particle is long and slender or short and rounded and is given by²⁰⁵:

$$\text{Aspect ratio} = \frac{\text{Major axis}}{\text{Minor axis}} \quad (\text{Eqn. 4.3})$$

whereas the degree of flatness is a ratio given by the formula²⁰⁵:

$$\text{Degree of flatness} = \frac{\text{Minor axis}}{\text{Thickness}} \quad (\text{Eqn. 4.4})$$

The SLN aspect ratio, degree of flatness, thickness, length and width in nm initially and after 24 wk are shown in Table 4.8.

Table 4.8: SLN particle shape from AFM analysis initially and after 24 wk. All data are means \pm standard deviations ($\bar{X} \pm s$) for $n = 3$ replicates per run. No significant differences were observed after 24 wk ($p > 0.05$).

Parameter	Initial	24 wk
Aspect ratio	1.4 ± 0.1	1.4 ± 0.1
Degree of flatness	4.6 ± 0.8	5.1 ± 0.6
Thickness (nm)	24.9 ± 7.3	23.4 ± 6.8
Length (nm)	155.5 ± 25.2	162.8 ± 28.9
Width (nm)	110.7 ± 19.9	117.3 ± 25.7

As per the TEM micrographs, over 24 wk, the particle dimensions, aspect ratio and degree of flatness remained essentially unchanged.

4.4.2 Characterization of SLN decorated oil-in-water emulsions

4.4.2.1 Particle size analysis

The o/w emulsions were prepared by high pressure homogenization using GSC SLNs as the sole emulsifying agent. The resultant o/w emulsions had a pH of ~ 4.6 and a pale pink appearance due to addition of Nile Red to the oily phase. The emulsion-making

protocol was highly-reproducible, based on the particle size distribution measured by LD (Table 4.9 and Figure 4.16).

Table 4.9: LD measurements showing the particle size distribution data of 3 batches of SLN decorated o/w emulsions. All data are means \pm standard deviations ($\bar{X} \pm s$) for $n = 3$ replicates per batch. No significant differences were observed between batches ($p > 0.05$).

Parameters	Batch 1	Batch 2	Batch 3
$D [4, 3]$ (nm)	460.0 \pm 3.0	459.0 \pm 1.0	459.4 \pm 2.0
$D [3, 2]$ (nm)	324.3 \pm 2.1	323.0 \pm 4.4	321.0 \pm 1.4
$D (v, 0.1)$ (nm)	169.0 \pm 1.0	168.0 \pm 3.5	166.0 \pm 2.6
$D (v, 0.5)$ (nm)	399.7 \pm 2.5	401.3 \pm 2.3	400.4 \pm 1.5
$D (v, 0.9)$ (nm)	842.3 \pm 4.5	838.3 \pm 4.6	841.9 \pm 2.4
Span	1683.3 \pm 3.1	1670.3 \pm 29.7	1686.0 \pm 10.1

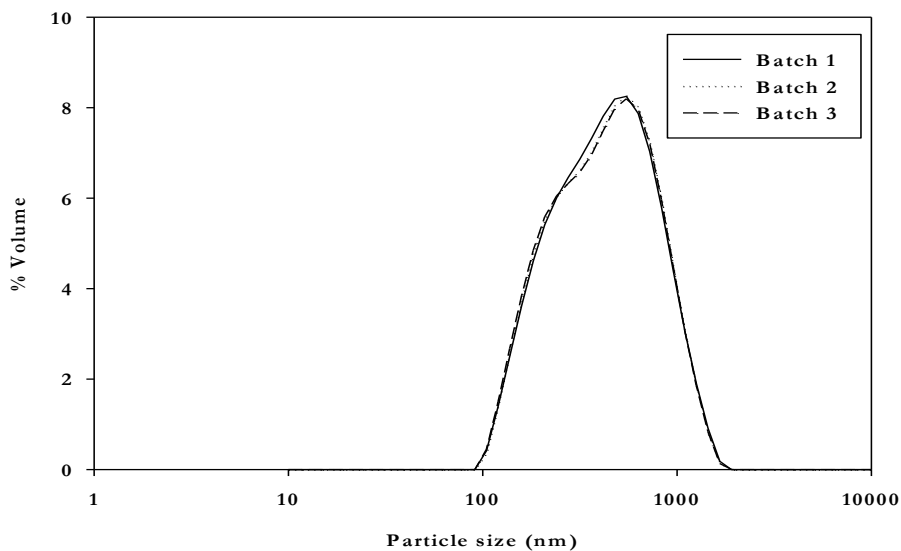


Figure 4.16: LD-measured droplet size distributions showing the reproducibility of 3 batches of SLN decorated o/w emulsions.

The initial average volume-weighted diameter of the dispersed oil droplets was 459.5 \pm 0.5 nm and $D (v, 0.9)$ was 840.8 \pm 2.2 nm. The span of the distribution was 1679.9 \pm 8.4 nm, which indicated a broad particle size distribution. The volume distribution curve displayed a shoulder at \sim 200 nm that resulted from the presence of the GSC SLNs (Figure

4.16). The breadth of the emulsion distributions was relatively high as it consisted of SLN-covered dispersed droplets and perhaps free SLNs not associated with oil droplets.

The emulsions were aged 24 wk and the evolution in their particle size distribution noted (Table 4.10). No significant differences in the LD measurements were observed in emulsions up to 12 wk ($p > 0.05$). At 24 wk, however, the emulsions had a significant ($p < 0.05$) secondary population of droplets of a much larger size (Figure 4.17).

Table 4.10: LD measurements showing the particle size distribution data of refrigerated samples of SLN decorated o/w emulsions at various time points. All data are means \pm standard deviations ($\bar{X} \pm s$) for $n = 3$ replicates per time point.

Parameter	Initial	4 wk	12 wk	24 wk
$D [4, 3]$ (nm)	460.0 ± 3.0	460.3 ± 2.3	452.7 ± 4.5	$1992.7 \pm 1139.4^*$
$D [3, 2]$ (nm)	324.3 ± 2.1	320.0 ± 2.6	321.7 ± 2.3	$372.3 \pm 6.0^*$
$D (v, 0.1)$ (nm)	169.0 ± 1.0	165.3 ± 1.5	166.4 ± 1.4	$179.3 \pm 2.5^*$
$D (v, 0.5)$ (nm)	399.7 ± 2.5	398.0 ± 2.6	392.3 ± 4.0	$477.3 \pm 9.1^*$
$D (v, 0.9)$ (nm)	842.3 ± 4.5	851.3 ± 3.2	835.0 ± 11.1	$1226.0 \pm 144.7^*$
Span	1683.3 ± 3.1	1724.7 ± 8.5	1715.3 ± 13.1	$2190.0 \pm 270.2^*$

* Statistically significant at $p < 0.05$

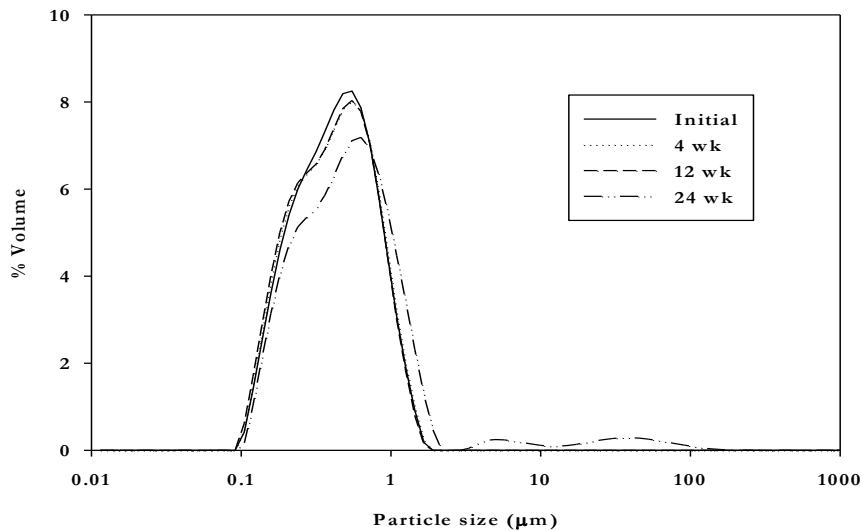


Figure 4.17: LD measurements showing the particle size distributions of refrigerated samples of SLN decorated o/w emulsions at various time points.

The distribution data revealed a decrease in the amount of particles sized 100-700 nm, while the portion of particles with diameters of 800-1700 nm increased, due to SLN Ostwald ripening or particle aggregation. This was coupled with an increase in particle size (up to $\sim 200 \mu\text{m}$), resulting from flocculation and/or coalescence of oil droplets (Figure 4.17). Visually, a thin, creamy pink-coloured oily layer was present on the emulsions after 12 wk. Over 24 wk, the breadth of the distribution widened $\sim 1.3 \times$ whereas the $D [4, 3]$ increased 5 x. Overall, the emulsions remained stable for 12 wk. By 24 wk, there was an increase in droplet and/or SLN particle diameter as the emulsions started to destabilize.

4.4.2.2 Surface charge measurement

GSC SLNs present in our o/w emulsions had a negative ζ potential as discussed earlier (Section 4.4.1.2). Thus, the emulsions showed a net negative charge of ca. -42 mV, which was constant up to 12 wk. By 24 wk, ζ potential had dropped significantly to -33 mV ($p < 0.05$) (Table 4.11).

Table 4.11: Zeta potential measurements of refrigerated samples of SLN decorated o/w emulsions at various time points. All data are means \pm standard deviations ($\bar{X} \pm s$) for $n = 3$ replicates per time point.

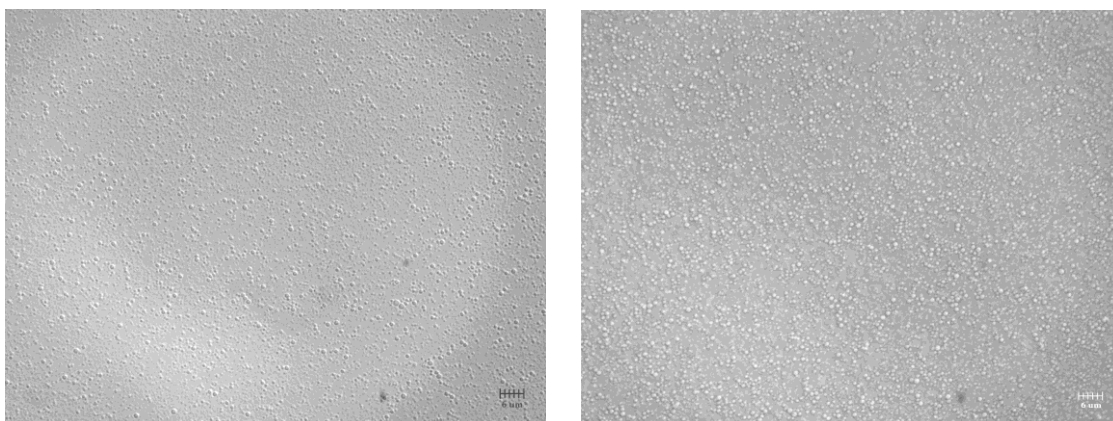
Parameter	Initial	4 wk	12 wk	24 wk
$\zeta(\text{mV})$	-42.5 ± 1.5	-43.1 ± 2.1	-43.8 ± 2.8	$-32.9 \pm 1.8^*$

* Statistically significant at $p < 0.05$

The drop in ζ potential was due to droplet-droplet aggregation and/or coalescence as no ζ potential reduction was observed for the SLNs, in spite of their aggregation. Hence, in the emulsions, ζ potential reflected demulsification, likely as a result of SLN desorption or probable dissolution, which resulted in droplet-droplet interactions leading to aggregation and/or coalescence events, and subsequent emulsion instability.

4.4.2.3 Inverted light microscopy

Particle size analysis by LD showed that the dispersed oil droplets were micron-sized. Hence, inverted microscopy was used to observe any macroscopic changes such as droplet flocculation or coalescence during storage. The images of the emulsions are displayed in Figure 4.18 A and B for the initial and 24 wk samples respectively.



(A) Initial

(B) At 24 wk

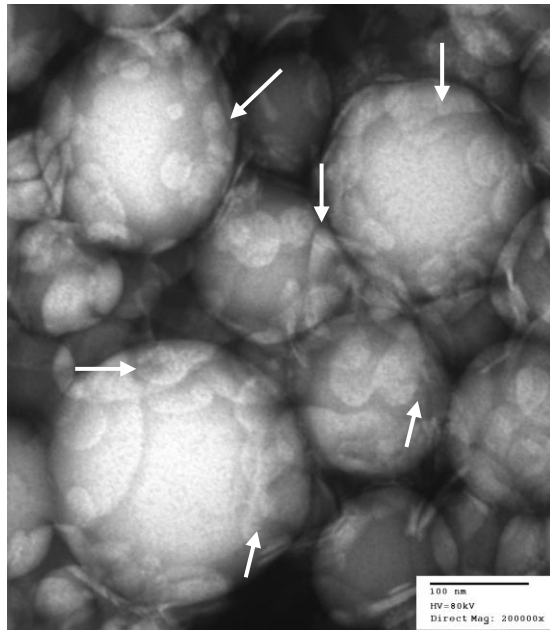
Figure 4.18: Inverted light microscopy of SLN decorated o/w emulsions at initial (A) and 24 wk (B) after emulsion preparation.

As can be seen from Figure 4.18(A), the freshly-prepared emulsions showed a uniform distribution of individual oil droplets. At 24 wk (B), aggregated and larger droplets were present, the result of flocculation-induced coalescence.

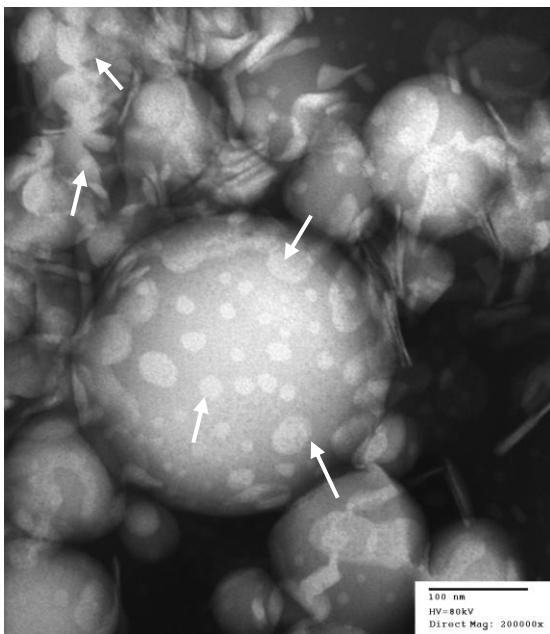
4.4.2.4 Transmission Electron Microscopy (TEM)

TEM scans of the SLN decorated o/w emulsions were visualized initially, and at 4, 12, 15 and 24 wk after preparation (Figures 4.19 A - E).

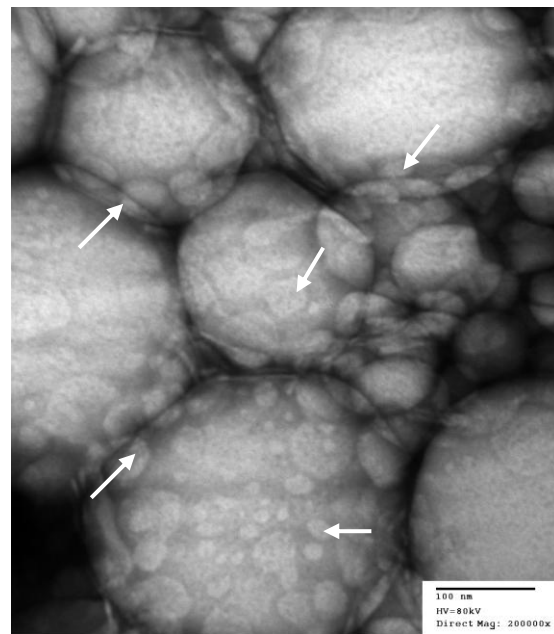
The images showed GSC SLNs adsorbed onto the oil droplets as mono- and/or multi-layers (white solid arrows). Surface coverage by the SLNs appeared to depend on droplet size, with smaller droplets much more densely covered than larger ones. The particle size of the GSC SLNs was in the range of 20-120 nm, in agreement with the particle size distribution of the GSC SLNs. Oil droplets were about 250-400 nm in diameter, in agreement with the LD measurements. Free SLNs could be seen in the images around the dispersed droplets.



(A) Initial



(B) At 4 wk



(C) At 12 wk

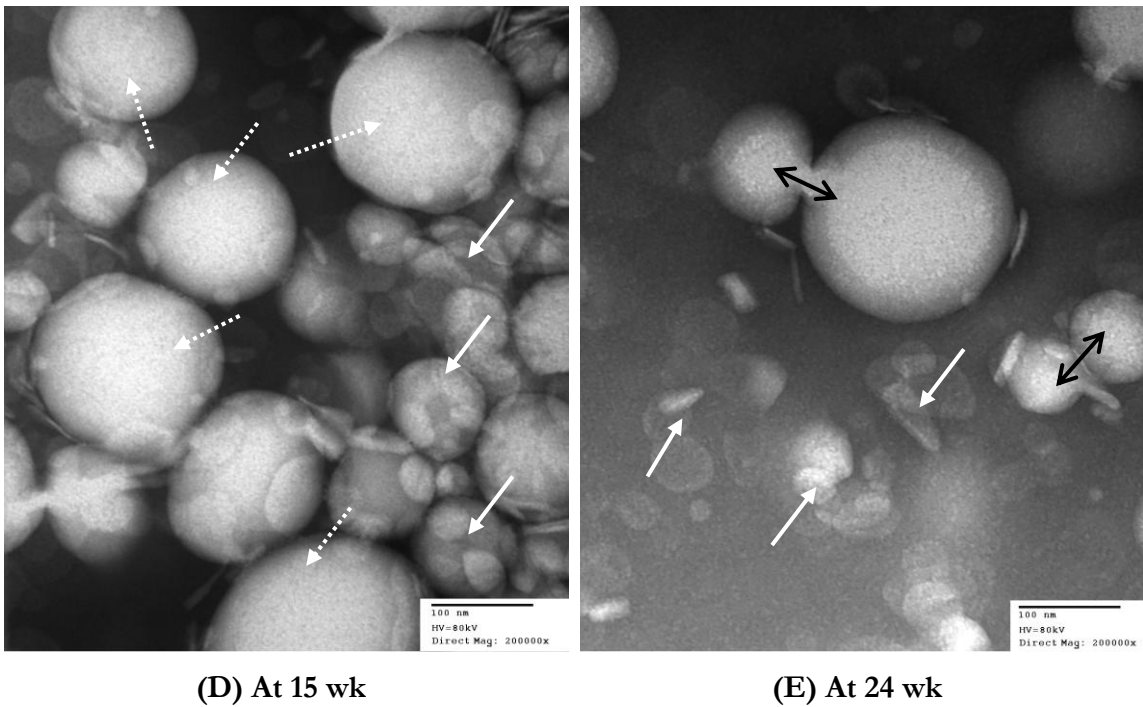


Figure 4.19: TEM micrographs of SLN decorated o/w emulsions at various time points (Arrows explained in text).

TEM images confirmed the adsorption of GSC SLNs onto oil droplets for up to 12 wk. At 15 wk, it was observed that although smaller oil droplets were still covered with SLNs (white arrows), the surface of the larger oil droplets were devoid of SLNs (white dotted arrows), an indication that the emulsions were starting to destabilize, though the oil droplets were still intact and hadn't coalesced. At 24 wk, there was a clear and almost complete dissociation of the SLNs (white solid arrows) from the droplet surface, with the oil droplets now coalescing (black solid arrows).

It is well known that better Pickering-type stabilization is achieved with complete droplet coverage by particles. However, our oil droplets did not show complete coverage by solid SLN particles. Vignati *et al.* have reported stable o/w emulsions with only 5 % droplet coverage of monodisperse, hydrophobic silica colloidal particles⁸ and they proposed monolayer bridging between particles as the mechanism responsible for preventing coalescence between droplets. There was no evidence of such monolayer bridging between lipid particles from TEM images in our emulsion samples.

However, as pointed earlier, if $\gamma_{ow} > \gamma_{sw} + \gamma_{so}$, the particles will be wetted by both phases and position themselves at the interface. From Equations 4.1 and 4.2 and our calculated interfacial tension values as mentioned in section 4.4.1.3, the SLNs would be positioned at the interface due to favourable θ as represented below (Figure 4.20). The equilibrium distance of a single spherical SLN particle of radius ~ 100 nm, immersed within the oil-water interface is given by $1 - \cos \theta$ and the free energy of displacement (ΔG_d) for this particle will be given by Eqn. 2.9^{16, 152}. Thus, the equilibrium distance calculated with equilibrium θ of 108.7° through oil phase will be 1.32° and the ΔG_d will be $3.94 \times 10^5 kT$, at room temperature. Thus, the particle embedded at the oil-water interface is trapped in a deep energy well, indicating that the repulsion potential is much larger than the attraction potential.

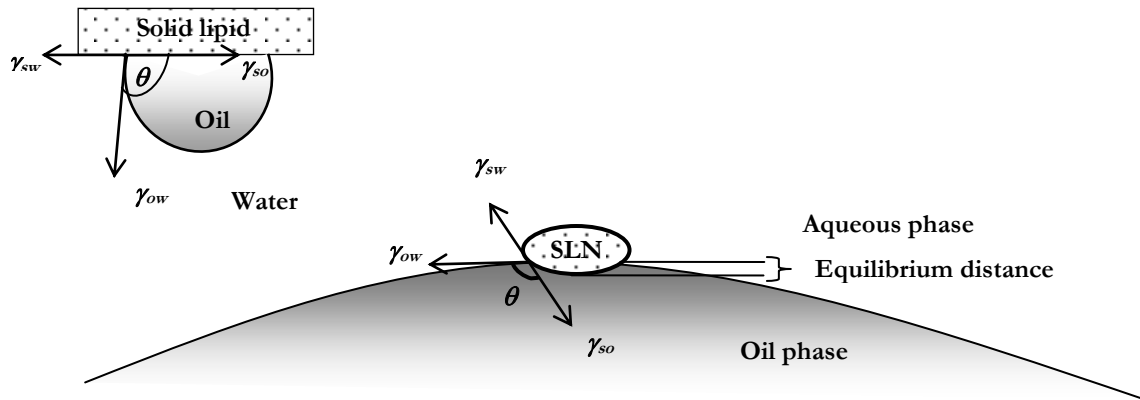


Figure 4.20: Probable positioning of GSC SLN at the oil-water interface in SLN decorated o/w emulsions.

In regards to o/w emulsion destabilization and apparent removal of the SLNs from the interface, there are two possible mechanisms. As previously discussed and confirmed by the TEM images, there appeared to be SLN desorption from the interface into the continuous aqueous phase. This was somewhat unusual as their interfacial attachment energy was many orders above kT . LD measurements, however, did not support this possibility. If the SLNs indeed desorbed from the interface, there should have been a concomitant increase in the LD peak intensity associated with free SLNs, which was not the case.

Another possible destabilization mechanism was based on Ostwald ripening. As explained in section 1.3.5, the Laplace pressure differential ΔP is directly proportional to

interfacial tension between the solid substrate and liquid droplet surface and inversely proportional to the radius of the droplet. Thus, the internal pressure of a water droplet increases from 1.4×10^{-3} atm with a 1 mm water droplet radius to 1.4×10^2 atm with a 10 nm radius. Thus, ΔP becomes enormous when droplet size approaches molecular dimensions. As the SLNs had a very high Laplace pressure on account of their nano-size, they were likely subjected to Ostwald ripening leading to an increase in SLN size and/or dissolution into the dispersed oil phase. This ultimately led to their disappearance from the interface. This hypothesis is supported by the lack of change in the LD peak component associated with free, desorbed SLNs and the gradual appearance of larger-sized particles up to 100 μm .

As the high SLN attachment energy would have made it unlikely for the SLNs to desorb from the interface, larger SLN particles were formed at the expense of smaller SLNs, which eventually disappeared, thus causing an increase in average particle/droplet diameter. Comparison of the SLN and emulsion size distributions by LD also indicated the presence of similar-sized particles after 24/28 weeks.

4.5 Conclusion

Obtaining a stable emulsion system is strongly dependent on the selection of an appropriate emulsifier. The concept of using SLNs as emulsion stabilizers in food products is relatively new and in its developmental stage. SLNs of the lipid GSC were prepared successfully and were found to retain their particle size, shape and surface charge for a period of up to 24 wk. These nanoparticles were able to emulsify and stabilize oil-in-water emulsions for at least 12 wk. GSC SLNs were adsorbed at the oil/water interface and prevented coalescence of oil droplets by steric hindrance. Overall, the GSC SLNs were effectively used as emulsifiers to generate oil-in-water emulsions. Efforts now need to be directed towards maintaining the stability over a longer period of time.

Chapter 5

OVERALL CONCLUSIONS

5.0 Overall conclusions

Solid lipid nanoparticles (SLNs) were fabricated from the GRAS food-grade lipid glyceryl stearate citrate (GSC), which possesses emulsifying properties. SLNs were prepared by hot-melt emulsification and high-pressure homogenization. The resultant oil-in-water nanoemulsion was flash-cooled to obtain GSC SLNs, which were characterized for particle size and size distribution, surface charge measurement, thermal analysis and ultra-structure by TEM and AFM studies.

The SLNs were negatively-charged with an effective mean diameter of ~ 180 nm (DLS analysis) and a volume-weighted mean diameter ~ 152 nm (LD measurement). They remained stable for 24 wk, although evidence of particle aggregation was visible from 12 wk onwards. Ultra-structure studies by TEM and AFM revealed anisometric SLNs with circular to elliptical shapes. The particle size of SLNs obtained from these studies corroborated the DLS and LD results.

The GSC SLNs were studied for their effectiveness as oil-in-water (o/w) emulsifiers. Stable o/w emulsions with a negative surface charge and volume-weighted mean droplet size of ~ 459 nm were obtained. Macroscopically, these emulsions were stable for 12 wk. TEM analysis revealed the adsorption of SLNs onto the oil globules, resulting in Pickering-type steric stabilization of emulsions. With time, the SLNs desorbed from the interface into the continuous water phase which, coupled with Ostwald ripening, resulted in emulsion destabilization.

Overall, this research demonstrated the feasibility of stabilizing o/w emulsions using SLNs as the sole emulsifiers, a new concept not reported to date in the literature.

Chapter 6

FUTURE STUDIES

6.0 Future studies

Amongst its many findings, this research work has highlighted the importance of SLN particle shape and size for the effective stabilization of o/w emulsions. However, there are several areas for future studies:

1. Reduction of SLN aggregation and particle growth. In this study, melt-emulsification and homogenization were used to generate the SLNs. The generated SLNs, albeit consisting of strongly polar groups, showed particle aggregation within 12 wk. The high concentration (7.5% w/w) of SLNs was partly responsible for this aggregation. In this light, lower lipid concentrations or similarly-concentrated dispersions stabilized with steric stabilizers should be attempted. This would nullify the novelty of emulsion stabilization solely by SLNs, but would lead to improvement in the stability of the starting SLN dispersions.
2. As mentioned, the concentration of lipid used in this study was 7.5% (w/w). Since the specific surface area of a particle increases tremendously at the nanoscale, ideally SLNs should be able to emulsify effectively at even lower concentrations. By increasing the hydrophobicity of the lipid surface, it will be possible to manipulate the contact angle of the particles at the oil-water interface, thereby effectively reducing the concentration of lipid required for emulsification.
3. The fundamental mechanism of stabilization provided by particle-stabilized emulsions is elusive and concrete evidence of the adsorption and desorption kinetics needs to be investigated. An improved determination of the contact angle at the oil-water interface could aid in unravelling the fundamental mechanisms of particle-stabilized emulsions and provide a basis to better understand interfacial phenomena.

Chapter 7

REFERENCES

7.0 References

1. Binks, B. P., Particles as Surfactants - Similarities and Differences. *Current Opinion in Colloid and Interface Science* **2002**, 7, 21-41.
2. Binks, B. P., Rocher, A. , Effects of temperature on water-in-oil emulsions stabilised solely by wax microparticles. *Journal of Colloid and Interface Science* **2009**, 335, 94-104.
3. Macierzanka, A., Szeląg, H., Szumala, P., Pawłowicz, R., Mackie, A. R., Ridout, M. J., Effect of crystalline emulsifier composition on structural transformations of water-in-oil emulsions: Emulsification and quiescent conditions. . *Journal of Colloids Surface: Physicochemical & Engineering Aspects* **2009**, 334, (1-3), 40-52.
4. Mishra, B., Patel, B. B., Tiwari, S., Colloidal Nanocarriers: A Review on Formulation Technology, Types and Applications toward Targeted Drug Delivery. *Nanomedicine - Nanotechnology, Biology, and Medicine* **2010**, 6, (1), 9 - 24.
5. Heurtault, B., Saulnier, P., Pech, B., Proust, J. E., Benoit, J. P. , Physico-chemical Stability of Colloidal Lipid Particles. *Biomaterials* **2003**, 24, (23), 4283-4300.
6. Barnes, G. T., Gentle, I. R., *Interfacial Science - An Introduction*. Oxford University Press Inc.: New York, 2005; p 1 - 32.
7. Leal-Calderon, F., Bibette, J., Schmitt, V., *Emulsion Science: Basic Principles*. 2nd ed.; Springer: New York, 2007; p 9 -12.
8. Vignati, E., Piazza, R., Lockhart, T. P., Pickering Emulsions: Interfacial Tension, Colloidal Layer Morphology, and Trapped-Particle Motion. *Langmuir* **2003**, 19, (17), 6650-6656.
9. Tcholakova, S., Denkov, N. D., Lips, A., Comparison of Solid Particles, Globular Proteins and Surfactants as Emulsifiers. *Physical Chemistry Chemical Physics* **2008**, 10, (12), 1608-1627.
10. Dickinson, E., Flocculation of Protein-Stabilized Oil-in-Water Emulsions. *Colloids and Surfaces B: Biointerfaces* **2010**, 81, (1), 130-140.
11. Jutz, G., Böker, A., Bio-inorganic Microcapsules from Templating Protein- and Bionanoparticle-stabilized Pickering Emulsions. *Journal of Material Chemistry* **2010**, 20, 4299-4304.
12. Frelichowska, J., Bolzinger, M. A., Chevalier, Y., Effects of Solid Particle Content on Properties of o/w Pickering Emulsions *Journal of Colloid and Interface Science* **2010**, 351, (2), 348-356.
13. Whitby, C. P., Fornasiero, D., Ralston, J., Structure of Oil-in-Water Emulsions Stabilised by Silica and Hydrophobised Titania Particles *Journal of Colloid and Interface Science* **2010**, 342, (1), 205-209.
14. Dickinson, E., Food Emulsions and Foams: Stabilization by Particles *Current Opinion in Colloid and Interface Science* **2010**, 15, (1-2), 40-49.
15. Rousseau, D., Fat Crystals and Emulsion Stability - A Review. *Food Research International* **2000**, 33, 3-14.

16. Rousseau, D., Fat Crystal Behavior in Food Emulsions. In *Physical Properties of Lipids*, Marangoni, A. G., Narine, S. S., Ed. Marcel Dekker, Inc.: New York, 2002; pp 219-264.
17. Kraft, D. J., de Folter, J. W. J., Luigjes, B., Castillo, S. I. R., Sacanna, S., Philipse, A. P., Kegel, W. K., Conditions for Equilibrium Solid-Stabilized Emulsions. *The Journal of Physical Chemistry B* **2010**, 114, (32), 10347-10356.
18. Liang, Y., Hilal, N., Langston, P., Starov, V., Interaction Forces between Colloidal Particles in Liquid: Theory and Experiment *Advances in Colloid and Interface Science* **2007**, 134-135, 151-166.
19. Barnes, G. T., Gentle, I. R., *Interfacial Science - An Introduction*. Oxford University Press Inc.: New York, 2005; p 200-211.
20. Eastman, J., Stability of Charge-stabilized Colloids. In *Colloid Science: Principles, Methods and Applications*, 2nd ed.; Cosgrove, T., Ed. John Wiley & Sons Ltd.: Chichester, 2010; pp 45-59.
21. McClements, D. J., *Food Emulsions: Principles, Practices, and Techniques*. 2nd ed.; CRC Press: Florida, 2005.
22. Cao, Z. Electrostatic Stabilization *Periodical* [Online], 2010. [http://depts.washington.edu/solgel/pages/courses/MSE_502/Electrostatic Stabilization.html](http://depts.washington.edu/solgel/pages/courses/MSE_502/Electrostatic_Stabilization.html) (accessed January 16, 2010).
23. Kamiya, H., Characteristics and Behavior of Nanoparticles and its Dispersion Systems. In *Nanoparticle Technology Handbook*, 1st ed.; Hosokawa, M., Nogi, K., Naito, M., Yokoyama, T., Ed. Elsevier: Amsterdam, 2007; pp 115-119.
24. Dagastine, R. R., Stevens, G. W. , Direct Force Measurement at Liquid/Liquid Interfaces. In *Interfacial Nanochemistry: Molecular Science and Engineering at Liquid-Liquid Interfaces*, Watarai, H., Teramae, N., Sawada, T., Ed. Kluwer Academic/ Plenum Publishers: New York, 2005; pp 77-95.
25. Anton, N., Benoit, J. P., Saulnier, P., Design and Production of Nanoparticles Formulated from Nano-Emulsion Templates - A Review. *Journal of Controlled Release* **2008**, 128, 185-199.
26. Fredrick, E., Walstra, P., Dewettinck, K. , Factors Governing Partial Coalescence in Oil-in-Water Emulsions. *Advances in Colloid and Interface Science* **2010**, 153, 30-42.
27. McClements, D. J., Lipid-Based Emulsions and Emulsifiers. In *Food Lipids Chemistry, Nutrition and Biotechnology*, 2nd ed.; Akoh, C. C., Min, D. B., Ed. Marcel-Dekker, Inc.: New York, 2002; pp 81-119.
28. Larsson, K., Tailoring Lipid Functionality in Foods. *Trends in Food Science and Technology* **1994**, 5, 311-315.
29. Martin, A., Swarbrick, J., Cammarata, A., *States of Matter and Phase Equilibria*. 3rd ed.; Lea and Febiger: Philadelphia, 1983; p 62-92.
30. Bunjes, H., Characterization of Solid Lipid Nano- and Microparticles. In *Lipospheres in Drug Targets and Delivery: Approaches, Methods, and Applications*, Nastruzzi, C., Ed. CRC Press: Boca Raton, FL, 2005; pp 41-66.
31. Owusu-Apenten, R. K., *Introduction to Food Chemistry*. CRC Press: Philadelphia, 2005; p 61-79.
32. Metin, S., Hartel, R. W. , Crystallization of Fats and Oils. In *Bailey's Industrial Oil and Fat Products*, 6th ed.; Shahidi, F., Ed. Wiley-Interscience, John Wiley and Sons, Inc., Publication: New Jersey, 2005; Vol. 1, pp 45-76.

33. Hughes, R., An Introduction to Colloids. In *Colloid Science: Principles, Methods and Applications*, 2nd ed.; Cosgrove, T., Ed. John Wiley & Sons Ltd.: Chichester, 2010; pp 1-21.
34. Manoharan, C., Basarkar, A., Singh, J., Various Pharmaceutical Disperse Systems. In *Pharmaceutical Suspensions: From Formulation Development to Manufacturing*, Kulshreshtha, A. K., Singh, O. N., Wall, G. M., Ed. Springer: New York, 2010; pp 1-37.
35. Barnes, G. T., Gentle, I. R., *Interfacial Science - An Introduction*. Oxford University Press Inc.: New York, 2005; p 123-126.
36. Moorthaemer, B., Sprakel, J. Improving the Stability of a Suspension *Periodical* [Online], 2006.
<http://pharmtech.findpharma.com/pharmtech/article/articleDetail.jsp?id=306687>
(accessed October 27, 2010).
37. Somasundaran, P., Chakraborty, S., Deo, P., Deo, N., Somasundaran, T., Contribution of Surfactants to Personal Care Products. In *Surfactants in Personal Care Products and Decorative Cosmetics*, 3rd ed.; Rhein, L. D., Schlossman, M., O'Lenick, A., Somasundaran, P., Ed. CRC Press, Taylor & Francis Group: Boca Raton, 2006; pp 121-175.
38. Landfester, K., Antonietti, M., Miniemulsions for the Convenient Synthesis of Organic and Inorganic Nanoparticle and "Single Molecule" Applications in Materials Chemistry. In *Colloids and Colloid Assemblies: Synthesis, Modification, Organization and Utilization of Colloid Particles*, Caruso, F., Ed. Wiley-VCH Verlag GmbH & Co. KGaA: Weinheim, 2004; pp 175-215.
39. Jain, S. C., Hughes, A. E., Ostwald Ripening and Its Application to Precipitates and Colloids in Ionic Crystals and Glasses. *Journal of Materials Science* **1978**, 13, 1611-1631.
40. Binks, B. P., Lumsdon, S. O., Catastrophic Phase Inversion of Water-in-Oil Emulsions Stabilized by Hydrophobic Silica. *Langmuir* **2000**, 16, (6), 2539-2547.
41. Freitas, C., Müller, R. H., Spray Drying of Solid Lipid Nanoparticles (SLN TM). *European Journal of Pharmaceutics and Biopharmaceutics* **1998**, 46, (2), 145-151.
42. Manjunath, K., Reddy, J. S., Venkateswarlu, V., Solid Lipid Nanoparticles as Drug Delivery Systems. *Methods and Findings in Experimental and Clinical Pharmacology* **2005**, 27, (2), 127-144.
43. Müller, R. H., Mäder, K., Gohla, S., Solid Lipid Nanoparticles (SLN) for Controlled Drug Delivery - A Review of the State of the Art. *European Journal of Pharmaceutics and Biopharmaceutics* **2000**, 50, (1), 161-177.
44. Üner, M., Preparation, Characterization and Physico-Chemical Properties of Solid Lipid Nanoparticles (SLN) and Nanostructured Lipid Carriers (NLC) : Their Benefits as Colloidal Drug Carrier Systems. *Pharmazie* **2006**, 61, (5), 375-386.
45. Kuntsche, J., Koch, M. H. J., Steiniger, F., Bunjes, H., Influence of Stabilizer Systems on the Properties and Phase Behavior of Supercooled Smectic Nanoparticles. *Journal of Colloid and Interface Science* **2010**, 350, 229-239.
46. Kuntsche, J., Koch, M. H. J., Drechsler, M., Bunjes, H., Crystallization Behavior of Supercooled Smectic Cholesteryl Myristate Nanoparticles containing Phospholipids as Stabilizers. *Biointerfaces* **2005**, 44, 25-35.
47. Müller, R. H., Maassen, H., Schwarz, C., Mehnert, W., Solid Lipid Nanoparticles (SLN) as Potential Carrier for Human Use: Interaction with Human Granulocytes. *Journal of Controlled Release* **1997**, 47, (3), 261-269.
48. Kalam, M. A., Sultana, Y., Ali, A., Aqil, M., Mishra, A. K., Chuttani, K., Preparation, Characterization, and Evaluation of Gatifloxacin Loaded Solid Lipid Nanoparticles

- as Colloidal Ocular Drug Delivery System. *Journal of Drug Targeting* **2010**, 18, (3), 191-204.
49. Bunjes, H., Koch, M. H. J., Saturated Phospholipids promote Crystallization but slow down Polymorphic Transitions in Triglyceride Nanoparticles. *Journal of Controlled Release* **2005**, 107, (2-3), 229-243.
 50. Bunjes, H., Koch, M. H. J., Westesen, K., Influence of Emulsifiers on Crystallization of Solid Lipid Nanoparticles. *Journal of Pharmaceutical Sciences* **2003**, 92, (7), 1509-1520.
 51. Radomska-Soukharev, A., Stability of Lipid Excipients in Solid Lipid Nanoparticles. *Advanced Drug Delivery Reviews* **2007**, 59, 411-418.
 52. Bunjes, H., Westesen, K., Koch, M. H. J., Crystallization Tendency and Polymorphic Transitions in Triglyceride Nanoparticles. *International Journal of Pharmaceutics* **1996**, 129, 159-173.
 53. Lopetinsky, R. J. G., Masliyah, J. H., Xu, Z., Solids-Stabilized Emulsions: A Review. In *Colloidal Particles at Liquid Interfaces*, Binks, B. P., Horozov, T. S., Ed. Cambridge University Press: Cambridge, 2006; pp 186-224.
 54. Horozov, T. S., Binks, B. P., Particle-Stabilized Emulsions: A Bilayer or a Bridging Monolayer? *Angewandte Chemie* **2006**, 45, 773-776.
 55. Abend, S., Lagaly, G., Bentonite and Double Hydroxides as Emulsifying Agents. *ClayMinerals* **2001** 36, 557-570.
 56. Brigger, I., Dubernet, C., Couvreur, P., Nanoparticles in Cancer Therapy and Diagnosis. *Advanced Drug Delivery Reviews* **2002**, 54, 631-651.
 57. Mehnert, W., Mader, K., Solid Lipid Nanoparticles - Production, Characterization and Applications. *Advanced Drug Delivery Reviews* **2001**, 47, 165-196.
 58. Wissing, S. A., Kayser, O., Müller, R. H., Solid Lipid Nanoparticles for Parenteral Drug Delivery. *Advanced Drug Delivery Reviews* **2004**, 56, 1257-1272.
 59. Müller, R. H., Mehnert, W., Lucks, J. S., Schwarz, C., zur Mühlen, A., Weyhers, A., Freitas, C., Rühl, D., Solid Lipid Nanoparticles (SLN) - An Alternative Colloidal Carrier System for Controlled Drug Delivery. *European Journal of Pharmaceutics and Biopharmaceutics* **1995**, 41, 62-69.
 60. Garcia-Fuentes, M., Alonso, M. J., Torres, D., Design and Characterization of a New Drug Nanocarrier made from Solid-Liquid Lipid Mixtures. *Journal of Colloid and Interface Science* **2005**, 285, 590-598.
 61. Cavalli, R., Peira, E., Caputo, O., Gasco, M. R., Solid Lipid Nanoparticles as Carriers of Hydrocortisone and Progesterone Complexes with B-Cyclodextrins. *International Journal of Pharmaceutics* **1999**, 182, 59-69.
 62. Yuan, H., Jiang, S., Du, Y., Miao, J., Zhang, X., Hu, F., Strategic Approaches for Improving Entrapment of Hydrophilic Peptide Drugs by Lipid Nanoparticles. *Colloids and Surfaces B: Biointerfaces* **2009**, 70, (2), 248-253.
 63. Ravi Kumar, M. N. V., Nano and Microparticles as Controlled Drug Delivery Devices. *Journal of Pharmaceutics and Pharmaceutical Sciences* **2000**, 3, (2), 234-258.
 64. Reddy, L. H., Sharma, R. K., Chuttani, K., Mishra, A. K., Murthy, R. R., Etoposide-Incorporated Tripalmitin Nanoparticles with Different Surface Charge: Formulation, Characterization, Radiolabeling, and Biodistribution Studies. *The AAPS Journal* **2004**, 6, (3), 1-10.
 65. Vivek, K., Reddy, H., Murthy, R. S. R., Investigations of the Effect of the Lipid Matrix on Drug Entrapment, *In Vitro* Release, and Physical Stability of Olanzapine-Loaded Solid Lipid Nanoparticles. *AAPS PharmSciTech* **2007**, 8, (4), Article 83, E1-E9.

66. Kesisoglou, F., Panmai, S., Wu, Y. H., Application of Nanoparticles in Oral Delivery of Immediate Release Formulations. *Current Nanoscience* **2007**, 3, (2), 183-190.
67. Munchow, M., Maincent, P., Muller, R. H., Lipid Nanoparticles with a Solid Matrix (SLN, NLC, LDC) for Oral Drug Delivery. *Drug Development and Industrial Pharmacy* **2008**, 34, (12), 1394-1405.
68. Silva, A. C., Santos, D., Ferreira, D. C., Souto, E. B., Oral Delivery of Drugs by Means of Solid Lipid Nanoparticles. *Minerva Biotechnologica* **2007**, 19, (1), 1-5.
69. Huang, Z. R., Hua, S. C., Yang, Y. L., Fang, J. Y., Development and Evaluation of Lipid Nanoparticles for Camptothecin Delivery: A Comparison of Solid Lipid Nanoparticles, Nanostructured Lipid Carriers and Lipid Emulsion. *Acta Pharmacologica Sinica* **2008**, 29, (9), 1094-1102.
70. Lippacher, A., Muller, R. H., Mader, K., Liquid and Semi-solid SLN TM Dispersions for Topical Application: Rheological Characterization. *European Journal of Pharmaceutics and Biopharmaceutics* **2004**, 58, 561-567.
71. Maia, C. S., Mehnert, W., Schafer-Korting, M., Solid Lipid Nanoparticles as Drug Carriers for Topical Glucocorticoids. *International Journal of Pharmaceutics* **2000**, 196, 165-167.
72. Müller, R. H., Radtke, M., Wissing, S. A., Solid Lipid Nanoparticles (SLN) and Nanostructured Lipid Carriers (NLC) in Cosmetic and Dermatological Preparations. *Advanced Drug Delivery Reviews* **2002**, 54, (Supplement 1), S131-S155.
73. Pardeike, J., Hommoss, A., Müller, R. H., Lipid Nanoparticles (SLN, NLC) in Cosmetic and Pharmaceutical Dermal Products. *International Journal of Pharmaceutics* **2009**, 366, (1-2), 170-184.
74. Wissing, S. A., Müller, R. H., Solid Lipid Nanoparticles (SLN) - A Novel Carrier for UV Blockers. *Die Pharmazie* **2001**, 56, (10), 783-786.
75. Wissing, S. A., Müller, R. H., Cosmetic Applications for Solid Lipid Nanoparticles (SLN). *International Journal of Pharmaceutics* **2003**, 254, 65-68.
76. Wissing, S. A., Muller, R. H., The Influence of Solid Lipid Nanoparticles on Skin Hydration and Viscoelasticity - *In Vivo* Study. *European Journal of Pharmaceutics and Biopharmaceutics* **2003**, 56, 67-72.
77. Acosta, E., Bioavailability of Nanoparticles in Nutrient and Nutraceutical Delivery. *Current Opinion in Colloid and Interface Science* **2009**, 14, 3-15.
78. Leser, M. E., Sagalowicz, L., Michel, M., Watzke, H. J., Self-Assembly of Polar Food Lipids. *Advances in Colloid and Interface Science* **2006**, 123-126, 125-136.
79. McClements, D. J., Decker, E. A., Weiss, J., Emulsion-Based Delivery Systems for Lipophilic Bioactive Components. *Journal of Food Science R: Concise Reviews and Hypotheses in Food Science* **2007**, 72, (8), R109-R124.
80. McClements, D. J., Decker, E. A., Park, Y., Weiss, J., Designing Food Structure to Control Stability, Digestion, Release and Absorption of Lipophilic Food Components. *Food Biophysics* **2008**, 3, 219-228.
81. McClements, D. J., Decker, E. A., Park, Y., Weiss, J., Structural Design Principles for Delivery of Bioactive Components in Nutraceuticals and Functional Foods. *Critical Reviews in Food Science and Nutrition* **2009**, 49, 577-606.
82. McClements, D. J., Yan, L., Structured Emulsion-Based Delivery Systems: Controlling the Digestion and Release of Lipophilic Food Components. *Advances in Colloid and Interface Science* **2010**, 159, 213-228.
83. McClements, D. J., Emulsion Design to Improve the Delivery of Functional Lipophilic Components. *Annual Reviews in Food Science Technology* **2010**, 1, 241-269.

84. Sagalowicz, L., Leser, M. E., Delivery Systems for Liquid Food Products. *Current Opinion in Colloid and Interface Science* **2010**, 15, 61-72.
85. Ubbink, J., Burbidge, A., Mezzenga, R., Food Structure and Functionality : A Soft Matter Perspective. *Soft Matter* **2008**, 4, 1569-1581.
86. Velikov, K. P., Pelan, E., Colloidal Delivery Systems for Micronutrients and Nutraceuticals. *Soft Matter* **2008**, 4, 1964-1980.
87. Weiss, J., Decker, E. A., McClements, D. J., Kristbergsson, K., Helgason, T., Awad, T., Solid Lipid Nanoparticles as Delivery Systems for Bioactive Food Components. *Food Biophysics* **2008**, 3, 146-154.
88. Chen, H., Weiss, J., Shahidi, F., Nanotechnology in Nutraceuticals and Functional Foods. *Food Technology* **2006**, 60, (3), 30-36.
89. Biello, D. Do Nanoparticles in Food Pose a Health Risk? *Periodical* [Online], 2008. <http://www.scientificamerican.com/article.cfm?id=do-nanoparticles-in-food-pose-health-risk> (accessed October 20, 2010).
90. Morris, V. J. Is Nanotechnology Going to Change the Future of Food Technology? *Periodical* [Online], 2005. <http://www.foodtech-international.com/papers/nanotechnology.htm> (accessed October 20, 2010).
91. Shefer, A. The Application of Nanotechnology in the Food Industry *Periodical* [Online], 2005. <http://www.foodtech-international.com/papers/application-nano.htm> (accessed October 20, 2010).
92. Morris, V. J. Nanotechnology in Functional Foods *Periodical* [Online], 2006. <http://www.functionalfoodnet.eu/asp/default.asp?p=62> (accessed October 20,2010).
93. Morris, V. J., Parker, R. Natural and Designed Self-assembled Nanostructures in Foods *Periodical* [Online], July 2008. <http://www.worldfoodscience.org/cms/?pid=1004050> (accessed October 20, 2010).
94. Sanguansri, P., Augustin, M .A., Nanoscale Materials Development - A Food Industry Perspective. *Trends in Food Science and Technology* **2006**, 17, (10), 547-556.
95. Chen, L., Remondetto, G. E., Subirade, M., Food Protein-based Materials as Nutraceutical Delivery Systems. *Trends in Food Science and Technology* **2006**, 17, 272-283.
96. Huang, Q., Yu, H., Ru, Q., Bioavailability and Delivery of Nutraceuticals Using Nanotechnology. *Journal of Food Science R: Concise Reviews and Hypotheses in Food Science* **2010**, 75, (1), R50-R57.
97. Dingman, J., Nanotechnology: Its Impact on Food Safety. *Journal of Environmental Health* **Jan/Feb 2008**, 70, (6), 47-50.
98. Siegrist, M., Stampfli, N., Kastenzholz, H., Keller, C., Perceived Risks and Perceived Benefits of Different Nanotechnology Foods and Nanotechnology Food Packaging. *Appetite* **2008**, 51, 283-290.
99. Chau, C., Wu, S., Yen, G., The Development of Regulations for Food Nanotechnology. *Trends in Food Science and Technology* **2007**, 18, 269-280.
100. Sekhon, B. S., Food Nanotechnology - An Overview. *Nanotechnology, Science and Applications* **2010**, 3, 1-15.
101. Lee, S. J., McClements, D. J., Fabrication of Protein-Stabilized Nanoemulsions using a Combined Homogenization and Amphiphilic Solvent Dissolution/ Evaporation Approach. *Food Hydrocolloids* **2010**, 24, 560-569.
102. McClements, D. J., Design of Nano-Laminated Coatings to Control Bioavailability of Lipophilic Food Components. *Journal of Food Science R: Concise Reviews and Hypotheses in Food Science* **2009**, 75, (1), R30-R42.

103. Al-Haj, N. A., Abdullah, R., Ibrahim, S., Bustamam, A., Tamoxifen Drug Loading Solid Lipid Nanoparticles Prepared by Hot High Pressure Homogenization Techniques. *American Journal of Pharmacology and Toxicology* **2008**, 3, (3), 219-224.
104. Bunjes, H., Drechsler, M., Koch, M. H. J., Westesen, K., Incorporation of the Model Drug Ubidecarenone into Solid Lipid Nanoparticles. *Pharmaceutical Research* **2001**, 18, (3), 287-293.
105. Dingler, A., Gohla, S., Production of Solid Lipid Nanoparticles (SLN): Scaling-up Feasibilities. *Journal of Microencapsulation* **2002**, 19, (1), 11-16.
106. Kristl, J., Volk, B., Ahlin, P., Gombac, K., Sentjurc, M., Interactions of Solid Lipid Nanoparticles with Model Membranes and Leukocytes studied by EPR. *International Journal of Pharmaceutics* **2003**, 256, 133-140.
107. Lippacher, A., Müller, R. H., Mader, K., Investigation on the Viscoelastic Properties of Lipid Based Colloidal Drug Carriers. *International Journal of Pharmaceutics* **2000**, 196, 227-230.
108. Müller, R. H., Rühl, D., Runge, S., Schulze-Forster, K., Mehnert, W., Cytotoxicity of Solid Lipid Nanoparticles as a Function of the Lipid Matrix and the Surfactant. *Pharmaceutical Research* **1997**, 14, (4), 458-462.
109. zur Mühlen, A., Schwarz, C., Mehnert, W., Solid Lipid Nanoparticles (SLN) for Controlled Drug Delivery - Drug Release and Release Mechanism. *European Journal of Pharmaceutics and Biopharmaceutics* **1998**, 45, (2), 149-155.
110. Souto, E. B., Wissing, S. A., Barbosa, C. M., Müller, R. H., Development of a Controlled Release Formulation based on SLN and NLC for Topical Clotrimazole Delivery. *International Journal of Pharmaceutics* **2004**, 278, 71-77.
111. Souto, E. B., Anselmi, C., Centini, M., & Müller, R. H., Preparation and Characterization of n-Dodecyl-Ferulate-Loaded Solid Lipid Nanoparticles (SLN®). *International Journal of Pharmaceutics* **2005**, 295, 261-268.
112. Viriyaroj, A., Ritthidej, G. C., Diazepam-Glycerol Behenate Nanoparticles for Parenteral Delivery Prepared by the Hot Homogenization Process. *Asian Journal of Pharmaceutical Sciences* **2006**, 1, 17-26.
113. Westesen, K., Bunjes, H., Koch, M. H. J., Physicochemical Characterization of Lipid Nanoparticles and Evaluation of their Drug Loading Capacity and Sustained Release Potential. *Journal of Controlled Release* **1997**, 47, (2-3), 223-236.
114. Helgason, T., Awad, T. S., Kristbergsson, K., Decker, E. A., McClements, D. J., Weiss, J., Impact of Surfactant Properties on Oxidative Stability of B-Carotene Encapsulated within Solid Lipid Nanoparticles. *Journal of Agricultural and Food Chemistry* **2009**, 57, 8033-8040.
115. Hentschel, A., Gramdorf, S., Müller, R. H., Kurz, T., B-Carotene-Loaded Nanostructured Lipid Carriers. *Journal of Food Science N: Nanoscale Food Science, Engineering, and Technology* **2008**, 73, (2), N1-N6.
116. Almeida, A. J., Runge, S., Müller, R. H., Peptide-Loaded Solid Lipid Nanoparticles (SLN): Influence of Production Parameters. *International Journal of Pharmaceutics* **1997**, 149, (2), 255-265.
117. Schubert, M. A., Muller-Goymann, C. C., Characterisation of Surface-Modified Solid Lipid Nanoparticles (SLN): Influence of Lecithin and Nonionic Emulsifier. *European Journal of Pharmaceutics and Biopharmaceutics* **2005**, 61, 77-86.
118. Hou, D. Z., Xie, C. S., Huang, K. J., Zhu, C. H., The Production and Characteristics of Solid Lipid Nanoparticles (SLNs). *Biomaterials* **2003**, 24, 1781-1785.

119. Cavalli, R. C., Carlotti, M. E., Trotta, M., Scarnecchia, C., Gasco, M. R., Sterilization and Freeze-Drying of Drug-Free and Drug-Loaded Solid Lipid Nanoparticles. *International Journal of Pharmaceutics* **1997**, 148, 47-54.
120. Marengo, E., Cavalli, R., Caputo, O., Rodriguez, L., Gasco, M. R., Scale-Up of the Preparation Process of Solid Lipid Nanospheres: Part I. *International Journal of Pharmaceutics* **2000**, 205, 3-13.
121. Ugazio, E., Cavalli, R., Rosa, G. M., Incorporation of Cyclosporin A in Solid Lipid Nanoparticles (SLN). *International Journal of Pharmaceutics* **2002**, 241, 341-344.
122. Igartua, M., Saulnier, P., Heurtault, B., Pech, B., Proust, J. E., Pedraz, J. L., Benoit, J.P., Development and Characterization of Solid Lipid Nanoparticles Loaded with Magnetite. *International Journal of Pharmaceutics* **2002**, 233, (149-157).
123. Subedi, R. K., Kang, K. W., Choi, H. K., Preparation and Characterization of Solid Lipid Nanoparticles Loaded with Doxorubicin. *European Journal of Pharmaceutical Sciences* **2009**, 37, (3-4), 508-513.
124. Zhang, J., Fan, Y., Smith, E., Experimental Design for the Optimization of Lipid Nanoparticles. *Journal of Pharmaceutical Sciences* **2009**, 98, (5), 1813-1819.
125. Wong, H. L., Yongqiang, L., Bendayan, R., Rauth, M. A., Wu, X. Y., Solid Lipid Nanoparticles for Anti-Tumor Drug Delivery. In *Nanotechnology for Cancer Therapy*, Amiji, M. M., Ed. CRC Press, Taylor & Francis: Massachusetts, 2007; pp 741-776.
126. Heurtault, B., Saulnier, P., Pech, B., Vernier-Julienne, M. C., Proust, J. E., Phan-Tan-Luu, R., Benoit, J. P., The Influence of Lipid Nanocapsule Composition on their Size Distribution. *European Journal of Pharmaceutical Sciences* **2003**, 18, (1), 55-61.
127. Gallarate, M., Trotta, M., Battaglia, L., Chirio, D., Preparation of Solid Lipid Nanoparticles from w/o/w Emulsions: Preliminary Studies on Insulin Encapsulation. *Journal of Microencapsulation* **2009**, 26, (5), 394-402.
128. Bunjes, H., Siekmann, B., Manufacture, Characterization and Applications of SLNs as Drug Delivery Systems. In *Microencapsulation: Methods and Industrial Applications*, 2nd ed.; Benita, S., Ed. CRC Press: 2006; pp 213-268.
129. Westesen, K., Drechsler, M., Bunjes, H., Colloidal Dispersions Based on Solid Lipids. In *Food Colloids: Fundamentals of Formulation*, Dickinson, E., Miller, R., Ed. Royal Society of Chemistry: UK, 2001; pp 103-115.
130. Schubert, M. A., Harms, M., Muller-Goymann, C. C., Structural Investigations on Lipid Nanoparticles Containing High Amounts of Lecithin. *European Journal of Pharmaceutical Sciences* **2006**, 27, 226-236.
131. Jores, K., Mehnert, W., Drechsler, M., Bunjes, H., Johann, C., Mader, K., Investigations on the Structure of Solid Lipid Nanoparticles (SLN) and Oil-Loaded Solid Lipid Nanoparticles by Photon Correlation Spectroscopy, Field-Flow Fractionation and Transmission Electron Microscopy. *Journal of Controlled Release* **2004**, 95, (217-227).
132. Herrera, J. E., Sakulchaicharoen, N., Microscopic and Spectroscopic Characterization of Nanoparticles. In *Drug Delivery Nanoparticles Formulation and Characterization: Drugs And The Pharmaceutical Sciences*, Pathak, Y., Thassu, D., Ed. Informa Healthcare USA, Inc.: New York, 2009; pp 239-251.
133. Fukui, T., Basic Properties and Measuring Methods of Nanoparticles. In *Nanoparticle Technology Handbook*, 1st ed.; Hosokawa, M., Nogi, K., Naito, M., Yokoyama, T., Ed. Elsevier: Amsterdam, 2007; pp 23-28.
134. Müller-Goymann, C. C., Physicochemical Characterization of Colloidal Drug Delivery Systems such as Reverse Micelles, Vesicles, Liquid Crystals and Nanoparticles for

- Topical Administration. *European Journal of Pharmaceutics and Biopharmaceutics* **2004**, 58, 343-356.
135. Application Note - Nanostructures in the Cryo FEG SEM *Periodical* [Online], 2007, p. 1-4. (accessed October 20, 2010).
 136. Esposito, E., Fantin, M., Marti, M., Drechsler, M., Paccamiccio, L., Mariani, P., Sivieri, E., Lain, F., Menegatti, E., Morari, M., Cortesi, R., Solid Lipid Nanoparticles as Delivery Systems for Bromocriptine. *Pharmaceutical Research* **2008**, 25, (7), 1521-1530.
 137. Bunjes, H., Steiniger, F., Richter, W., Visualizing the Structure of Triglyceride Nanoparticles in Different Crystal Modifications. *Langmuir* **2007**, 23, 4005-4011.
 138. Sanna, V., Kirschvink, N., Gustin, P., Gavini, E., Roland, I., Delattre, L., Evrard, B., Preparation and *In Vivo* Toxicity Study of Solid Lipid Microparticles as Carrier for Pulmonary Administration. *AAPS Pharm.SciTech* **2004**, 5, (2), Article 27.
 139. Erdal, M. S., Güngör, S., Özsoy, Y., Araman, A., Preparation and *In Vitro* Evaluation of Indomethacin Loaded Solid Lipid Microparticles. *Acta Pharmaceutica Scientia* **2009**, 51, 203-210.
 140. El-Kamel, A. H., Al-Fagih, I. M., Alsarra, I. A., Testosterone Solid Lipid Microparticles for Transdermal Drug Delivery: Formulation and Physicochemical Characterization. *Journal of Microencapsulation* **2007**, 24, (5), 457-475.
 141. Hatziantoniou, S., Deli, G., Nikas, Y., Demetzos, C., Papaioannou, G. Th., Scanning Electron Microscopy Study on Nanoemulsions and Solid Lipid Nanoparticles containing High Amounts of Ceramides. *Micron* **2007**, 38, 819-823.
 142. Misra, A., Kalariya, M., Padhi, B. K., Chougule, M. Methotrexate-Loaded Solid Lipid Nanoparticles for Topical Treatment of Psoriasis: Formulation and Clinical Implications *Periodical* [Online], October 2004, p. Posted on March 28, 2008. (accessed October 30, 2010).
 143. Urbán-Morlán, Z., Ganem-Rondero, A., Melgoza-Contreras, L. M., Escobar-Chávez, J. J., Nava-Arzaluz, M. G., Quintanar-Guerrero, D., Preparation and Characterization of Solid Lipid Nanoparticles Containing Cyclosporine by the Emulsification-Diffusion Method. *International Journal of Nanomedicine* **2010**, 5, 611-620.
 144. zur Mühlen, A., zur Mühlen, E., Niehus, H., Mehnert, W., Atomic Force Microscopy Studies of Solid Lipid Nanoparticles. *Pharmaceutical Research* **1996**, 13, (9), 1411-1416.
 145. Du, B., Yan, Y., Li, Y., Wang, S. Y., Zhang, Z. Z., Preparation and Passive Target of 5-Fluorouracil Solid Lipid Nanoparticles. *Pharmaceutical Development and Technology* **2009**, 1-8.
 146. Dingler, A., Blum, R. P., Niehus, H., Müller, R. H., Gohla, S., Solid Lipid Nanoparticles (SLN™/Lipopearls™) A Pharmaceutical and Cosmetic Carrier for the Application of Vitamin E in Dermal Products. *Journal of Microencapsulation* **1999**, 16, (6), 751-767.
 147. Gualbert, J., Shahgaldian, P., Lazar, A., Coleman, A. W., Solid Lipid Nanoparticles (SLNs): Preparation and Properties of Calix[4]resorcinarene-Derived Systems. *Journal of Inclusion Phenomena and Macrocyclic Chemistry* **2004**, 48, 37-44.
 148. You, J., Wan, F., de Cui, F., Sun, Y., Du, Y. Z., Hua, Q. F., Preparation and Characteristic of Vinorelbine Bitartrate-Loaded Solid Lipid Nanoparticles. *International Journal of Pharmaceutics* **2007**, 343, 270-276.
 149. Dubes, A., Parrot-Lopez, H., Abdelwahed, W., Degobert, G., Fessi, H., Shahgaldian, P., Coleman, A. W. , Scanning Electron Microscopy and Atomic Force Microscopy

- Imaging of Solid Lipid Nanoparticles Derived from Amphiphilic Cyclodextrins. *European Journal of Pharmaceutics and Biopharmaceutics* **2003**, 55, 279-282.
150. Schubert, M. A., Schicke, B. C., Müller-Goymann, C. C., Thermal Analysis of the Crystallization and Melting Behavior of Lipid Matrices and Lipid Nanoparticles Containing High Amounts of Lecithin. *International Journal of Pharmaceutics* **2005**, 298, 242-254.
 151. Awad, T. S., Helgason, T., Kristbergsson, K., Weiss, J., Decker, E. A., McClements, D. J., Temperature Scanning Ultrasonic Velocity Study of Complex Thermal Transformations in Solid Lipid Nanoparticles. *Langmuir* **2008**, 24, 12779-12784.
 152. Binks, B. P., Horozov, T. S., Colloidal Particles at Liquid Interfaces: An Introduction. In *Colloidal Particles at Liquid Interfaces*, Binks, B. P., Horozov, T. S., Ed. Cambridge University Press: Cambridge, 2006; pp 1-74.
 153. Kulozik, U., Structuring Dairy Products by Means of Processing and Matrix Design. In *Food Materials Science: Principles and Practice*, Aguilera, J. M., Lillford, P. J., Ed. Springer Science + Business Media, LLC New York, 2008; pp 439-473.
 154. Zisman, W. A., Relation of the Equilibrium Contact Angle to Liquid and Solid Constitution. In *Contact Angle, Wettability, and Adhesion*, Fowkes, F., Ed. American Chemical Society: Washington DC, 1964; pp 1-51.
 155. Donaldson, E. C., Alam, W., *Wettability*. Gulf Publishing Company: Houston, 2008; p 1-55.
 156. APV Lab Series Homogenizers. In *APV Lab Series Homogenizers 1000/2000 Series Brochure*, SPX Corporation: 08/2008; pp 1-4.
 157. deMendoza, A. E. H., Campanero, M. A., Mollinedo, F., Blanco-Prieto, M. J. , Lipid Nanomedicines for Anticancer Drug Therapy. *Journal of Biomedical Nanotechnology* **2009**, 5, (4), 323-343.
 158. Luykx, D. M. A. M., Peters, R. J. B., vanRuth, S. M., Bouwmeester, H., A Review of Analytical Methods for the Identification and Characterization of Nano Delivery Systems in Food. *Journal of Agricultural and Food Chemistry* **2008**, 56, 8231-8247.
 159. Werner, M., Crossley, A., Johnston, C., Characterization of Nanostructured Materials. In *Handbook of Surface and Interface Analysis - Methods for Problem-Solving*, 2nd ed.; Riviere, J. C., Myhra, S., Ed. CRC Press, Taylor & Francis Group: USA, 2009; pp 319-350.
 160. *Instruction Manual for 90 Plus/ BI-MAS Multi Angle Particle Sizing Option*. Brookhaven Instruments Corporation: New York, January 1995; p 1-25.
 161. Wedd, M. W., Determination of Particle Size Distributions using Laser Diffraction. *Educational Resources for Particle Technology* **2003**, 032Q-Wedd, 1-4.
 162. Rawle, A. *Technical Paper: Basic Principles of Particle Size Analysis*; Malvern Instruments Ltd: Worcestershire, pp 1-8.
 163. Boom, R. M., Emulsions: Principles and Preparation. In *Food Materials Science: Principles and Practice*, Aguilera, J. M., Lillford, P. J., Ed. Springer Science + Business Media, LLC: New York, 2008; pp 305-339.
 164. MRK654-01 *Zeta Potential : An Introduction in 30 Minutes*; Malvern Instruments Ltd.: Worcestershire, 2001; pp 1-6.
 165. Nutan, M. T. H., Reddy, I. K., General Principles of Suspensions. In *Pharmaceutical Suspensions - From Formulation Development to Manufacturing*, Kulshreshtha, A. K., Singh, O. N., Wall, G. M., Ed. Springer: New York, 2010; pp 39-65.

166. Campbell, I. J., The Role of Fat Crystals in Emulsion Stability. In *Food Colloids*, Bee, R. D. R., P.;Mingins, J., Ed. Royal Society of Chemistry: Cambridge, 1989; pp 272-282.
167. ASTM D971 - 99a Standard Test Method for Interfacial Tension of Oil Against Water by the Ring Method *Periodical* [Online], 2004. <http://www.astm.org/Standards/D971.html> (accessed December 15, 2010).
168. Bunjes, H., Unruh, T., Characterization of Lipid Nanoparticles by Differential Scanning Calorimetry, X-Ray and Neutron Scattering. *Advanced Drug Delivery Reviews* **2007**, 59, 379-402.
169. *Operating Manual Axiovert 200 / Axiovert 200 M Inverted Microscopes*. Carl Zeiss Light Microscopy: Gottingen, 2001; Vol. B 40-080 e, p 0-2 - 4-6.
170. *Bioscope™ SPM Instruction Manual*. Digital Instruments, Inc.: California, 1998; p 1-1 - 15-28.
171. *Nanoscope Command Reference Manual Version 4.42*. Digital Instruments, Inc.: California, 1999; p 1-1 - 15-1.
172. Saupe, A., Rades, T., Solid Lipid Nanoparticles. In *Nanocarrier Technologies: Frontiers of Nanotherapy*, Mozafari, M. R., Ed. Springer: Amsterdam, 2006; pp 41-50.
173. Yokoyama, T., Basic Properties and Measuring Methods of Nanoparticles. In *Nanoparticle Technology Handbook*, 1st ed.; Hosokawa, M., Nogi, K., Naito, M., Yokoyama, T., Ed. Elsevier: Amsterdam, 2007; pp 5-10.
174. Krog, N. J., Sparso, F. V., Food Emulsifiers: Their Chemical and Physical Properties. In *Food Emulsions*, 4th ed.; Friberg, S. E., Larsson, K., Sjoblom, J., Ed. Marcel Dekker, Inc.: New York, 2004; pp 45-91.
175. Lautenschläger, H., Emulsifiers Enable Mixtures. *Kosmetische Praxis* **2004**, 3, 8-10.
176. Euston, S. R., Emulsifiers in Dairy Products and Dairy Substitutes. In *Food Emulsifiers and Their Applications*, 2nd ed.; Hasenhuettl, G. L., Hartel, R. W., Ed. Springer Science + Business Media, LLC: New York, 2008; pp 195-232.
177. Hasenhuettl, G. L., Synthesis and Commercial Preparation of Food Emulsifiers. In *Food Emulsifiers and Their Applications*, 2nd ed.; Hasenhuettl, G. L., Hartel, R. W., Ed. Springer Science + Business Media, LLC: New York, 2008; pp 11-37.
178. Gaupp, R., Adam, W., Acid Esters of Mono- and Diglycerides. In *Emulsifiers in Food Technology*, 1st ed.; Whitehurst, R. J., Ed. Wiley-Blackwell Publishing: Malden, 2004; pp 59-85.
179. *Product Information Immvitor 372P* Sasol Germany, GmbH: Witten, 07/02/2006, 2006; pp 1-4.
180. *Excipients for Pharmaceuticals*; Sasol Germany, GmbH: Witten, 2010; pp 1-28.
181. Ash, M., Ash, I., *Handbook of Green Chemicals*. 2nd ed.; Synapse Information Resources, Inc.: Endicott, 2004.
182. Garti, N., Food Emulsifiers: Structure-Reactivity Relationships, Design, and Applications. In *Physical Properties of Lipids*, Marangoni, A. G., Narine, S. S., Ed. Marcel Dekker, Inc.: New York, 2002; pp 265-386.
183. Prestidge, C. A., Simovic, S., Nanoparticle Encapsulation of Emulsion Droplets. *International Journal of Pharmaceutics* **2006**, 324, 92-100.
184. Aveyard, R., Clint, J. H., Horozov, T. S., Aspects of the Stabilisation of Emulsions by Solid Particles: Effects of Line Tension and Monolayer Curvature Energy. *Physical Chemistry Chemical Physics* **2003**, 5, 2398-2409.
185. Glyceryl Stearyl Citrate *Periodical* [Online], 2010. <http://pubchem.ncbi.nlm.nih.gov/summary/summary.cgi?cid=62110>.

186. *Mastersizer 2000 User Manual*. Malvern Instruments Limited: Worcestershire, March 2007; p 1.1-10.8.
187. Attama, A. A., Schicke, B. C., Paepenmüller, T., Müller-Goymann, C. C., Solid Lipid Nanodispersions Containing Mixed Lipid Core and a Polar Heterolipid: Characterization. *European Journal of Pharmaceutics and Biopharmaceutics* **2007**, 67, 48-57.
188. MRK656-01 *Dynamic Light Scattering: An Introduction in 30 Minutes*; Malvern Instruments Ltd.: Worcestershire, 2001; pp 1-8.
189. MRK1357-01 *Intensity-Volume-Number: Which Size is Correct?*; Malvern Instruments Ltd.: Worcestershire, 2009; pp 1-3.
190. Attama, A. A., Müller-Goymann, C. C., Investigation of Surface-Modified Solid Lipid Nanocontainers Formulated with a Heterolipid-Templated Homolipid. *International Journal of Pharmaceutics* **2007**, 334, 179-189.
191. Higashitani, K., Characteristics and Behavior of Nanoparticles and Its Dispersion Systems. In *Nanoparticle Technology Handbook*, 1st ed.; Hosokawa, M., Nogi, K., Naito, M., Yokoyama, T., Ed. Elsevier: Amsterdam, 2007; pp 139-142.
192. Abe, H., Characteristics and Behavior of Nanoparticles and Its Dispersion Systems. In *Nanoparticle Technology Handbook*, 1st ed.; Hosokawa, M., Nogi, K., Naito, M., Yokoyama, T., Ed. Elsevier: Amsterdam, 2007; pp 159-162.
193. Schwarz, C., Mehnert, W., Lucks, J. S., Muller, R. H., Solid Lipid Nanoparticles (SLN) for Controlled Drug Delivery I: Production, Characterization and Sterilization. *Journal of Controlled Release* **1994**, 30, 83-96.
194. Shaw, D. J., *Introduction to Colloid and Surface Chemistry*. 4th ed.; Butterworth-Heinemann: Oxford, 1992.
195. Bunjes, H., Koch, M. H. J., Westesen, K., Effect of Particle Size on Colloidal Solid Triglycerides. *Langmuir* **2000**, 16, 5234-5241.
196. Siekmann, B., Westesen, K., Thermoanalysis of the Recrystallization Process of Melt-Homogenized Glyceride Nanoparticles. *Colloids and Surfaces B: Biointerfaces* **1994**, 3, 159-175.
197. Higami, M., Ueno, S., Segawa, T., Iwanami, K., Sato, K., Simultaneous Synchrotron Radiation X-ray Diffraction-DSC Analysis of Melting and Crystallization Behavior of Trilauroylglycerol in Nanoparticles of Oil-in-Water Emulsion. *JAACS* **2003**, 80, (8), 731-739.
198. Liu, X. Y., Heterogeneous Nucleation or Homogeneous Nucleation? *Journal of Chemical Physics* **2000**, 112, (22), 9949-9955.
199. McClements, D. J., Weiss, J., Lipid Emulsions. In *Bailey's Industrial Oil and Fat Products*, 6th ed.; Shahidi, F., Ed. Wiley-Interscience, John Wiley and Sons, Inc., Publication: New Jersey, 2005; Vol. 3, pp 457-502.
200. Sonoda, T., Takata, Y., Ueno, S., Sato, K., DSC and Synchrotron-Radiation X-ray Diffraction Studies on Crystallization and Polymorphic Behavior of Palm Stearin in Bulk and Oil-in-Water Emulsion States. *JAACS* **2004**, 81, (4), 365-373.
201. Krog, N., Larsson, K., Crystallization at Interfaces in Food Emulsions - A General Phenomenon. *Lipid* **1992**, 94, (2), 55-57.
202. Sato, K., Ueno, S., Yano, J., Crystal Growth of Organic Soft Materials in Template-Controlling Systems. *Journal of Optoelectronics and Advanced Materials* **2000**, 2, (5), 441-450.
203. Ueno, S., Hamada, Y., Sato, K., Controlling Polymorphic Crystallization of n-Alkane Crystals in Emulsion Droplets through Interfacial Heterogeneous Nucleation. *Crystal Growth & Design* **2003**, 3, (6), 935-939.

204. Arima, S., Ueno, S., Ogawa, A., Sato, K., Scanning Microbeam Small-Angle X-ray Diffraction Study of Interfacial Heterogeneous Crystallization of Fat Crystals in Oil-in-Water Emulsion Droplets. *Langmuir* **2009**, 25, (17), 9777-9784.
205. Suzuki, M., Basic Properties and Measuring Methods of Nanoparticles. In *Nanoparticle Technology Handbook*, 1st ed.; Hosokawa, M., Nogi, K., Naito, M., Yokoyama, T., Ed. Elsevier: Amsterdam, 2007; pp 12-14.
206. Boker, A., He, J., Emrick, T., Russel, T. P., Self-assembly of Nanoparticles at Interfaces. *Soft Matter* **2007**, 3, 1231-1248.